



University of
Stavanger

Faculty of Science and Technology

MASTER'S THESIS

| | |
|--|--|
| Study program/ Specialization: MSc in Petroleum Engineering/ Natural Gas Engineering | Spring 2017 Open access |
| Writer: Madhan Nur Agista | (Writer's signature) |
| Faculty supervisor: Professor Zhixin Yu | |
| Thesis title: A Literature Review and Transport Modelling of Nanoparticles for Enhanced Oil Recovery | |
| Credits (ECTS): 30 | |
| Keywords: <ul style="list-style-type: none">- Nanotechnology- Petroleum industry- Enhanced Oil Recovery- Nanoparticle- Simulation- Transport model | Pages: 77 + enclosure: 7 Stavanger, 15 th June 2017 |

Abstract

Nanotechnology has been envisioned to transform every sector of industries, particularly in the petroleum industry. Numerous researches, especially on nano-EOR, have been done in the past few years and shown promising results for improving oil recovery. Injected nanoparticles (NPs) are believed to be able to form adsorption layers on the top of grain surface. The adsorption layers then alter the wettability of the rock and reduce the interfacial tension. Due to the importance of the adsorption, numerous theoretical studies were performed to simulate the transport behavior of NPs in the porous media.

The purpose of this thesis is to i) review the state-of-the-art progress of nanoparticles application in the petroleum industry especially in EOR, and ii) simulate the transport and adsorption of nanoparticles in the porous media.

Literatures show that various types of nanoparticles can improve oil recovery through several mechanisms such as wettability alteration, interfacial tension reduction, disjoining pressure and mobility control. Parameters such as salinity, temperature, size, and concentration are substantial for nano-EOR. Several experiments indicate that NPs can improve the oil recovery significantly up to 20% after the primary recovery period.

Classical Advection-Dispersion Equation (ADE) is commonly used to simulate particles flow in the porous media, but it fails to simulate NPs flow due to the adsorption that occurs. The colloidal filtration theory (CFT) is used in the study to accommodate the adsorption. Several modifications on CFT, such as dual site model (ISTM), increase the number of unknown variables that reduce the efficiency and the accuracy of the model. Therefore, a simple modified linear adsorption model (ML) is proposed by the author, followed by parameter sensitivity study to reduce the unknown parameters and understand each parameter affecting on the model.

The simulation result indicates that CFT model is unable to predict the effluent history data. Differently, ML model demonstrates that it can predict the effluent history quite well. The comparison with ISTM indicates that both can simulate the behavior of NPs, and our ML model gives slightly better result than ISTM model. Therefore, the transport and adsorption of NPs can be predicted by the simple linear adsorption model.

Acknowledgement

First and foremost, I would like to express my greatest gratitude to my supervisor, Professor Zhixin Yu, for his invaluable guidance, knowledge, and support during this research. His patience and enthusiasm for the research mean so much for me while finishing this master's thesis. Also, thanks to Dr. Pål Andersen for the assistance and support during the simulation study.

I would like to acknowledge Professor Ole Torsæter, NTNU for providing the material and Dr. Tiantian Zhang, UT for the discussion on the simulation part. Also, the best appreciation to all professors and staff at the Department of Petroleum Technology, University of Stavanger.

An extraordinary thanks and love to my family, relatives, and friends in Indonesia and Norway who always support me during my study. Especially to my parents that always pray the best for me, thank you very much. I would like to appreciate my sister (Debia Nur Epita) and her best friend (Citra Istiqomah) that helped me with the writing correction.

Last but not least, I would like to express my special appreciation to Norwegian State Educational Load Fund for the financial support during my master's degree via Quota Scheme Program.

Table of Contents

| | |
|---|------------|
| Abstract | ii |
| Acknowledgement | iii |
| Table of Contents | iv |
| List of Tables | vi |
| List of Figures | vii |
| Abbreviations | ix |
| Chapter 1 Introduction | 1 |
| 1.1 Background | 1 |
| 1.2 Research Objective..... | 2 |
| 1.3 Outline..... | 2 |
| Chapter 2 Fundamentals | 4 |
| 2.1 Introduction | 4 |
| 2.2 Nanomaterials: Nanoparticles and Nanofluids..... | 4 |
| 2.3 Nanoparticles: Structure and Synthesis Process..... | 5 |
| 2.3.1 Nanoparticles Structure..... | 5 |
| 2.3.2 Nanoparticles Synthesis Process..... | 6 |
| 2.4 Nanofluids: Preparation and Stability | 9 |
| 2.4.1 Preparation of Stable Nanofluids | 9 |
| 2.4.2 DLVO Theory in Particles Stability | 10 |
| Chapter 3 Nanoparticle Application in Petroleum Industry | 12 |
| 3.1 Exploration and Reservoir Characterization | 14 |
| 3.2 Drilling and Completion..... | 15 |
| 3.3 Production and Stimulation..... | 16 |
| 3.4 Enhanced Oil Recovery..... | 17 |
| 3.5 Refinery | 18 |
| Chapter 4 Experimental Studies of Nano-EOR | 20 |
| 4.1 Introduction | 20 |
| 4.2 Laboratory Experiments | 20 |
| 4.2.1 Inorganic Nanoparticles | 20 |
| 4.2.2 Organic Nanoparticles | 27 |
| 4.3 Mechanism | 29 |
| 4.3.1 Wettability Alteration | 29 |
| 4.3.2 Interfacial Tension Reduction..... | 31 |
| 4.3.3 Disjoining Pressure | 33 |
| 4.3.4 Viscosity Control | 34 |
| 4.4 The Effect of Nanoparticle Parameters | 35 |

| | | |
|---------------------|--|-----------|
| 4.4.1 | Nanoparticle size..... | 35 |
| 4.4.2 | Nanoparticle concentration | 36 |
| 4.4.3 | Salinity | 37 |
| 4.4.4 | Temperature | 37 |
| 4.4.5 | Wettability..... | 38 |
| Chapter 5 | Simulation of Nanoparticle Transport..... | 39 |
| 5.1 | Introduction | 39 |
| 5.2 | Nanoparticle Flow in Porous Media..... | 39 |
| 5.3 | Numerical Study Overview | 40 |
| 5.3.1 | Filtration Model | 42 |
| 5.3.2 | Kinetic Langmuir Model..... | 45 |
| 5.3.3 | Dual Sites Model..... | 46 |
| 5.3.4 | Modified Linear Adsorption Model..... | 46 |
| 5.4 | Model Development and Parameter Study..... | 47 |
| 5.4.1 | Visualization Model..... | 47 |
| 5.4.2 | Transport Model..... | 48 |
| 5.5 | Experimental Data Validation | 56 |
| Chapter 6 | Conclusion and Future Research | 65 |
| 6.1 | Conclusion Remarks | 65 |
| 6.2 | Challenges and Future Research | 66 |
| Bibliography | | 68 |
| Appendix | | 78 |

List of Tables

| | |
|---|----|
| Table 3.1 Summary of the literature studies | 13 |
| Table 4.1 Experimental studies summary | 21 |
| Table 4.2 Measured interfacial tension data of certain nanofluid [123] | 32 |
| Table 5.1 Transport flow model (modified from [237]) | 42 |
| Table 5.2 Single Collector Efficiency..... | 43 |
| Table 5.3 Data input for sensitivity study..... | 53 |
| Table 5.4 Collector and particle diameter sensitivity study result..... | 54 |
| Table 5.5 Sensitivity study result on the different dispersion coefficient and distribution coefficient | 56 |
| Table 5.6 Experimental Data [240]..... | 57 |
| Table 5.7 Colloidal Filtration Theory Result..... | 57 |
| Table 5.8 Modified Linear Result..... | 60 |
| Table 5.9 Independent Two-site Model (Zhang) | 63 |
| Table 5.10 Model Comparison Result with the Dual Site Model [4] | 63 |

List of Figures

| | |
|--|----|
| Figure 2.1 Size domains of colloids and nanoparticles [33]..... | 4 |
| Figure 2.2 Surface area to volume ratio of particle with different dimension [37] | 5 |
| Figure 2.3 A nanoparticle structure (modified from [39])..... | 6 |
| Figure 2.4 Nanoparticle fabrication methods (Modified from [36])..... | 6 |
| Figure 2.5 Stable and unstable suspension [67]..... | 9 |
| Figure 2.6 Interaction between two colloidal particles, DVLO theory (modified from [67])..... | 11 |
| Figure 4.1 Oil-air contact angle on rock surface before (a) and after (b) treatment with 100 ppm alumina nanofluid [161]..... | 23 |
| Figure 4.2 SEM image of different nanofluids (a) Al ₂ O ₃ , (b) SiO ₂ , (c) CeO ₂ , (d) TiO ₂ , (f) MgO and (f) ZrO ₂ [164] | 24 |
| Figure 4.3 Oil recovery mechanism by magnetic nanoparticle (MNP) [166] | 25 |
| Figure 4.4 Single-walled carbon nanotube (SWCNT) (left), double & triple walled carbon nanotube (MWCNT) (mid and right) [183] | 28 |
| Figure 4.5 Wettability variation on oil-water system | 30 |
| Figure 4.6 SEM and atomic force microscopy image of calcite surface. (A) Calcite surface before; (B) Calcite surface after nanofluid treatment; (C) High resolution ; (D) Max resolution; Topography picture before (E) and after (F) nanofluid treatment [193]. | 30 |
| Figure 4.7 Contact angle variation of oil-brine system in different concentration [146] | 31 |
| Figure 4.8 The effect of carbon nanotube and activated carbon on the interfacial tension [62]..... | 32 |
| Figure 4.9 Nanoparticle wedge shape structuring and the forces (A), Wedge contact pressure (B) [205] | 33 |
| Figure 4.10 Glass micromodel picture of the oil displacement process with nanopolymer solution at different NPs concentrations [214]..... | 34 |
| Figure 4.11 Recovery comparison between Nanoparticle-Polymer-Flood (NPF), Polymer Flood (PF) and Water Flood (WF) [217])..... | 35 |
| Figure 4.12 The effect of nanoparticle size [221]..... | 36 |
| Figure 4.13 Concentration Effect on nano-EOR [216]..... | 36 |
| Figure 4.14 Temperature effect [221]..... | 38 |
| Figure 5.1 Filtration mechanism of colloidal particle transport in porous media [239] | 40 |

| | |
|--|----|
| Figure 5.2 Particle-collector interaction mechanism [245]..... | 40 |
| Figure 5.3 Visualization result of nanoparticle flow model | 48 |
| Figure 5.4 Velocity effect on particle flow behavior..... | 48 |
| Figure 5.5 One dimension ADE solution [263]..... | 49 |
| Figure 5.6 Advection-Dispersion Result..... | 50 |
| Figure 5.7 3-D plot of the effect of dispersion coefficient (D) on concentration distribution | 50 |
| Figure 5.8 Comparison of the single-collector efficiency models at different particle diameters (10^{-5} - 10^{-9} m) and velocities (5×10^{-6} - 5×10^{-1} m/s)..... | 51 |
| Figure 5.9 Normalized model at different particle diameters (10^{-5} - 10^{-9} m) and velocities (5×10^{-6} - 5×10^{-1} m/s) | 52 |
| Figure 5.10 Comparison of Yao-Habibian (YH), Logan et al. (LOG), Tufenkji-Elimelech (TE), Messina et al. (MMS) single-collector efficiency model at low velocity, 5×10^{-6} m/s (left) and low permeability, 10% (right)..... | 52 |
| Figure 5.11 Sensitivity of collector diameter and particle diameter | 54 |
| Figure 5.12 Dispersion coefficient, particle velocity and attachment efficiency sensitivity..... | 54 |
| Figure 5.13 Linear relation on distribution coefficient..... | 55 |
| Figure 5.14 Sensitivity study result of: A. the concentration profile at effluent (left) and B. nanoparticle recovery (right)..... | 56 |
| Figure 5.15 Effluent data and simulation using Colloidal Filtration Theory (CFT) result of experiments 66 and 67 | 58 |
| Figure 5.16 Effluent data and simulation using Colloidal Filtration Theory (CFT) result of experiments 91 and 92..... | 59 |
| Figure 5.17 Effluent data and simulation using Modified Linear (ML) result of experiments 66 and 67 | 61 |
| Figure 5.18 Effluent data and simulation using Modified Linear (ML) result of experiments 91 and 92 | 62 |
| Figure 5.19 Model comparison for experiment 91 and experiment 92..... | 63 |

Abbreviations

| | |
|-------|--|
| ADE | Advection-Dispersion Equation |
| ADR | Advection-Dispersion-Reaction Equation |
| BET | Brunauer–Emmett–Teller |
| CFT | Colloidal Filtration Theory |
| CNF | Carbon Nanofiber |
| CNT | Carbon Nanotube |
| DLVO | Derjaguin-Landau-Verwey-Overbeek |
| EOR | Enhanced Oil Recovery |
| GNP | Graphene nano-platelets |
| HLP | Hydrophobic and Lipophilic Polysilicon |
| HPHT | High Pressure High Temperature |
| IFT | Interfacial Tension |
| ITSM | Independent Two Site Model |
| LHP | Lipophobic and Hydrophilic Polysilicon |
| ML | Modified Linear |
| MWCNT | Multi-walled Carbon Nanotube |
| NP | Nanoparticle |
| NWP | Neutrally Wettable Polysilicon |
| OOIP | Original Oil in Place |
| PNP | Polymer Nanoparticle |
| PVI | Pore Volume Injection |
| PVP | Polyvinylpyrrolidone |
| SEM | Scanning Electron Microscope |
| STM | Scanning Tunneling Microscope |
| SWCNT | Single-walled Carbon Nanotube |
| VES | Viscoelastic Surfactant |

Chapter 1 Introduction

1.1 Background

Nanotechnology is a relatively new technology developed since the 90's. It was envisaged to revolutionize every sector of industries and significantly shape human civilization and has already been realized in areas such as antibiotics, plastics, computer and silicon transistor industry [1]. Initially, the core idea of nanotechnology had been proposed by Richard Feynman in 1959. However, the first term "nanotechnology" was introduced by Norio Taniguchi in 1974 [2]. Then, nanotechnology became more popular after Dr. Heinrich Rohrer (a Nobel laureate and the founding father of nanotechnology) invented the scanning tunneling microscope (STM) in 1981 which later presented the promising opportunities of nanotechnology in 1996 [3]. This invention was the stepping stone of the atomic era that enables identification of individual atom and mapping its surface topology [4]. The definition of nanotechnology has been generalized by National Nanotechnology Initiative of the US as the technology in manipulating matter with sizing from 1 to 100 nanometers [5]. Recently, nanotechnology has been applied in various area such as pharmacy [6, 7], medical [8, 9], biotechnology [10, 11], material and chemical engineering [12, 13]. Novel applications of nanotechnology were also proposed in the petroleum industry for exploration [14], drilling [15], enhanced oil recovery (EOR) [16, 17], and refinery [18, 19].

Hydrocarbon or fossil fuel plays a major role in today's human civilization. During industrialization era coal was the dominant source, until today oil and gas are the major fuel for all transportation sectors. Hydrocarbon is still predicted to be the primary source of energy for the upcoming decades, and the consumption of hydrocarbon will significantly increase over the years. However, there are numerous oil and gas fields in the world which have already reached plateau period and the production will likely to decline. To meet the energy demand for the next decades, methods for extracting residual hydrocarbon trapped in reservoir need to be developed economically. Based on U.S Department of Energy data, 67% of total oil in the United States of America will remain in the reservoir because of the limitation of the technology to extract residual hydrocarbon [17]. There are various enhanced oil recovery (EOR) technologies which have been applied and were proven to increase hydrocarbon recovery significantly such as thermal methods, miscible methods, chemical methods, as well as some new technologies (microbial, low salinity flooding). More recently, nanotechnology is proposed to be one of the promising EOR methods, since it can penetrate the pore throat easily and change the reservoir properties to increase the oil recovery [16, 17, 20-22].

Nanotechnology has shown its potential to revolutionize the petroleum industry for both upstream and downstream sectors in the recent years. Many types of research, especially for nano-EOR, have been done in the past few years and shown a promising

result on the recovery improvement. Laboratory works have shown that surface-coated silica NPs can stabilize emulsion which improves mobility control in EOR process [23, 24]. Hydrophilic silica NPs were reported to alter the rock wettability and reduce interfacial tension, and can potentially be used as EOR agent [16, 25]. Other attempts were made by Onyekonwu et al. [26] with silica NPs dispersed in ethanol that could improve oil recovery up to 38% of the original oil in place (OOIP). Several parameters of nanoparticles such as size, concentration, ionic compositions and NP types had been studied in relation to EOR [26, 27]. Hendraningrat et al. [28] showed that the optimal silica NPs concentration was 0.05 wt.% and concluded that the smaller size of NPs leads to better recovery.

Moreover, nanoparticles were proven to be able to form adsorption layers on the surface of the grain and significantly changes the wettability and interfacial tension of reservoir system [29, 30]. Thus, the adsorption of nanoparticles is one of the important aspects that needs to be understood for a successful EOR implementation. However, nanoparticles' flow in porous media is quite complex and is dominated by the physicochemical interaction between each particle and solid surface, due to their nano-scale size. Several models have been built to predict the adsorption of NPs during the nanofluid flooding based on classical Advection-Dispersion Equation (ADE). Since ADE is only limited for passive tracer model, several modifications are proposed such as maximum adsorption sites, detachment parameter, reversible and irreversible adsorption. Based on all those models, the author proposed a modified linear model which is simpler and quite reliable for predicting NPs adsorption behavior by assuming that linear adsorption occurs.

1.2 Research Objective

The goal of this research is to deeply understand the mechanism of NPs for EOR with the affecting parameters and to simulate the NPs adsorption on the grain surface during the flooding process. This research is divided into two main parts which are experimental studies and numerical studies. The experimental study part discusses the laboratory research existing in the literature on NP for EOR and elaborates the mechanisms and parameters affecting recovery improvement. In the simulation part, mathematical models were developed based on several existing models for NP adsorption. Then, a sensitivity study of parameters affecting NPs flow was done to deeply understand the model and NP behavior in porous media. In the end, comparison and validation using experimental data were done by using those models.

1.3 Outline

This master's thesis consists of six chapters. The focus and coverage of each chapter are briefly as follows:

Chapter 1 provides a brief overview regarding the potential of nanotechnology implementation in the petroleum industry, especially for EOR. The purpose of the study is explained as well as the structure of the thesis and outline.

Introduction

Chapter 2 discusses the fundamental theory of nanoparticle and nanofluid. The fabrication process of nanoparticle and the preparation of stable nanofluid will be elaborated with the theoretical background in colloidal particle stability.

Chapter 3 covers the recent application of nanoparticles and nanofluids in the petroleum industry. The chapter will summarize the utilization of nanoparticles for exploration, drilling, production, and refinery briefly.

Chapter 4 investigates the experimental research on nanofluids which have been done for EOR purpose. In this chapter, the mechanism on how nanoparticle could improve oil recovery is elaborated. Thereafter the parameters which affect the performance of nanoparticle during EOR process are illustrated.

Chapter 5 delivers the simulation studies on nanoparticle flow in porous media. In this part, existing numerical studies on nanoparticle transport will be explained briefly. At the end of this chapter our own numerical models will be built, and sensitivity study of the parameters is done, followed by experimental data validation and model comparison.

Chapter 6 includes the conclusion of both literature and simulation study. Then, the future challenges and promises of nanotechnology for petroleum industry especially for EOR are proposed.

Appendix contains the MATLAB codes that are used for the simulation study.

Chapter 2 Fundamentals

2.1 Introduction

This chapter discusses the fundamental concept of nanotechnology, including both nanoparticles and nanofluids. Structures of nanoparticles are explained together with various methods to synthesize nanoparticle. Then the preparation of nanofluid will be discussed with the theoretical background on nanofluid stability.

2.2 Nanomaterials: Nanoparticles and Nanofluids

After the invention of the scanning tunneling microscope (STM) by Gerd Binnig and Heinrich Rohrer in 1981, the miniaturization of materials and nanotechnology became an intensive scientific research focus worldwide [31]. Das et al. [1] defined nanotechnology as the modification of materials, devices, and systems by controlling matters at the nanoscale size (10^{-9} m) with the exploitation of phenomena and properties at that scale. IUPAC [32] defined nanoparticles as a sub-fraction of the colloid within size ranged from 10^{-9} to 10^{-7} meters (Figure 2.1). Since the only difference between NPs and colloids is the magnitude of the size, dispersed NPs are often considered as a part of the colloidal system. However, NP cannot fully be classified as a colloid nor a molecule since it is smaller than most colloidal particle and more complex than just a simple molecule [33].

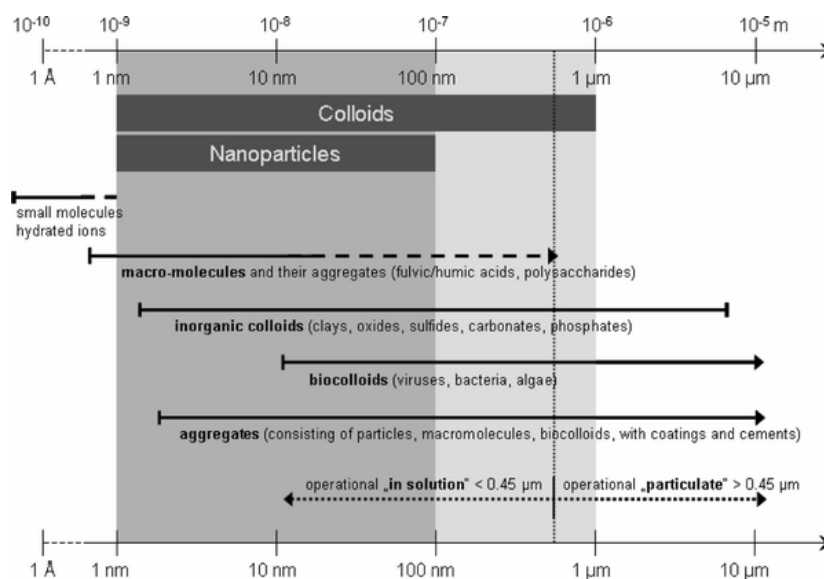


Figure 2.1 Size domains of colloids and nanoparticles [33]

2.3 Nanoparticles: Structure and Synthesis Process

Nanoparticle (NP) is defined as an aggregate of atoms bonded to each other within radius 1 and 100 nm that typically contains $10-10^5$ atoms [34]. Generally, any nanostructure materials will have higher surface area to volume ratio due to its smaller size. A good analogy to understand how a smaller particle can yield higher surface area to volume ratio is presented in Figure 2.2. In comparison to micro-particle, the nanoparticle has 1000 times higher surface area to volume ratio. Due to the larger surface area to volume ratio, a nanoparticle has different surface properties compared to its bulk material that increases its potential utilization to a wider range. Moreover, the nanostructure of one material has unique properties which cannot be found in its macro-size analogy [35]. Nanoparticles especially metallic NPs exhibit different physical and chemical characteristic from bulk metals such as higher total surface areas, low melting point, unique optical properties and unique magnetizing behavior [36]. As Kong and Ohadi [17] explained that since the dimension of NP is closer to or even less than the wavelength of conduction electrons, the periodic boundary conditions are damaged, and so that magnetism, internal pressure, optical absorption, thermal resistance, chemical activity, catalysis and melting point undergo great changes that are different from those of normal particles.

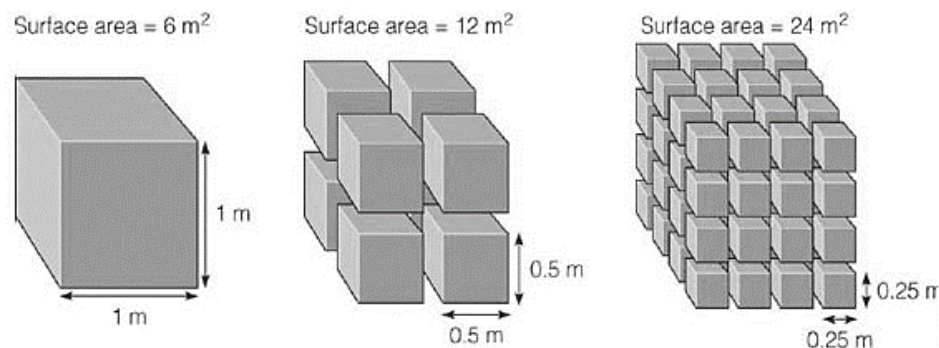


Figure 2.2 Surface area to volume ratio of particle with different dimension [37]

2.3.1 Nanoparticles Structure

In general, nanoparticle consists of several layers, the core, a surface and an additional shell (see Figure 2.3). The core of a nanoparticle is located at the center of its structure, and it is used to identify the type of NPs. Generally, the properties of NPs are associated with the composition of the core which is mostly made of inorganic material [33, 38]. The surface of the nanoparticle is an outer layer of the core which is functionalized by using metal ion, a surfactant or a polymer [33]. The shell is an outer layer of structures with chemically different materials. It is constructed from oxide, nitride or an organic material (surfactant or polymer). In some inorganic NPs (e.g. silica NPs), the extension layer of a core can be considered as a shell [38]. Moreover, the molecular shell consists of three different groups which are, the tail group, the hydrocarbon chain and the active head group [31].

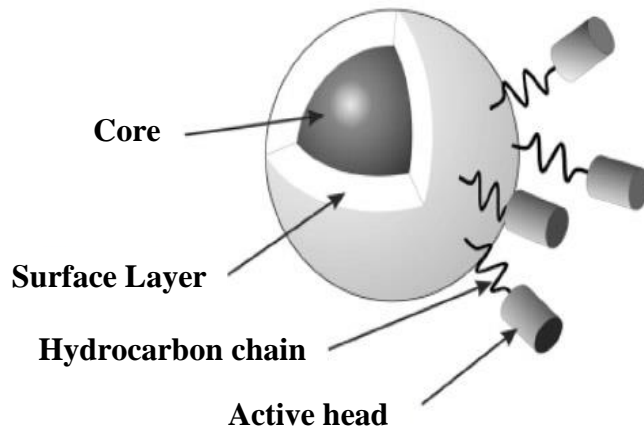


Figure 2.3 A nanoparticle structure (modified from [39])

2.3.2 Nanoparticles Synthesis Process

In general, there are two methods in manufacturing NPs which are the top-down and bottom-up process. In the top-down process, external forces are implemented to breakdown the original solid material into the smaller particle. On the other hand, bottom-up process form NP by the coalition of atoms based on molecular condensation or atomic transformation [36]. Figure 2.4 shows the typical methods used in the top-down process and bottom-up process.

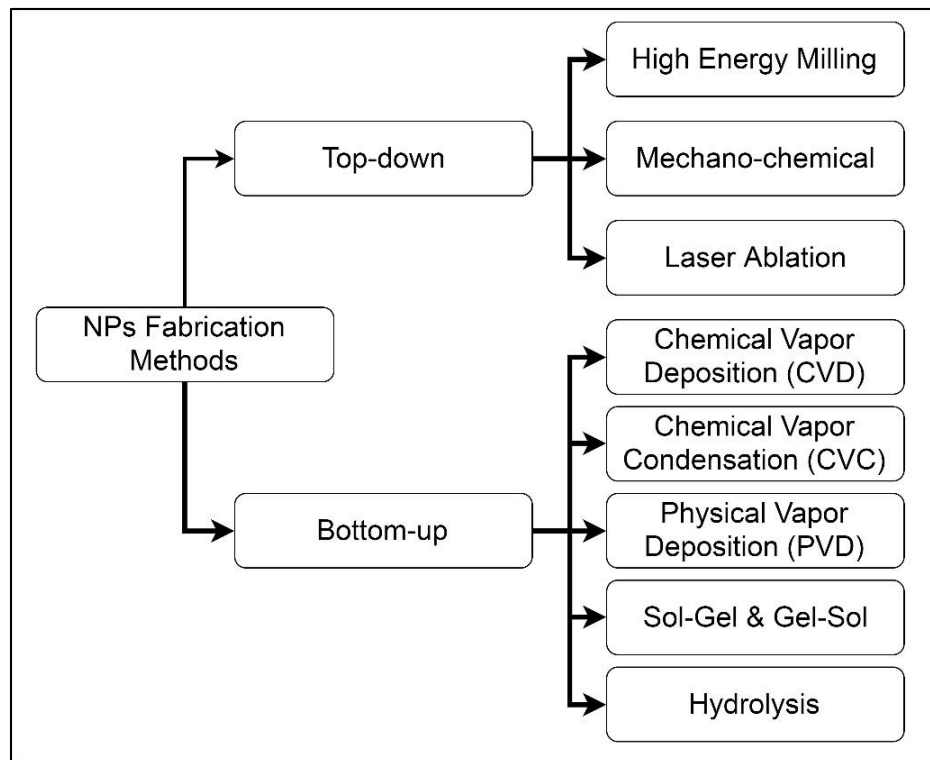


Figure 2.4 Nanoparticle fabrication methods (Modified from [36])

Top-down method

This process produces NPs by removing building blocks from the substrate to form smaller size particles. It simply means reducing the bulk particle size to produce smaller size (nanoscale) particles. The advantages of this process are the simplicity of the process, lower production cost, and scalability. The top-down method can be divided into three broad categories such as physical process (high energy milling), physical-chemical process (chemical-mechanical milling) and mechanical alloying [36, 40].

High energy milling

In 1970, Benjamin et al. [41] synthesized powder material for the first time by using the high energy milling principle. The high energy milling process involves applying physical forces to bulk solid material in order to break the material into smaller size [40]. The forces employed in this process mostly are the combination of impact and shear. The breakdown of solid material can occur by different mechanisms such as attrition, abrasion, fragmentation or chipping [42]. Mechanical milling has the ability to induce defects and activate the frozen state of NP which resulted in stable composition [43]. There are several types of mills that are commonly used such as vibratory mills and planetary mills.

Grinding process is affected by the size and frequency of the force, material properties (size and strength), the amount of energy applied in the system, and efficiency of the process [40]. Temperature also affects the grinding process due to the diffusivity and the concentration of defects in the powder that further influence phase transformation. Increasing temperature will lead to the formation of intermetallic compounds. On the other hand, a lower temperature will result in amorphous phases when energy is sufficient [43].

Chemical-mechanical milling

Basically, the concept of chemical-mechanical milling is combined the physical and chemical forces in order to improve the overall process [40]. During the milling process, chemical reactions occur at the nano-sized particle interface and continuously happens during the milling [44]. The chemical reactions can occur at low temperature without external heating process needed [45]. Lu et al. [46] synthesized nanocomposite of Mg, Al, and Ti by using mechanochemical process, and the resulting nanocomposite showed higher yield strength and ductility. Ding et al. [47] fabricated ultrafine Co and Ni NPs using mechanochemical principal. They succeeded in producing uniform sized NPs (10-20 nm) by chemical reduction of Co and NiCl₂ by grinding with Na. Sheibani et al. [48] reduced Cu₂O with graphite to produce nano-crystalline copper with an average size of 27 nm in high energy planetary ball mill. They found out that increasing milling time will increase the amount of fine Cu powder to an optimum point, after which agglomeration of the particle will dominate. By milling for about 30 hours, they could get Cu NPs with an average size of 27 nm.

Bottom-up method

During the bottom-up process, NPs are synthesized by adding the building blocks into the substrate. It means that by this approach NPs are synthesized by reacting each atom in the solution to form larger structures. During the process, the size of NP is controlled by regulating concentration, functionalizing the surface, and applying micelle for setting the growth [33]. It has various advantages compared to the top-down process such as better quality of the product (fewer defects NPs), higher homogenous chemical composition, and better stability. There are numerous processes involving the bottom-up principle.

Chemical Vapor Deposition

Chemical vapor deposition (CVD) is one of the bottom-up processes where a solid is deposited due to the reaction from the vapor phase [36]. There are several variations in the CVD process such as thermal, plasma and photo-laser. In thermal CVD, the reaction occurs at high temperatures above 900 °C. In plasma CVD, the reaction is activated by plasma at temperatures around 300 to 700 °C. While in photo-laser CVD, the reaction is initiated by ultraviolet radiation to break the chemical bond between the molecules and the deposition will occur at room temperature [36].

Chemical Vapor Condensation

Chemical vapor condensation (CVC) process was developed in Germany in 1994. This method involves pyrolysis of metal-organic-precursors' vapors in a reduced pressure [36]. The metal-organic-precursor vapors are led into the reactor by using mass flow controllers. The process can achieve above 20 gr/hour and can be improved by adjusting the reactor and mass flow of the input. This process has a limitation in size, morphology and phase control for the NPs product. However, CVC is widely used for fabricating silica NP from silicon tetrachloride.

Sol-gel

The sol-gel process is the well-known method to fabricate metal oxides NPs [36]. Compared to the chemical and physical deposition, the sol-gel technique is very cost-efficient. Sol is defined as a colloidal or a molecular suspension of solid particles in a solvent. While the gel is a semi-rigid mass of continuous network of particles and ions, taking shape when the solvent began to evaporate. This process involves a combination of metal precursors in solution and the deposition of the precursors. The deposition will occur on suitable substrate and heat condition, leading to the oxidation and sintering to the final product. Wang et al. [49] had successfully fabricated TiO₂ based NP with sol-gel technique. The sol-gel method is one versatile fabrication process that can be scaled up with further advances in the synthesizing technology.

2.4 Nanofluids: Preparation and Stability

Nanofluids are engineered fluids that disperse the nano-scale materials in the specific fluid [50]. The fluid can be polar (water or alcohol) and non-polar (oil or toluene) [38]. It means that a nanofluid is made of solid and liquids, in which NPs as solid are dispersed in the liquid called base fluid [31]. As NPs are dispersed into the base fluid, the characteristic of the nanofluids will not be similar to its pure base fluid. Nanofluids were proven to have higher thermal conductivity, diffusivity, viscosity and heat transfer than its pure base fluids that enable a wide range of application in many areas [50].

Due to the specific characteristics that can be engineered, nanofluid has wide potential applications such as mass and heat transfer [51, 52], friction reduction [53, 54], magnetic enhancement [51, 55], and many other uses [6, 7, 39]. It is also proposed for the petroleum industries application as drilling fluid enhancement [53, 56-59], exploration [14] and reservoir characterization [60, 61], refinery [18, 19] and EOR [20, 24, 30, 62-66]. Several nanofluids are proposed as the successor of the existing chemical EOR as nanofluids are relatively cheaper and possess tremendous potential for the future applications.

2.4.1 Preparation of Stable Nanofluids

Since NPs tend to aggregate to make bigger particle, preparing stable nanofluid is a challenging task [30]. When NPs are dispersed in a liquid, high surface energy of each nanoparticle tends to be stabilized by forming bigger particles (agglomerates). As seen in Figure 2.5, stable condition is achieved when the repulsion forces are relatively high. However, once the attraction force starts to overcome the repulsion, the particles will stick to each other. Particles dimers and trimers will form at the beginning, then as the aggregation and agglomeration occur continuously, sedimentation will likely follow. At some condition, unstable suspension or dispersion can be reversed and the process is known as peptization [67]. In general, nanofluid can be prepared by using two different methods, one-step and two-steps [50, 52].

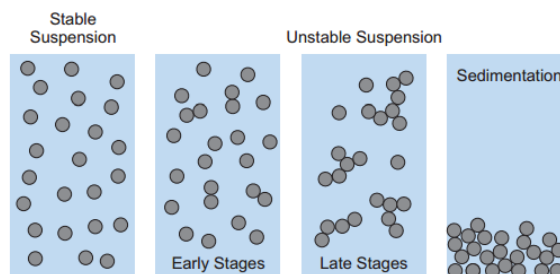


Figure 2.5 Stable and unstable suspension [67]

The two-step method is the most common process that has been used to prepare nanofluids. In this process, dry NP powders produced from mechanical or chemical synthesis are dispersed in a base fluid [50]. However, due to the high surface energy of NPs, agglomeration of some particles cannot be avoided which then reduce the homogeneity of the nanofluids [52]. Due to the quick agglomeration, several attempts can be done such as adding a surfactant to improve the dispersion could be carried out.

The stability could thus be improved, but limited to the high-temperature application. One of the advantages of this process is the economic feasibility for a larger scale production since the production of NP powders has been already induced in industrial scale [50].

One-step method is a process that simultaneously synthesizes nanoparticle and nanofluid [50]. The base fluid is formed at the same time as the NP synthesis. The processes such as drying, storing and transporting process associated with nano-powder fabrication are removed, minimizing the agglomeration and improving the fluid stability. By using one-step process, the uniformity of the dispersed particle and the stability became higher. However, this process has several disadvantages and limitations, e.g., limited to the small scale production, only applies to low vapor pressure host fluids, and produces the remaining residuals due to incomplete reaction or stabilization [52].

2.4.2 DLVO Theory in Particles Stability

Dispersed nanoparticles have a tendency to adhere and form aggregates that later led to the gravitational deposition [50]. This unstable condition is caused by the high surface to volume ratio of the NPs. High surface to volume ratio leads to the higher surface energy between each particle, making them faster to react and forming aggregates to stabilize [31]. Particles are stable in dispersion when they do not aggregate at a significant rate, which is determined by the collisions frequency and cohesion probability. Derjaguin, Landau, Verwey, and Overbeek (DLVO) developed the theory of colloidal suspension stability, or the so-called DLVO theory [68-70]. It describes the relation between two forces that acts between particles, whilst the free energy per unit area is the sum of the van der Waals attraction and double layer repulsion energy [67].

$$W = W_{vdW} + W_{dl}$$

Van der Waals forces are the result of the dipoles rotation or fluctuation between molecules and atoms, which always present in every particle interaction. The vdW interaction can be expressed as,

$$W_{vdW} = -\frac{A_h}{12\pi h^2}$$

where h is the distance between two particles and A_h is the Hamaker constant that defines the attraction strength between two particles in a medium with typical value 10^{-21} - 10^{-19} J. This attraction interaction may decrease due to increasing salt level in the dispersion [67].

On the contrary, double layer repulsion (also called electrostatic repulsion) is the counter force of the vdW forces that becomes significant when double layers begin to interact with two approaching particles [31]. The surface charge of the particles in the dispersion acts as double layer repulsion that can be expressed as,

$$W_{dl} = \frac{2\sigma_+\sigma_-}{\epsilon_o\epsilon\kappa} \exp(-\kappa h)$$

where σ_+ and σ_- are the surface charge density per unit area of both surface sides, ϵ_o is the vacuum permittivity, ϵ is water dielectric constant, κ is the inverse Debye length serving as a function of ionic strength.

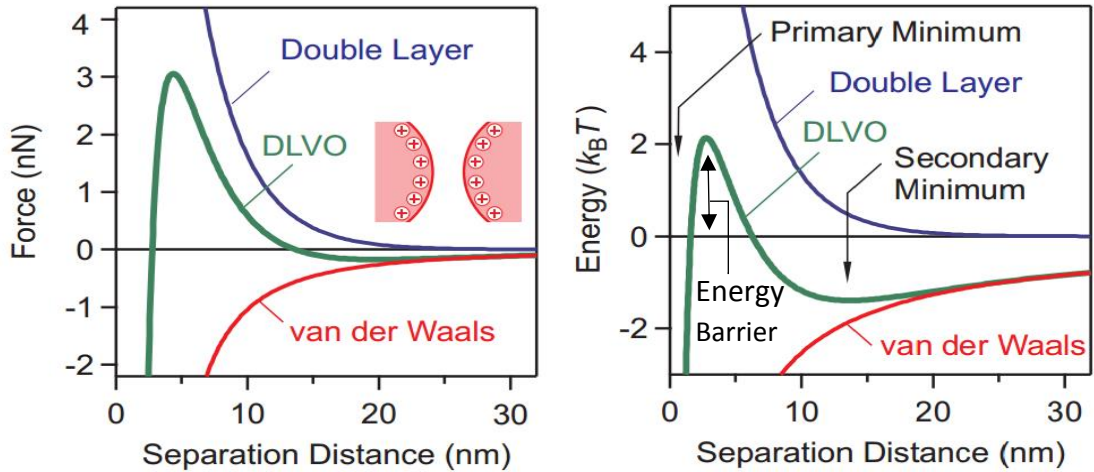


Figure 2.6 Interaction between two colloidal particles, DLVO theory (modified from [67])

Thus, the stability of the formation is determined by the sum of vdW attraction and double layer repulsion as shown in Figure 2.6. When the attractive force is higher than the repulsive force, it means the collision between particles will occur. Otherwise, if the repulsion is high enough, the dispersion will be stable. Therefore, in order to get stable dispersion, both particles need enough energy barrier which is commonly expressed as zeta potential. Higher zeta potential means more stable dispersion, while lower zeta potential will lead to the rapid coagulation of flocculation.

The most common method to enhance the stability of nanofluid is by adding stabilizer, mostly in chemical solution form, to reduce agglomeration [31]. The widely used stabilizers are surfactants and polymers. Cationic surfactants such as octadecyl amine (ODA), are proven to increase the stability of silver-based nanofluids [50]. However, the application of surfactant as a stabilizer is limited since it will degrade under high-temperature condition. Polymers are used as the alternatives to stabilize nanofluids. Polyethylene Glycol (PEG) is proven to be a good stabilizer for TiO₂ [71]. Adding polyvinylpyrrolidone (PVP) to AgNO₃ [72] and SiO₂ [31] based nanofluid have been demonstrated to prevent sedimentation for more than a month. By adding stabilizers, surface charges between particles went through an increase, leading higher energy barrier that could prevent agglomeration of smaller particles [31].

Chapter 3 Nanoparticle Application in Petroleum Industry

Nanoparticle could potentially revolutionize the petroleum industry for both upstream and downstream, including exploration, drilling, production, and EOR as well as refinery processes [17]. It provides a wide range of alternatives for technologies and material to be utilized in petroleum engineering. Nanoscale materials in various forms such as solid composite, complex fluids, and functional NP-fluid combinations are the key to the new technological advances [4]. Studies on nanotechnology related to petroleum industry have been growing rapidly in the past few years. Figure 3.1 presents the number of scientific journals published in this field, displaying high research activities even during the down time of petroleum industry [73].

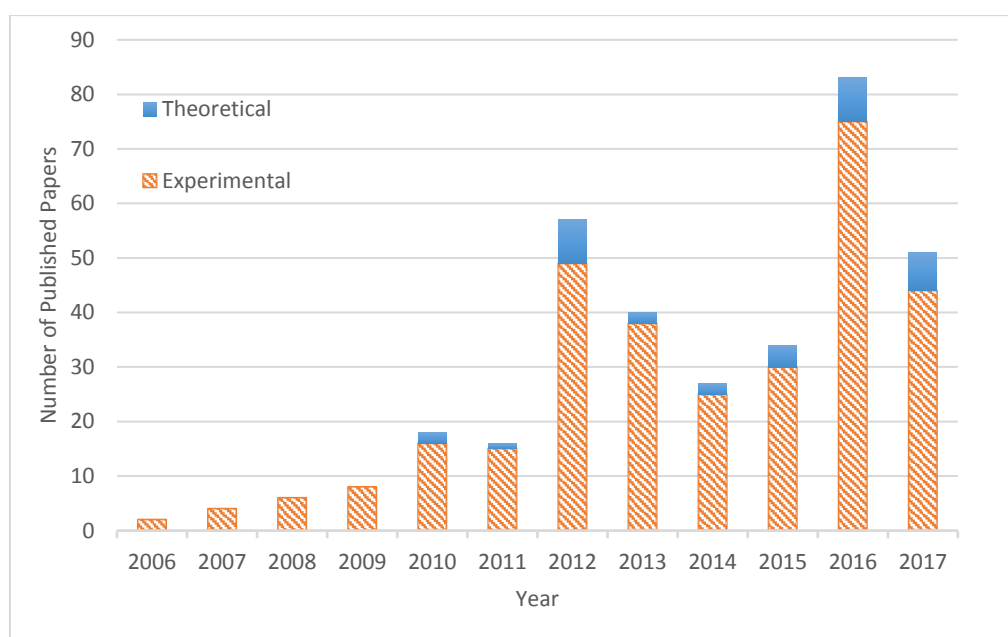


Figure 3.1 Nanotechnology in petroleum industry research (Taken until March 2017 and modified from [73])

Engineered nanoparticles have been studied in many potential applications in the petroleum industry, especially as nano-sensors in exploration [14], mud additive in drilling [56], emulsion stabilizer and wettability alteration in enhanced oil recovery (EOR) [16] and nano-catalyst in refinery process [19]. The summary of important studies related to the utilization of nanotechnology is presented in Table 3.1. The detailed summary of each area is elaborated in the next sub-section.

Nanoparticle Application in Petroleum Industry

Table 3.1 Summary of the literature studies

| Area | References | Nano Type | Purpose |
|--------------------------|---|--|---|
| Exploration | Song and Marcus (2007) | Hyperpolarized silicon NPs | Imaging sensors of oil in a hydrocarbon reserve |
| | Jahagirdar (2008) | Nano-optical fiber | Detecting oil-microbe, which able to estimate reservoir pressure and temperature |
| | Pratyush and Sumit (2010) | Nano-robots | Well logging and borehole measurement (patent) |
| | Li and Meyyappan (2011) | Coated carbon-nano structure | Real-time oil reservoir evaluation with two-dimensional detection technology |
| | Berlin et al. (2011) | Polyvinyl alcohol functionalized oxidized carbon black | Synthesizing engineered NPs for hydrocarbon detection in reservoir |
| | Al-Shehri et al. (2013) | Magnetic NP | Detect flood front, fluid contact, hydrocarbon bypass and fracture |
| | Rahmani et al. (2013) | Superparamagnetic NP | Crosswell magnetic sensor for tracking flood front |
| Drilling & Completion | Sharma et al. (2012), Hoelscher et al. (2012), Xu (2012), Cai et al. (2012) Chakraborty et al. (2012) | Silica NPs | Reduce or stop water invasion to shale by plugging shale pore |
| | Santra et al. (2012) | Nanodiamond | Improve drilling process in harsh and demanding environment |
| | Gurluk et al. (2013) | Silica & Alumina NPs | Cement accelerator |
| | Murtaza et al. (2016) | MgO and ZnO NPs | Improving thermal stability of drilling fluid |
| | Khan et al. (2016) | Nanoclay | Reduce permeability and porosity of cement and enhanced compressive strength |
| | Sun et al. (2017) | Carbon Nanotubes (CNT) | Improve compressive strength in HPHT |
| | | Cellulose nanofibers (CNF) & graphene nano-platelets (GNP) | Increased yield stresses, degree of hydration (DOH), flexural and compressive strengths |
| | | Pyroelectric NP | Additive for fracturing + viscoelastic surfactant to increase efficiency in fracturing |
| Stimulation & Production | Crews et al. (2008) | Ni-Fe NPs | Hydrate mitigation in the well |
| | Crews and Gomaa (2012) | ZnO NPs | Increase low shear rate viscosity on Threadlike micelle (TLM) fluids and more stable |
| | Fakoya and Shah (2013) | Silica NPs | Rheological studies on surfactant based and polymeric fluids |
| | Li et al. (2016) | Metal oxides based | Improves fracturing fluids stability and viscosity in height temperature (300 F). |
| | Hamed et al. (2010,2011) | Cu and Ni NPs | Thermal recovery by metallic NPs |
| | Suleimanov et al. (2011) | Non-ferrous NPS | Combine with surfactant for IFT reduction |
| EOR | Ju et al. (2006), Maghzi et al. (2013), Hendraningrat et al. (2013) | Silica NPs | Wettability alteration, improving oil recovery |
| | Saien et al. (2013) | Alumina NPs | IFT study of methylbenzene–water with alumina NPs |
| | Mensah et al. (2013) | Cu and Al based NPs | Emulsion stability effect study |
| | Espinosa et al. (2013) | Silica NPs | Generate very stable CO ₂ -in-water foam |
| | Moghadam and Azizian (2014) | ZnO NPs | IFT study on anionic surfactant liq-liq interface |
| | Ehtesabi et al. (2014) | TiO ₂ NPs | Heavy oil recovery in sandstone core |
| | Alomair et al. (2015) | Al, Ni, Si, and Ti based NPs | Recovery factor sensitivity study |
| Refinery | Mohajeri et al. (2009) | Nano-supported HDS | Patent on nano-supported hydrodesulphurization (HDS) catalyst |
| | Kong & Ohadi (2010) | Nano membranes | Gas stream separation |
| | Hansen et al. (2011) | MoS ₂ nano-catalyst | Observing atomic-scale edge structures of MoS ₂ |
| | Sotto et al. (2011) | TiO ₂ NPs | Improving water treatment by reducing fouling effect |
| | Mohammadi et al. (2011) | TiO ₂ , ZrO ₂ , and SiO ₂ NPs | Additive for stabilizing asphaltene in oil under acidic condition |
| | Ko et al. (2014) | Magnetic NPs | Accelerate oil removal in water-oil emulsion |
| | Patiño and Cortés (2016) | Nickel oxides and alumina NPs | Patent on Nanocatalyst for hydrocracking |

3.1 Exploration and Reservoir Characterization

Exploration is the initial phase of oil and gas field development. Recently, exploration of hydrocarbon began to be carried out in the more challenging area and involves high risk and investment. Therefore, it is necessary to develop methods which are technically and economically feasible to develop exploration technology. "Nano-sensors" has been proposed in seismic characterization, interpretation, formation evaluation of geochemical exploration [73]. When NPs are injected into the reservoir, some of them will pass through pores while some others will be adsorbed, which can help to give information on chemical and physical properties of the rock, 3D distribution of the formation, and the sensing mechanism for reservoir monitoring and surveillance [74]. The size of nano allowed them to pass through pore-throats unhindered. NPs can be engineered by changing the core and surface characteristics to adapt harsh environments. That will induce significant changes in optical, magnetic, and electrical properties of NPs, making them ideal candidates for sensors or imaging agents [75].

At Schlumberger presentation in 2007, Song and Marcus [14] introduced their idea of using hyperpolarized silicon NPs for nanosensors in oil and gas exploration. Hyperpolarized NPs were first tested with a good result in bio-medical engineering as alternative tracker particles for magnetic resonance imaging (MRI) [76, 77]. Later on, Jahagirdar [78] proposed the idea on the detection of oil-microbe, using the principle of Resonance Raman Spectroscopy (RRS) which employed nano-optical fiber in the reservoir. As microbes survive only in a certain condition, this method will indirectly measure the reservoir properties such as pressure, temperature, and salinity. In 2011, Berlin et al. [79] synthesized polyvinyl alcohol functionalized oxidized carbon black, which could be potentially used for hydrocarbon detection. Li and Meyyappan [61] were granted a patent on real time two dimensional analysis for oil reservoir evaluation, using engineered carbon-nano structure and surface sensors.

Magnetic NPs for detecting flood front and oil-water were studied, and the result showed the capability of travel-time tomography to detect magnetic NP in different media, which was a big step in the utilization of magnetic nanosensors [60]. Similarly, Rahmani et al. [55] successfully employed superparamagnetic NP for tracking floodfront using Crosswell magnetic sensing method. The most recent progress in the nanotechnology on oil and gas exploration is the utilization of reservoir nano-robot by Liu et al. [80]. They successfully tested as a nano detection device, which integrates reservoir sensor, micro-dynamic system, and micro-signal transmission. In the same year, a patent on the nano-robots system for well logging and measurement was granted to Pratyush and Sumit [81].

Those studies show that NP can be potentially utilized for reservoir characterization and hydrocarbon exploration. However, the problem that needs to be solved for nanosensor lies on protecting the sensor from degradation by fouling while at the same time getting the sensors to reach reservoir fluids [21].

3.2 Drilling and Completion

Nanotechnology for drilling and completion has been widely studied for the past few years, including drilling fluids, cementing additive and drilling tools. In 2010, Amanullah [53] projected that various NPs can be an answer for several drilling operation challenges such as, shallow water, unconsolidated formation, borehole instability, lost circulation, torque and drag, pipe sticking problem, gumbo and bit bailing, gas hydrate zone, acid gas, HPHT, and fracturing fluids.

Utilization of nanomaterials such as silica, graphene and other NPs have been suggested for drilling fluids additive [56]. Nano based mud is defined when at least one additive of mud using nanomaterial with a size range between 1-100 nm [53, 57]. The use of silica-NP in drilling mud were studied by several researchers [15, 54, 82, 83]. By using silica NPs, Sharma et al. [15] observed improvements in the stability of the mud at elevated pressures and temperatures at different rheology by reducing 10-100 times of shale invasion. Hoelscher et al. [54] performed experiments on Marcellus and Mancos shales with 3 wt.% of silica NPs as additives in the water based mud. The result showed that silica NPs could physically plug the shale and significantly reduce the fluid invasion to shale zone at the lower loading level in the water based mud. Cai et al. [82] also performed experimental tests with 10 wt.% of 6 types of silica NPs for Atoka shale. They found a drastic reduction in shale permeability impairment and observed that the mud had a higher plastic viscosity, lower yield point, and fluid loss reduction. Potassium silicate function on handling shale formation had also been investigated by McDonald [84]. Srivatsa and Ziaja [85] conducted an experimental study using the combination of biopolymer- surfactant and nanoparticle for mud additives. They concluded that nanoparticle combined with bio-polymer and surfactant could be a solution to solid free fluids in horizontal drilling.

Metallic and metal oxides based NPs for enhancing the properties of drilling fluids also had been investigated [86-88]. Contreras et al. [87] studied the effect of iron and calcium NPs, and Gurluk et al. [88] employed MgO and ZnO NPs for the study. Both results showed that adding NPs could improve the thermal stability of the drilling fluids and control the filtration loss to the reservoir [87, 88]. Recently, in 2016, Ho et al. [89] investigated the effect of graphene nano-sheet with the concentration range from 25 ppm to 100 ppm. The result showed that graphene in oil based fluid exhibit higher viscosity with shear rate ranges from 0-140 s⁻¹ and behaves like a Newtonian fluid while it is classified as a Bingham fluid.

Nanoparticles also exhibit many advantages for cement additives. Many types of NPs such as nano-clay [90], silica [91, 92], alumina [91], magnesium oxide [93], etc. had been formerly studied. Silica NP has proved to improve cement slurry stability, rheology and hydration degree by acting as both accelerator and mechanical properties enhancer [91, 92]. The nanoparticle can also improve flexibility, reducing permeability and compressive strength of the cement [90, 94]. Carbon nanotube (CNT) had been shown to significantly improve cement compressive strength at high pressure high temperature condition (HPHT) [95]. In 2017, Sun et al. [96] combined cellulose nanofibers (CNF) and graphene nano-platelets (GNP) for oil well cement additives.

They concluded that CNF/GNP addition to cement increased yield stresses and degree of hydration which enhanced both flexural and compressive strength of the cement.

Nanotechnology for drilling and completion can also be applied to the drilling tools by nano-modification. Drilling process can be improved by nano-ceramic coating for drilling bits which can enhance the lifespan of the drilling tools [97]. The other alternative is by using nano-diamond for improving drilling effectivity in the harsh and demanding environment [98].

There have been several patents on the nanotechnology related to drilling [99, 100] and cementing [101-103], and will likely increase as the rising demand for new technology on drilling and completion process. It can be suggested that nanotechnology will bring the future of drilling and completion technology into “Smart Fluid” era [17, 53].

3.3 Production and Stimulation

During hydrocarbon production, various problems can reduce the production efficiency. Nanoparticles have been proposed by Junwen et al. [104] as the alternative solution of liquid loading problem in deep gas well during the production process. They proved that engineered silica NPs with a temperature resistance up to 150 °C, salinity resistance about 250 g/L, and H₂S resistance up to 0.04%, could solve the liquid loading problem by creating stable gas-liquid foams. Silica NPs are also beneficial in preventing the wax development at pipe during oil and gas production. Recently, Sun et al. [105] discovered that modified nano-silica/EVA (ethylene vinyl acetate) could prevent the development of wax crystals and disperse it by heterogeneous nucleation. Similar as wax, oil-water emulsion also becomes a problem in the hydrocarbon treatment facility. Silica NPs were proposed by Gavrielatos et al. [19] as one of the methods to handle an emulsion problem. They stated that the increase in NPs' concentration would reduce the rate of separation. The smaller size of NPs is favorable for treating the emulsion problem since it has a larger surface area which more efficient. Other production problems such as hydrate formation could be solved by injecting self-heating Ni-Fe NPs to the hydrate area. Ni-Fe NPs were chosen because they have high nucleation latency period, strong temperature rising and ecofriendly characteristic [106].

Nanoparticle has been studied for improving hydraulic fracturing and acidizing job in the field in stimulation process. The first attempt on the application of NP in hydraulic fracturing was done by Baker Hughes [107] with nano-structured metal composite, mixed with alloys (magnesium and aluminum) that improve the strength at a lower weight and dissolve ability at the specific condition. Huang and Crews [108] introduced nanoparticle coated proppant which has the ability to maintain viscosity at high temperature, control fluid loss and reduce fines migration. Nanoparticles can pass through pore throat and can be flowed back easily with the producing fluid which can preserve reservoir permeability. Later, Crews et al. [109] reported the use of pyroelectric NPs combined with a viscoelastic surfactant (VES) to increase the fracturing efficiency and improving production rates. Differently, Barati et al. [107] applied polyelectrolyte complex NPs for cleaning up fracturing fluids by delaying the released enzyme which enables to prevent gel premature breaking and improve the

fracturing efficiency. Crews and Goma [110] found that ZnO NPs could raise the low shear rate viscosity of threadlike micelles fluids that exhibit similar behavior as crosslinked polymer system. Li et al. [111] conducted experimental studies on the effect of metal oxides NPs on fracturing fluids. The result showed that by adding NPs to the fracturing fluid, viscosity improved by 23-116 % at elevated temperature and the polymer loading efficiency was reduced.

Therefore, nanoparticles have a large potential for stimulation and solving production problems. There are several patents granted to the nanotechnology for hydraulic fracturing. Some of the examples are the nano-proppant for fracture conductivity by Ghahfarokhi [112], and high temperature fracturing fluids using nano crosslinkers by Al-Muntasheri [113].

3.4 Enhanced Oil Recovery

Due to the continuous increase in the world energy demand, technology for finding hydrocarbon source or for enhancing oil recovery needs to be developed [17]. The fact that finding a new source of hydrocarbon is difficult and most of the oil field have 60 to 70 % of non-producible hydrocarbon in place, drives the development of novel technologies in EOR [38]. There are various studies which had been done on the application of nanoparticle on EOR. The use of NPs suspension for EOR has several advantages [107] such as: good stability because surface force is more dominant than gravity; nanoparticle properties depend on size and shape which can be easily modified during the manufacturing process; chemical properties of NPs correlates to the surface coating, that can be simply tailored from hydrophilic to hydrophobic; 99.8% of silica NPs are silicon dioxide which is a dominant substance in sandstone and making it environmentally friendly; the price is much cheaper than any other chemical EOR.

In 2006, Ju and Fan [16] observed the mechanism of EOR utilizing lipophobic and hydrophilic polysilicon (LHP) on wettability alteration by experimental and numerical approaches. They concluded that LHP could be absorbed on rock grain, leading to wettability alteration. The similar mechanism had been proposed previously in 2003 by Wasan and Nicolov [114]. They observed the spreading and adhesion behavior of nanofluids mixed with surfactant on a solid surface, enabling further research on nanotechnology for EOR [114]. Onyekonwu and Ogolo [115, 116] performed core flood experiment using silica NP, and later on with different types of NPs. Ju and Fan [117] developed a numerical model on the retention of nanoparticle flow in porous media. Recently, Ahmadi and colleagues employed silica NP dispersed with surfactant fluid for carbonate core flood and resulted in 25% additional oil recovery [118-120].

Metal oxides NPs also potential to be applied in EOR. In 2011, Suleimanov et al. [121] found that the use of non-ferrous NP dispersed in anionic surfactant able to increase oil recovery up to 18%. Interfacial tension reduction due to nanoparticle was observed by Saien et al. [122] when hydrophilic and hydrophobic alumina NPs were applied on the toluene-water system. Esmaelizadeh [123, 124] reported the effect of ZrO₂ NPs on interfacial tension of surfactant for both air-water and *n*-heptane-water interfaces, while Moghadam and Azizian [125] studied interfacial tension of anionic

surfactant in the presence of ZnO NPs. They concluded that IFT of surfactant-oil could be reduced significantly and in general, dynamic IFT will reduce faster if ZnO NPs are added into the system.

The nanoparticle as novel foam and emulsion stabilization additive had been investigated in the past few years. Zhang et al. [107] observed that nanoparticle could stabilize an emulsion of oil-in-water or water-in-oil in the absence of surfactant. The emulsions with nanoparticles were stable up to 2 years and could stand in harsh condition. A further study had been done by Mensah et al. [126] on the emulsion stability effect by utilizing copper and aluminum based NP. They correlated the effect of NPs concentration and water density with the emulsion behavior. Differently, Espinosa et al. [24] concluded that silica NPs dispersion could also stabilize supercritical CO₂ foams in porous media with co-injection of liquid and supercritical CO₂.

Nanoparticle especially metallic based NPs had been projected as the solution for improving heavy oil recovery [127, 128]. Hamed et al. [129-132] observed the use of copper and nickel for improving heavy oil recovery by thermal method. Later, Ehtesabi et al. [133] reported that TiO₂ NPs could improve the heavy oil recovery up to 51%.

3.5 Refinery

The downstream industry is facing challenges such as the limitation on sulfur and CO₂ emission to the atmosphere, while on the other hand it has to increase the production to meet the fast growing energy demand [17]. Those challenges are reforming refinery industry into cost effective, energy efficient and technologically focused development [38]. Therefore, nanoparticle had been proposed in oil refining in order to address the challenges.

The concept of nano-catalyst for handling heavy oil production was proposed in 1997 by Ying and Sun [127]. Then, nano catalyst became more popular in the refinery industry since it has higher surface area to volume ratio than conventional catalyst. The approach in imaging MoS₂ nanocatalyst performed by Kisielowski et al. [134] led to further research on the substitution of conventional MoS₂ into MoS₂ NPs as a catalyst for industrial oil refining [135]. Furthermore, Mohajeri et al. [107] patented their invention of a nano-supported hydrodesulfurization (HDS) catalyst for treating sulfur content in hydrocarbon feedstock. Their patent included the preparation, the content and the utilization of the nanocatalyst. Recently, Patiño and Cortés [136] were granted a patent on their invention of nanocatalyst for hydrocracking. The nanocatalyst specifically consists of nickel oxides NPs supported on alumina NPs which are able to enhance the thermal catalytic cracking of heavy oil.

Nanoparticle is not only projected for nanocatalyst but also for fluid treatment, e.g., a nanoparticle-coated membrane for improving water treatment [137], inhibitors for avoiding asphaltene and precipitation [51, 138], and for improving the separation of the water-oil emulsion during the treatment [139]. Sotto et al. [137] studied the effect of NP aggregation for polyether-sulfone (PES)-TiO₂ that can potentially improve the treatment by reducing the fouling effect. Mohammadi et al. [138] reported that TiO₂,

ZrO₂, and SiO₂ NPs have potential use for stabilizing asphaltene particles via hydrogen bonding between NPs and asphaltene at the acidic condition. Similarly, Davidson et al. [51] applied the hyperthermia concept of magnetic induction heating for preventing wax deposition during production and refining. In addition, NPs can also be utilized for separating oil-water emulsion that can be a beneficial solution for the refinery industry. It had been studied that magnetic NPs [139] and silica NPs [19] can remove oil droplet from the emulsion significantly faster than conventional demulsifier.

Chapter 4 Experimental Studies of Nano-EOR

4.1 Introduction

This chapter covers laboratory experiment conducted on different nanoparticles for EOR purpose. Then, the mechanisms on how NP could improve oil recovery are briefly explained. The parameters affecting the performance of nanoparticle in increasing oil recovery are discussed at the end of this chapter.

4.2 Laboratory Experiments

Several laboratory experiments on nano-EOR had been done in the past few years. From Table 4.1, it can be seen that all experimental research with different NP types and condition indicated the improvement of oil recovery. Various types of NPs had been discovered such as fullerenes, graphene, carbon-nanotube, polymers, metallic and metal oxides [140]. However, only some of them have been tested for EOR application. Negin et al. [141] divided nanoparticle used for EOR into three main categories, metal oxides, organic and inorganic NPs. However, in this section, NPs are discussed with respect to two major categories which are inorganic and organic NP.

4.2.1 Inorganic Nanoparticles

The inorganic nanoparticle is categorized based on the components of particles which have no carbon in the molecular structure and non-biologic origin. Silica-based NP and other metal oxides NP are the most well-known inorganic NP widely used as EOR agent. Metal based NPs are aimed for wettability alteration, interfacial tension and viscosity control [141].

Silica-based nanoparticles

Silica-based NP is the most common material used in the experimental studies. Silica NPs are one of the most preferred for EOR application since they can be produced easily with well-known physical-chemical properties and can be engineered into different characteristics such as hydrophobic to hydrophilic [142]. Silica NPs are also one of the most abundant non-toxic inorganic material [31] and have lower production cost than other nanoparticles [143]. There are many types of engineered silica NPs that have been synthesized. Ju et al. [25] categorized polysilicon nanomaterial based on their wettability behavior into three types: lipophobic and hydrophilic polysilicon (LHP); hydrophobic and lipophilic polysilicon (HLP); and neutral-wet polysilicon (NWP). They also reported that polysilicon NPs could change the wettability of porous surface when adsorbed on its surface. In addition, silica NPs have good thermal stability when heated at 650°C, as observed using infrared spectrum, x-ray diffraction, and SEM analysis, suitable for high-temperature reservoirs [144].

Table 4.1 Experimental studies summary

| Reference | NP type | NP concentration | Max additional RF | Fluids | Porous Media |
|-----------------------------------|---|-----------------------------------|---------------------------------------|---------------------------|-----------------|
| Ju et al. (2006) | SiO ₂ | 0.02-0.03 wt.% | - | water | sandstone core |
| Haroun et al. (2012) | FeO, CuO, NiO | 5 wt.% | 14 % | water | carbonate core |
| Onyekonwu and Ogolo (2012) | Al ₂ O ₃ , Ni ₂ O ₃ , MgO, Fe ₂ O ₃ , ZnO, ZrO ₂ , SnO, SiO ₂ | 0.3 wt.% | 12% (Al ₂ O ₃) | ethanol brine & water | sandstone core |
| Shahrabadi et al. (2012) | HLP & LHP SiO ₂ | 0.1-0.4 wt.% | 19.31% | ethanol | sandstone core |
| Maghzi et al. (2013) | SiO ₂ | 0.1 wt.% | 10 % | polyacrylamide | glass bed |
| Hendraningrat et al. (2013) | LHP SiO ₂ | 0.01- 0.1 wt.% | 10 % | brine (NaCl 3 wt.%) | berea sandstone |
| Ehtesabi et al. (2014) | TiO ₂ | 0.01 and 1 wt.% | 51 % | brine (NaCl 0.5 wt.%) | sandstone core |
| Joonaki and Ghanaatian (2014) | Fe ₂ O ₃ , Al ₂ O ₃ , SiO ₂ -silane | 0.05; 0.1; 0.15; 0.2 and 0.3 wt.% | 22.5% | propanol | sand pack |
| Hendraningrat and Torsæter (2014) | Al ₂ O ₃ TiO ₂ , SiO ₂ | 0.05 wt.% | 7-11% | brine (NaCl 3 wt.%) | sandstone core |
| Moradi et al. (2015) | SiO ₂ | 0.1 wt.% | 20 % | water | carbonate core |
| Sharma et al. (2015) | SiO ₂ | 1 wt.% | 21 % | surfactant and polymer | berea sandstone |
| El-Diasty (2015) | SiO ₂ | 0.01; 0.5 and 3 wt.% | 29 % | water | sandstone core |
| Cheraghian (2015) | Nanoclay | 0.9 wt.% | 5.8% | water | sandstone core |
| Nazari Moghaddam et al. (2015) | ZrO ₂ , TiO ₂ , MgO, Al ₂ O ₃ , CeO ₂ , CNT, CaCO ₃ , SiO ₂ | 5 wt. % | 8-9% | brine (3, 8, 10, 12 wt.%) | sandstone core |
| Cheraghian (2016) | TiO ₂ | 1.9; 2.1; 2.3; and 2.5 wt.% | 4 % | polymer and water | sandstone core |
| Ahmadi et al. (2016) | SiO ₂ | 5 wt% | 25 % | water and surfactant | carbonate core |
| Alnarabiji (2016) | MWCNT | 0.01; 0.05 and 0.10 wt% | 31.8% | MWCNT fluid | glass bed |
| Jafarnezhad et al. (2017) | SnO ₂ | 0.1 wt% | 22 % | brine | carbonate core |
| Towler et al. (2017) | Complex nanofluid | 1 wt% | 16%-21% | water, brine, surfactant | Tensleep core |

Ju et al. [16] continued their research by conducting experimental and theoretical studies on the utilization of hydrophilic silica NPs (LHP) for EOR. By injecting 2.0-3.0 % of LHP NPs, they concluded that NP could be adsorbed onto pore walls, which then change the wettability and obviously improve the oil recovery. Onyekonwu and Ogolo [116] did a further study on LHP, HLP and NWP silica NPs dispersed in different fluids (water, ethanol, and alcohol). During core flooding experiments, they observed that NWP and HLP silica NPs dispersed in ethanol not only change the wettability of water-wet core plug, but also behave as surfactant by reducing the interfacial tension between oil and water. Shahrabadi et al. [145] studies HLP silica NPs by using three scenarios of injection (1) nanofluid were injected after waterflood process, (2) sequenced injection of water and nanofluid, (3) HLP nanofluid injection since the beginning. They observed that by injecting nanofluid at the beginning, the highest ultimate oil recovery (93.65%) was achieved. Hendraningrat et al. [146] studied the effect of LHP silica NPs by implementing coreflood experiment on Berea sandstone core with various NPs concentration from 0.01 up to 0.1 wt.% dispersed in brine (NaCl 3.0 wt.%). They showed that the contact angle decreases when the concentration of NPs increases, but higher concentration tends to block the pore throat of the low-permeability Berea core sample.

Differently, Maghzi et al. [147] dispersed silica NP into polymer (polyacrylamide) solution to study the rheology of polyacrylamide solution when silica NPs are present in the mixture, observed in glass micromodel. By applying 0.1 wt. % of silica NP into the mixture, the pseudo-plasticity of the polymer solution was improved at low shear rate and overall viscosity of the mixture is increased, which lead to an additional oil recovery up to 10%. Sharma et al. [148] studied the utilization of silica NPs dispersed in polymer and surfactant mixture for chemical EOR. They found out that silica NPs could lower and stabilize the interfacial tension for Pickering emulsion, which leads to 21% additional recovery compared to conventional surfactant-polymer flood. Sharma et al. [149, 150] continued similar research, focusing on the interfacial properties and wettability alteration of NPs with and without surfactant. The conventional polymer and surfactant-polymer flood efficiency reduced when the temperature increases. Differently, the nanofluids mixture had stable behavior at higher temperatures which could be a potential solution of high-temperature chemical EOR.

Silica NP is not only proposed for water flooding and chemical flooding, but also for CO₂ flooding and water-alternating-gas flooding. Several problems such as viscous fingering, channeling, and poor sweep efficiency are experienced during conventional CO₂ flooding [151], and formation of CO₂-in-water foam is proposed to handle those problems [152]. AttarHamed et al. [153] investigated the effect of hydrophobic silica NP in CO₂-water foam by varying the size and concentration of NPs. They demonstrated that in a low concentration of NPs, bigger NPs size was favored for foam stability, while in high concentration smaller NPs size was preferred. Even though the size and concentration of NP influence the foam stability, the hydrophobic characteristic of silica NPs is the most important parameter on stability. Moradi et al. [154] conducted an experimental study on the application of silica NPs for water-alternating-gas injection. The coreflood result showed that by implementing silica NPs on water, 20% additional oil recovery was achieved. Recently, Kim et al. [155] performed an experimental study on CO₂-in-brine and decane-in-brine foam by using

silica NPs. They were able to synthesize stable foam with the smaller size of silica NPs since smaller size could be adsorbed easily at the CO₂-brine interface.

Jafarnezhad et al. [156] observed the impact of silica NPs in heavy oil recovery on carbonate rock. They found that heavy oil recovery could be improved by 39 to 61% after injecting silica NP dispersed in brine with concentration no more than 0.5 wt. %. Similarly, Magda et al. [157] were able to achieve 13.28% additional recovery on sandstone core with the optimum concentration at 0.1 wt.%. Moreover, the utilization of silica NP is considered to be the most economical and environmentally friendly, even though the risk of dried silica NPs should be assessed since it could be dangerous for the human when directly inhaled [30].

Aluminum oxides

Aluminum oxides (Al₂O₃), or alumina can be fabricated by several processes such as flame spray pyrolysis [158], modified plasma arch [159], mechanochemical [160] and several other ways. For EOR purpose, Ogolo and Onyekonwu [66] studied several metal oxides NPs (Al₂O₃, MgO, Fe₂O₃, Ni₂O₃, SnO, ZnO, and ZrO₂) by using coreflood experiment with sandstone core plugs. They concluded that the Al₂O₃ NPs with an average size of 40 nm and surface area 60 m²/g dispersed in water and brine gave the highest additional oil recovery (12.5%) than other metal oxides NPs. Giraldo et al. [161] focused their study on the wettability alteration by alumina based NPs. By using concentrations of alumina NPs varying from 0.01 to 1.00 wt.% dispersed in anionic surfactant, they observed that alumina NP and a surfactant solution could alter the wettability of rock from strong oil-wet surface to strong water-wet surface, as proved by the change of residual water saturation S_{wr} from 0.07 to 0.23 (Figure 4.1). Their hypothesis is that the Al₂O₃ NPs were able to be adsorbed onto the rock surface with a coating mechanism.

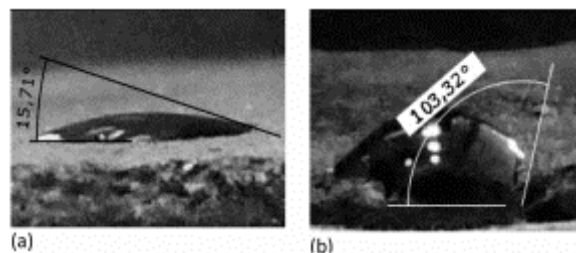


Figure 4.1 Oil-air contact angle on rock surface before (a) and after (b) treatment with 100 ppm alumina nanofluid [161]

Zaid et al. [162] investigated the effect of Al₂O₃ and ZnO dispersed in an aqueous surfactant (sodium dodecyl sulfate). Using two different kinds of Al₂O₃ (sol-gel and commercial product), they could achieve up to 53.5% ROIP. Interestingly, commercial Al₂O₃-RM achieved 63% more oil than Al₂O₃-SG (sol-gel) even though, the sol-gel alumina has lower IFT and smaller size. It proves that lower IFT does not always give higher recovery since other factors such as sweep efficiency and fluid rheology are also important.

Hendraningrat and Torsæter [20, 30] studied the potential of aluminum, titanium and silicon oxides NPs in two-phase coreflooding process on Berea core plug.

The dispersant of polyvinylpyrrolidone (PVP) was added to stabilize the nanofluid since the natural tendency of NPs to aggregate into a bigger molecule. Coreflood experiment results showed that the additional oil recovery was higher for other metal oxides NPs than silica NPs (especially in water-wet system) since other metal oxides are adsorbed into the pore surface easier than silica [20]. Even though the result showed that titanium oxides had better result in reducing the contact angle (up to 54°) between oil-water and rock, aluminum oxides still proved to be a good candidate for EOR. Similar experiment using both silica, alumina and iron oxides diluted in propanol solution proved that alumina has better result in oil displacement than iron oxides with almost similar effect as silica NPs [163]. Moreover, Alomair et al. [133] indicated that mixed alumina and silica NPs at 0.05 wt. % concentration resulted in the highest recoverable oil. They believed that the combination of alumina and silica NPs would be the best solution for EOR since it can handle the harsh reservoir condition (high temperature, salinity, and pressure) while also capable of controlling asphaltene precipitation.

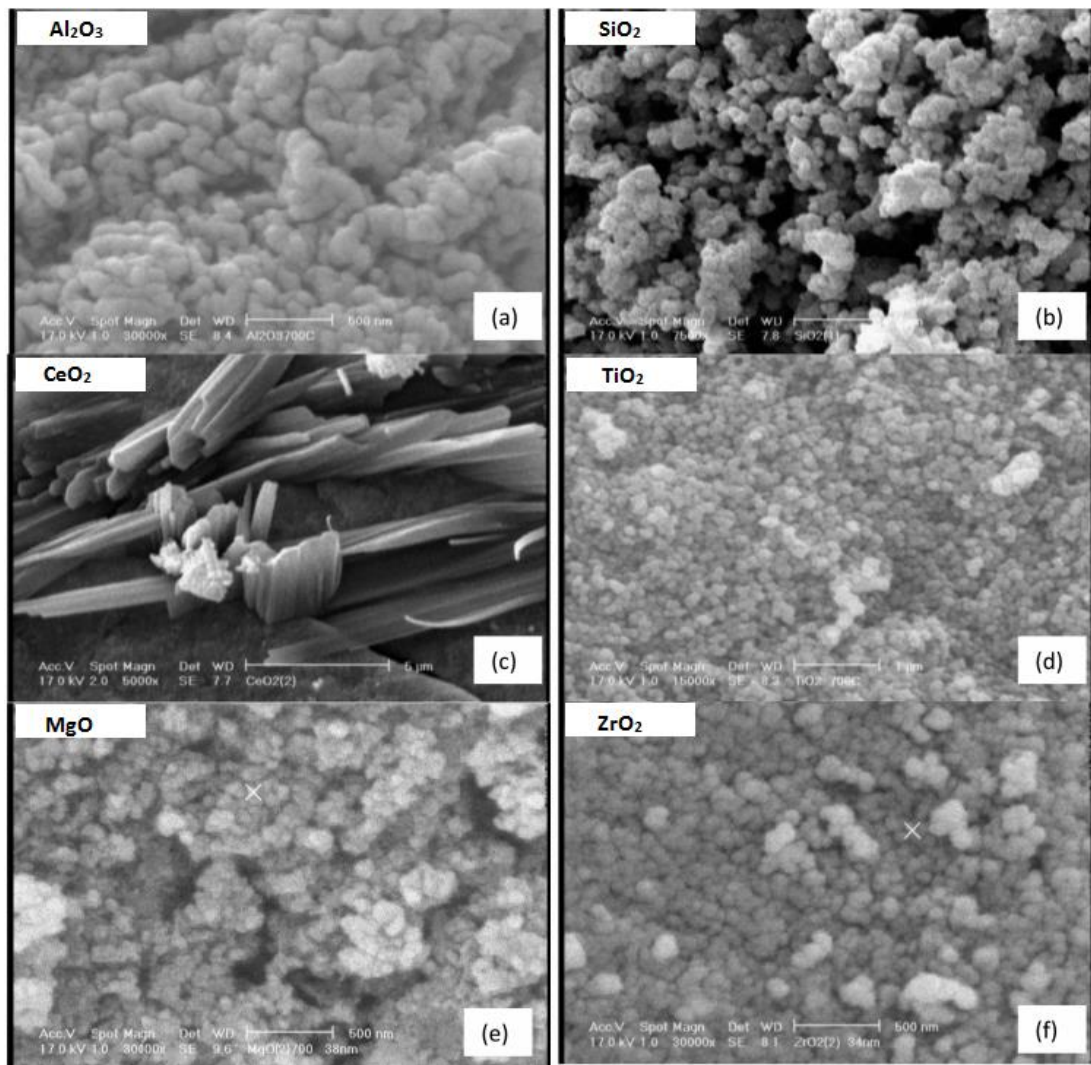


Figure 4.2 SEM image of different nanofluids (a) Al_2O_3 , (b) SiO_2 , (c) CeO_2 , (d) TiO_2 , (e) MgO and (f) ZrO_2 [164]

Iron oxide

With unique magnetic and electrical properties, iron oxides ($\text{Fe}_2\text{O}_3/\text{Fe}_3\text{O}_4$) NP is proposed by many researchers as sensor tracker (nano sensor) [141]. However, there is only a few research on the potential use of iron oxides for EOR. Haroun et al. [165] studied several metal oxide NPs such as Fe_2O_3 , CuO , and NiO on carbonate core plugs. The result on the iron oxides NPs was not so promising since it could only reach 57% ultimate recovery while other NPs can achieve up to 85%. However, others have shown that iron oxides were able to increase the recovery up to 24% (additional) when they are dispersed in water. Iron oxide has the possibility to increase the viscosity of the displacing fluid which also improves of sweep efficiency [66]. Joonaki et al. [163] reported that iron oxides were only able to recover 17% extra oil while other NPs i.e., Al_2O_3 and SiO_2 recovered around 20% additional oil.

Ferrofluids (Fe_3O_4) were proposed for magnetic heavy oil recovery by Shekhawat et al. [166]. Magnetic recovery is done by having an *in-situ* injection of magnetic NPs and pushing the NPs towards the reservoir using magnetic downhole tools. Then, inward magnetic forces are applied towards the borehole to recover magnetic NPs that already soaked with oil. Iron oxides NPs is shown to stabilize CO_2 foam which can improve sweep efficiency during the CO_2 injection process.

It seems that iron oxides NPs are not the best candidate for EOR. However, they still give a decent performance on recovery and viscosity enhancement.

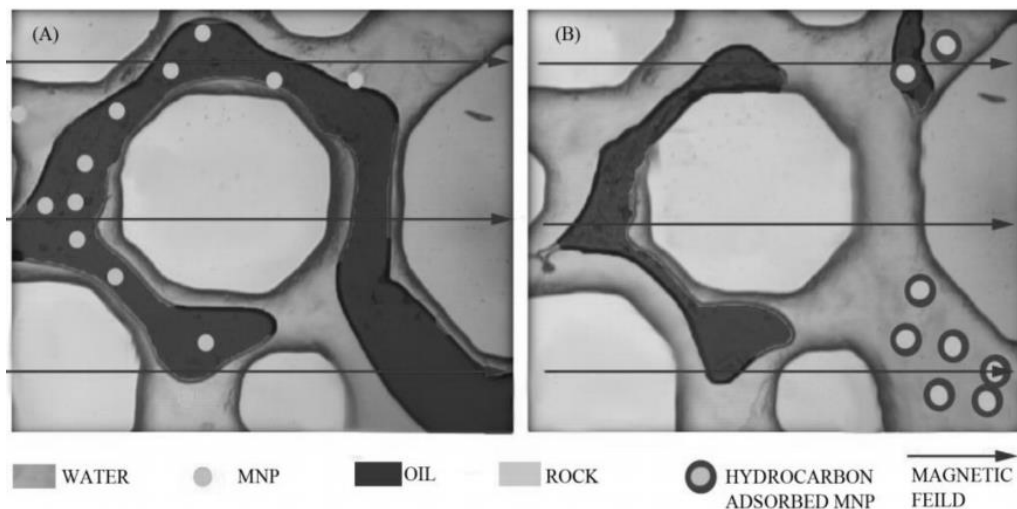


Figure 4.3 Oil recovery mechanism by magnetic nanoparticle (MNP) [166]

Nickel oxide

Nickel oxides ($\text{NiO}/\text{Ni}_2\text{O}_3$) as one of hydrophilic metal oxides has potential use for EOR [66, 167]. Ogolo et al. [107] found out that nickel oxides NPs dissolved in diesel and brine had positive result towards the improvement of oil recovery due to wettability alteration of the rock surface and viscosity enhancement of the brine. Nwidae et al. [168] studied the effect of NiO and ZrO_2 NP with fractured limestone core samples. They concluded that even though ZrO_2 gave the best result, NiO has potential use as EOR agent since it is able to reduce the water contact angle with increasing

concentration, injection time and salinity. Therefore, it has been shown NiO is not the best compared to other metal oxides (Al_2O_3 and ZrO_2) for EOR, but it still gave a positive improvement in recovery with its ability to alter wettability and enhance viscosity.

Titanium oxide

The potential use of titanium oxides NPs for EOR has been proposed by several researchers. Ehtesabi et al. [169] employed TiO_2 NPs in water for enhancing oil recovery in sandstone core plug. They discovered that TiO_2 NPs could improve recovery from 49% to 80% by altering the wettability due to uniform adsorption, as proved by SEM study. Similar experiments with lower concentrations of TiO_2 (0.01 and 0.05 wt %) [64] showed that TiO_2 was not significantly affecting viscosity and interfacial tension, but will change the wettability from oil-wet to water-wet. Hendraningrat and Torsæter [30] studied the effect of Al_2O_3 and TiO_2 on Berea sandstone. They showed that combined TiO_2 NPs with PVP as dispersant yield highest recovery compared with Al_2O_3 , SiO_2 , brine-only and dispersant-only. They concluded that TiO_2 NPs is the most effective nanoparticle for EOR compared to the other metal oxides NPs with wettability alteration as the dominant mechanism [20].

The possibility of combining TiO_2 NP with surfactants or polymer in chemical EOR had been investigated. Cheraghian [170] proved that oil recovery was increased by 4.85% when using 2.2 wt. % TiO_2 in surfactant compared with only surfactant. Similarly, by combining polymer with 2.3 wt.% TiO_2 , the recovery of oil was improved by 3.9% than conventional polymer flooding due to the viscosity improvement of the displacing fluid [171]. Moreover, Sedaghat et al. [107] observed the effect of TiO_2 on polymer-surfactant flooding which showed positive recovery improvement than conventional polymer-surfactant flooding.

Zinc oxide

Zinc oxides (ZnO) has been widely studied for wettability change in EOR in the past few years. Ogolo and Onyekonwu [107] showed that zinc oxides dispersed in brine and water caused permeability reduction due to the agglomeration of ZnO into larger particles, which blocked the pore throat of the core. Differently, Zaid et al. [162] proved that ZnO could be a good candidate for EOR agent. They found out that ZnO has better performance in oil recovery than Al_2O_3 (72% ROIP for ZnO vs. 53% for Al_2O_3) with lower IFT value. They also concluded that larger particle size of ZnO gives higher recovery for about 145% higher than smaller sizes. Similarly, Tajmiri et al. [172] investigated oil recovery by 0.2 wt.% ZnO NPs over heavy oil saturated sandstone and carbonate core samples. Improvement of oil recovery with both carbonate (8.89% of OOIP) and sandstone (up to 20.68% OOIP) core plugs was achieved. ZnO NP was able to reduce the heavy oil viscosity and alter the grain surface wettability.

Latiff et al. [173] proposed to use ZnO combined with non-invasive electromagnetic (EM) transmission. They investigated the effect of ZnO particle dispersed in water, on the oil recovery from glass micromodel saturated with heavy oil

(viscosity 12.31 cP). They successfully recovered 26% remaining oil by 30 minutes EM exposure with a simultaneous nanofluid injection.

Adil et al. [174] studied the stability of zinc oxides NP dispersed in water. By using different anionic surfactants as the stabilizer with various NPs concentration, they concluded 0.1 wt. % ZnO stabilized with 0.025 wt. % sodium dodecyl benzenesulfonate (SDBS) has the highest stability at 95°C with viscosity enhancement up to 11%. The combination of surfactant, pH and ultrasonication for ZnO nanofluid preparation to adjust their mobility properties were suggested.

Zirconium oxide

Zirconium oxide / zirconia (ZrO_2) NPs is widely used in catalysis, ceramics, thermal coating, etc. [141]. In EOR, zirconia is proposed as wettability alteration agent. Karimi et al. [175] studied zirconia as wettability alteration agent for carbonate core sample. They prepared zirconia using the sol-gel method, calcined at 800°C, and then dispersed in nonionic surfactant. It showed that ZrO_2 NPs could change the wettability of carbonate core from strong oil-wet to strong water-wet. The adsorption of NPs onto carbonate surface were confirmed by SEM studies. However, they noted that wettability alteration by zirconia (adsorption and growth) was a slow process taking 2 days. Recently, Nwideo et al. [168] investigated the wettability alteration on carbonate core samples by zirconia NPs injection. Water contact angle decreased with increased concentration, salinity and exposure times. Combining zirconia NPs and a surfactant could achieve better result in wettability alteration for carbonate rock [176], because cationic surfactant can form ion pairs to the cationic head and the acidic component of the crude, while NPs will develop continuous wedge film around the liquid-solid surface. Moreover, interfacial tension between two fluids can be considerably reduced by ZrO_2 [123], and higher adsorption energy is needed for oil-water interface than the air-water interface.

4.2.2 Organic Nanoparticles

Polymer and polymer-coated

Polymers are mainly used as stabilizer or coating to improve the stability of the nanofluids [30]. Nanoparticles with at least contain one polymer as a component are considered as polymer NPs (PNP) [177]. PNP can be fabricated from pre-formed polymers or direct polymerization of monomers. Several processes such as solvent evaporation, salting-out and dialysis, are used for preparing PNP from pre-formed polymers. It can also be directly fabricated by polymerization of monomers by implementing various methods such as mini-emulsion, micro-emulsion, surfactant free emulsion and interfacial polymerization [178]. PNPs are suggested to improve the mobility control and wettability alteration during EOR process [179].

Several types of research on using nano-size polymers for EOR purpose had been done to improve the injection efficiency and reduce the injection cost [17]. Wang et al. [180] conducted an experimental study on the effect of polyacrylamide (PAM)

microgel nanospheres on the recovery improvement. By using PAM nanospheres, they were able to recover 20% additional heavy oil recovery. PAM nanospheres could enhance the viscosity of the nanofluid and improve the sweep efficiency of the EOR [180].

However, more research needs to be done for PNP since only a few literatures were available on the potential of polymer and polymer-coated NPs as EOR agents.

Carbon nanotube

Carbon Nanotube (CNT) is cylindrical-shaped carbon structure within nano-size range, which was discovered by Iijima in 1991 [36] and classified as fullerene type [141]. Two most common CNT that have been used in various research are single-walled carbon nanotube (SWCNT) and multi-walled carbon nanotube (MWCNT) (Figure 4.4) [141]. There is only few research conducted on carbon nanotubes for EOR since this type of material is relatively new [141] and not yet economical to be applied in the field scale. However, CNTs possess unique structural, electronic properties [181] and hydrophobic nature [182], which can be potentially used in EOR.

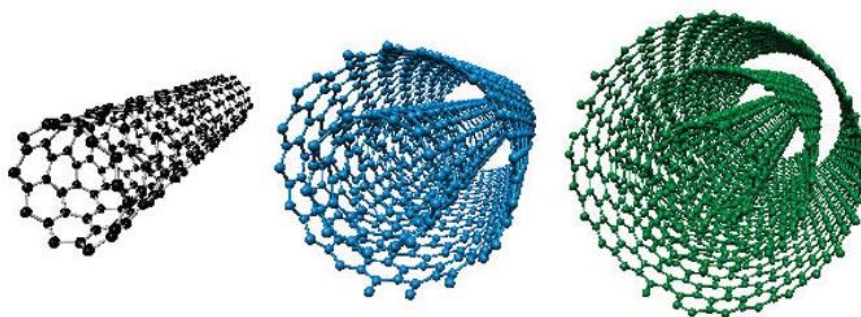


Figure 4.4 Single-walled carbon nanotube (SWCNT) (left), double & triple walled carbon nanotube (MWCNT) (mid and right) [183]

Shen and Resasco [181] investigated the stability of water-oil emulsion in the presence of CNT/silica nanohybrids NPs. Stability of the w/o emulsion increased when SWCNT-silica nanohybrids were added into the mixture. The emulsion could handle coalescence and sedimentation, and can be separated easily by filtration or centrifugation process. Similarly, Villamizar et al. [184] did a core flooding experiment by flooding SWCNT-silica nanohybrids solution into glass bed with crushed Berea sand. They found out that more energy was needed for injecting the emulsion into the sand packs, but the nanoparticle could effectively improve the recovery by the interfacial active catalytic reaction. Kadhum et al. [185] employed MWCNT which flowed into Berea core plug and sand packs. The result showed improvement in dispersion stability and propagation at high temperature and salinity conditions. The NPs retention was dependent on oil saturation, with more than 80% NP found in the effluent. Alnarabiji et al. [186] reported MWCNT resulted in 31.8% additional remaining oil in place (ROIP) for heavy crude oil recovery. AfzaliTabar et al. [62] did a comparative study on the performance of MWCNT, SWCNT and activated carbon for Pickering emulsion application in chemical EOR. The emulsions were formulated at pH 7 with distilled water. By using MWCNT, the Pickering emulsion exhibit the

highest stability at 0.1% and 1% salinity, moderate temperature (25°C to 90°C), and it successfully alters the wettability of oil-wet carbonate rock into water-wet.

4.3 Mechanism

As shown in the previous section, different nanoparticle types have been demonstrated that they could improve hydrocarbon recovery in EOR process. However, the detailed mechanism on how nanoparticle could increase the oil recovery is not clearly understood yet. Several mechanisms for the recovery improvement are proposed, such as interfacial tension reduction, wettability alteration, viscosity control, disjoining pressure, pore channel plugging and emulsification.

Those mechanisms take place because adsorption, desorption and transport of NP occur inside the pore throat [16]. Furthermore, since the size of NP is very small (1-100 nm) compared to the grain and pore throat size, five types of energy will be responsible for their interaction with the pore surface, (1) London-van der Waals attractive potential energy, (2) electric double layer repulsion energy, (3) Born repulsion, (4) acid-base interaction and (5) hydrodynamic energy [187]. Adsorption occurs when the attractive force is larger than the repulsion force while desorption will happen otherwise. In addition, the transport of NPs inside pore throat is driven by diffusion and convection. Blocking occurs due to agglomeration of NPs into bigger sizes larger than pore throat [16]. Thus, in order to understand deeply about the improved oil recovery mechanism between nanoparticle and reservoir we will elaborate each mechanism in the next sections.

4.3.1 Wettability Alteration

Wettability is defined as the tendency of a certain fluid to spread on the solid surface in the presence of other immiscible fluid in the same system [63]. It is directly related to the fluid-fluid and fluid-solid interaction which involves interfacial energy [73]. In general, wettability is rock properties which depend on the type of the minerals, pore distribution and surface area, and is also the function of fluid composition and temperature [63]. Wettability is usually measured in the laboratory by using the contact angle method, the Amott test and ore displacement test [188]. The Young equation is commonly used to distinguish the wettability type of the system by adopting the contact angle methods.

$$\cos \theta = \frac{\sigma_{sw} - \sigma_{so}}{\sigma_{wo}} \quad (4.1)$$

Where σ_{sw} is the solid-water interfacial tension, σ_{so} is the solid-oil interfacial tension and σ_{wo} is the water-oil interfacial tension. This equation is valid under equilibrium conditions with assumption on smooth, homogenous, rigid, and nonreactive surface [73]. Based on the contact angle, wettability of rock in oil-water system can be classified into three main types, i.e., water-wet ($\theta < 90^\circ$), neutral-wet ($\theta = 90^\circ$) and oil-wet ($\theta > 90^\circ$) [38]. This is illustrated in Figure 4.5.

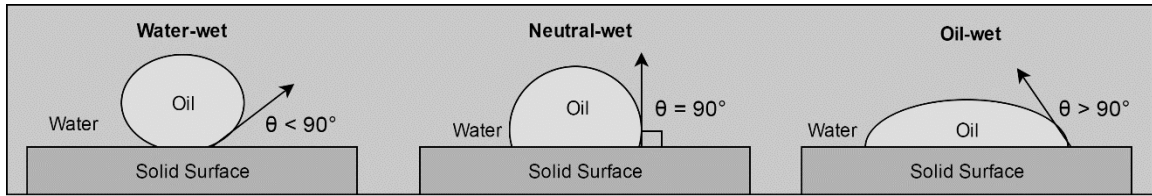


Figure 4.5 Wettability variation on oil-water system

Several studies concluded that wettability is an important factor for achieving highest oil recovery and understanding the multiphase flow during the hydrocarbon accumulation until production [189, 190]. Since wettability is significantly affecting capillary pressure and relative permeability, the oil flow inside the porous media can be improved considerably [73]. It also leads the spontaneous imbibition of water which helps to push the hydrocarbon out of the matrix blocks during water flooding [161]. Surfactant flooding is the well-known method for altering wettability. However, the efficiency of surfactant in the field scale is not so economical [191]. Thus, many researchers proposed nanoparticle to be used in EOR fluid as alternatives of wettability alteration agents.

Surfactant and nanoparticle have similarity in the mechanism of wettability alteration [161]. Hammond and Unsal [192] proposed two most possible mechanisms, the adsorption on the solid surface (coating mechanism) and removal of the absorbed molecule from the rock surface (cleaning mechanism). The adsorption process of NPs on the grain surface resulted in the formation of composite nanostructure-surface which improves the water-wetting behavior [175]. The SEM images in Figure 4.6 shows the adsorption of silica NPs on the calcite surface which forms a layer of the nanostructure with some agglomerated particles after 1 hour nanofluid treatment [193]. The surface modification by nanoparticles also increases the roughness of the surface as can be seen in Figure 4.6 [193]. Karimi et al. [175] added that the main factors on the wettability alteration are the area fractions of the nanostructure, partition coefficient and surface roughness.

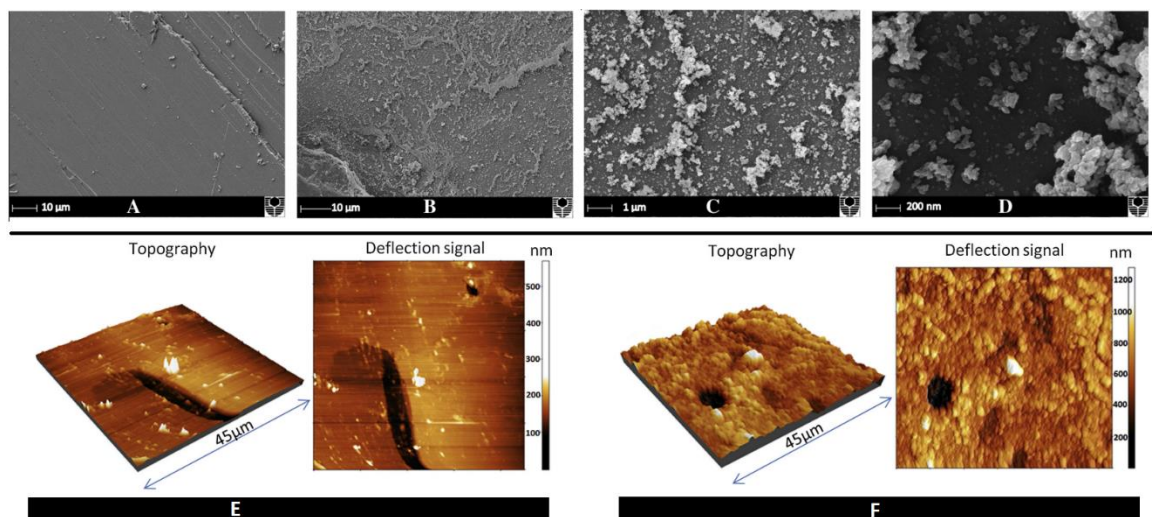


Figure 4.6 SEM and atomic force microscopy image of calcite surface. (A) Calcite surface before; (B) Calcite surface after nanofluid treatment; (C) High resolution ; (D) Max resolution; Topography picture before (E) and after (F) nanofluid treatment [193].

Furthermore, Hendraningrat et al. [28] investigated the effect of LHP silica NPs on the wettability alteration on the polished-synthetic-silica surface in different concentration. As shown in Figure 4.7, increasing concentration of NPs will reduce the contact angle of crude oil and change the wettability towards more water-wet. They stated that smaller size of NPs tends to decrease the contact angle more than bigger size particles, due to the higher electrostatic repulsion on smaller sizes [194]. Moreover, wettability alteration is the function of salinity, ionic composition, initial wettability, a solid system and the exposure time [29]. The potential of silica based NPs on wettability alteration in both carbonate [195] and sandstone rock [38] have been revealed. Moreover, Maghzi et al. [147] verified that silica NPs improved recovery significantly by wettability alteration mechanism for heavy oil systems. Similarly, several metal oxides such as aluminum oxides, titanium oxides, zirconium oxides and nickel oxides were proven as wettability alteration agent.

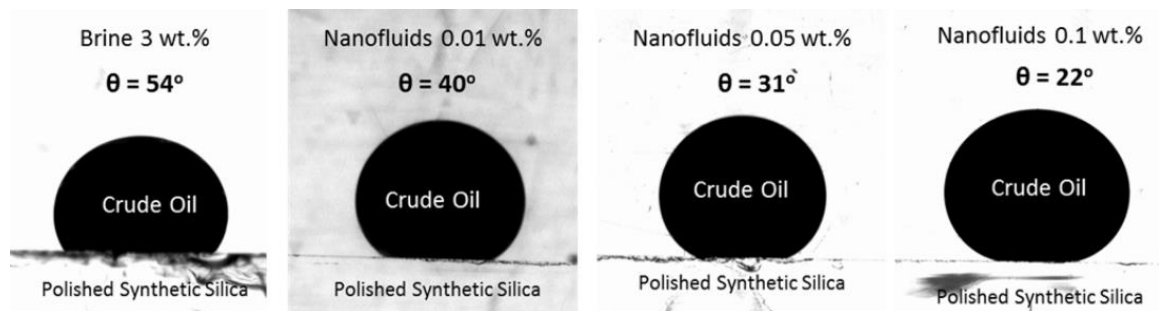


Figure 4.7 Contact angle variation of oil-brine system in different concentration [146]

4.3.2 Interfacial Tension Reduction

Capillary force is one of the most essential forces in reservoir system which restricts the oil recovery [196]. The value of capillary force is determined by interfacial tension (IFT) between the reservoir fluids and rock wettability [197]. By reducing the interfacial tension and alter the rock wettability, the capillary pressure will be reduced. It will lead to the improvement in the oil recovery [198]. In chemical EOR process, reducing the interfacial tension through surfactant is one of the important mechanisms for mobilizing the residual oil [196]. Nanoparticles are proposed to assist in decreasing IFT during EOR processes with or without surfactant. The presence of nanoparticle in surfactant mixture can improve the rheology of the solution and enhance the surfactant effect on IFT reduction [199]. Adsorption of NPs onto the surface of the fluid will effectively reduce the interfacial tension between those fluids [121].

Interfacial tension is usually measured with the pendant drop method [121] and the spinning drop method [38]. The ability of silica NPs in reducing the interfacial tension has been proved by several studies. Roustaie et al. [200] reported that NWP and HLP silica NPs were able to reduce the oil-water IFT from 26.3 mN/m to 2.55 mN/m and 1.75 mN/m (respectively). Hendraningrat et al. [28] added, that the magnitude of IFT reduction is directly related to nanoparticle concentration, with higher concentration favorable for lower IFT.

Table 4.2 Measured interfacial tension data of certain nanofluid [123]

| Fluids | <i>n</i> -Heptane–fluid interfacial tension (mN/m) | Air–fluid surface tension (mN/m) |
|---------------------------|--|----------------------------------|
| Water | 51.4 | 72.1 |
| 10 mg/l ZrO ₂ | 37.2 | 71.8 |
| 100 mg/l ZrO ₂ | 37.2 | 71.3 |
| 500 mg/l ZrO ₂ | 36.4 | 71.1 |
| 1 g/l ZrO ₂ | 36.8 | 71.2 |

Zirconium oxides mixed in a surfactant solution had been proven to reduce the IFT of heptane-fluid and air-fluid significantly, as shown in Table 4.2 [123]. Similarly, Moghadam [125] found out that zinc oxides could improve the efficiency of sodium dodecyl sulfate (SDS) surfactant in reducing IFT. The pH of the fluid had a significant effect on IFT with acidic and neutral pH favored. In addition, alumina NPs dispersed in brine were able to reduce brine-oil IFT from 19.2 mN/m to 12.8 mN/m, while silica based NPs are only able to reduce to 15.7 mN/m [20]. Moreover, carbon nanotubes (CNT) were also proven to reduce interfacial tension significantly (Figure 4.8), demonstrating a good potential for EOR agent [62].

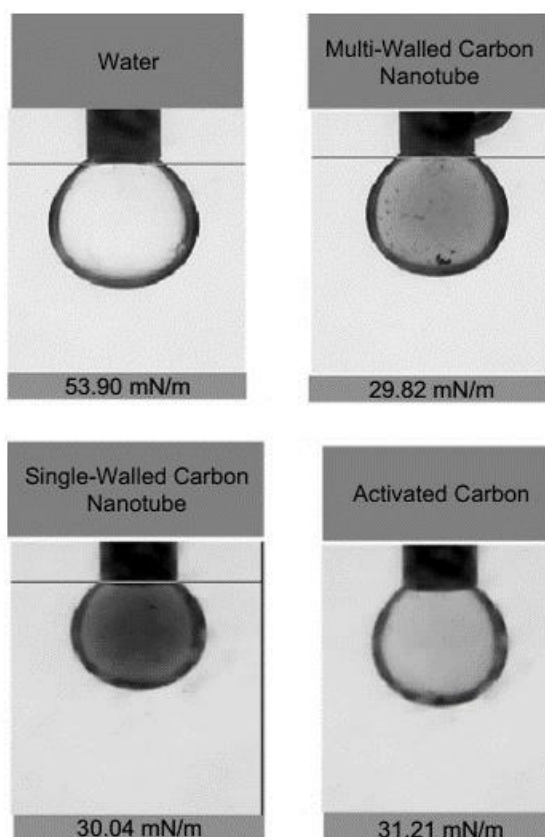


Figure 4.8 The effect of carbon nanotube and activated carbon on the interfacial tension [62]

4.3.3 Disjoining Pressure

The disjoining pressure mechanism is a novel concept to explain the effect of nanoparticle interaction with the reservoir surface to improve oil recovery. The theory of disjoining pressure itself is quite mature and has been widely studied [201, 202]. Disjoining pressure (Π_d) is defined as the attractive and repulsive forces between two thin layer of fluid surfaces [203]. Chengara et al. [204] defined disjoining pressure in the thin liquid film as the excess pressure in the film relative to that in the bulk solution. Therefore, nanofluid were considered to significantly affect disjoining pressure between two immiscible fluids.

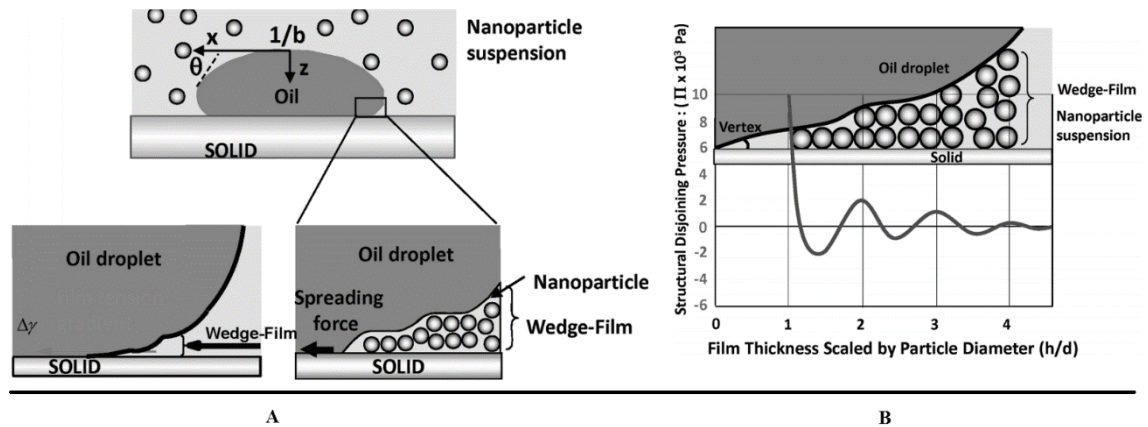


Figure 4.9 Nanoparticle wedge shape structuring and the forces (A), Wedge contact pressure (B) [205]

The spreading and adhesion behavior of nanofluid on a solid surface is quite complex. It is different from simple liquid behavior, since three-phase contact region does exist [114]. In three phase regions, nanoparticle dispersed in the liquid tend to develop wedge-shaped structures and forces towards oil-solid contact area (Figure 4.9 A). Those ordered structures in wedge film are enhancing the spreading and wetting strength of nanofluid on the solid surface [206]. The force created by a single particle is relatively small, however, the total forces of the massive number of NPs can reach up to 5×10^4 Pa at vertex region (Figure 4.9 B) [38]. The mechanisms that drive this phenomenon are Brownian motion and electrostatic repulsion. In short, the disjoining force is responsible for the detachment of oil from the solid surface while allowing the nanofluid to spread further.

Disjoining pressure is affected by several parameters such as, the nanoparticle size, concentration, charge density, temperature, salinity, and the surface characteristic [207]. Kondiparty et al. [205] concluded that higher concentration and smaller size of nanoparticle would lead to the increasing disjoining pressure. Moreover, the force at wedge film will increase when smaller sizes of nanoparticle with higher charge density and electrostatic repulsion are used [38]. However, a polydispersity of the nanoparticles needs to be considered since it could significantly affect the magnitude of the disjoining pressure [208].

4.3.4 Viscosity Control

During the EOR process high mobility of displacing fluid often results in viscous fingering which leads to poor sweep efficiency and conformance [188]. Thus, it is necessary to control the mobility of the injected fluid to achieve better sweep efficiency for higher oil recovery. The mobility ratio of the displacing fluid and reservoir fluid is the function of permeability and viscosity, and can be expressed as [209]:

$$M = \frac{k_{rinj}\mu_o}{k_{ro}\mu_{inj}} \quad (4.2)$$

Which M is the mobility ratio; k_{rinj} and k_{ro} are relative permeability of injection fluid and oil; μ_{inj} and μ_o are the viscosities of both injected fluid and oil. Polymer flooding has been successfully used as a viscosity control agent for increasing sweep efficiency [210, 211]. However, in the reservoir with harsh condition (high temperature, pressure, salinity, etc.), polymer solution is often degraded. The degradation will reduce its viscosity and sweep efficiency [212, 213]. Therefore, nanoparticle has been proposed to enhance the viscosity of the polymers in the injection fluid, since it improves the thermal stability of the polymer solution and prevents the degradation.

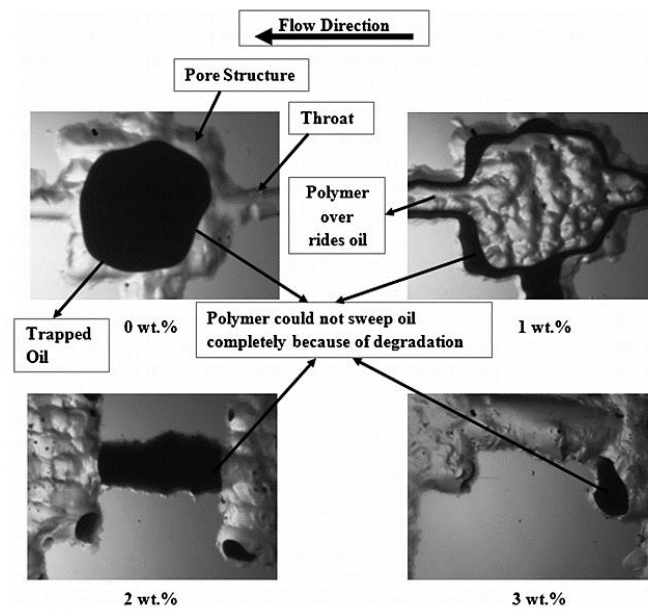


Figure 4.10 Glass micromodel picture of the oil displacement process with nano-polymer solution at different NPs concentrations [214]

Thickening of the solution occurs due to the ability of NP to form a network structure via hydrogen bonding [215], which will directly affect the fluid shear stress [216]. Zeyghami et al. [215] showed that viscosity enhancement by silica NPs in water solution is relatively low due to the high polarity of water. However, in the polymer solution, NPs seem to be able to enhance pseudoplasticity behavior considerably even in low shear rate [58, 214]. Moreover, they prevent premature degradation of the polymer in high salinity condition by preventing polymer to interact with ions, and NPs will substitute the polymer for attracting cation [214].

Maghzi et al. [214] investigated the effect of dispersion of silica NP on polymer flooding in different fluid salinity. As shown in Figure 4.10, by adding silica NP in the

polymer solution, degradation can be reduced significantly. The trapped oil can be mobilized efficiently by increasing the concentration. A comparison of different injection fluids (Figure 4.11) showed that silica nanoparticle-polymer-flood (NPF) has the highest oil recovery compared to water flood and conventional polymer flood [217]. Highest recovery was achieved due to the improvement on the fluid viscosity for about 35 cP while the conventional polymer only yields 8 cP.

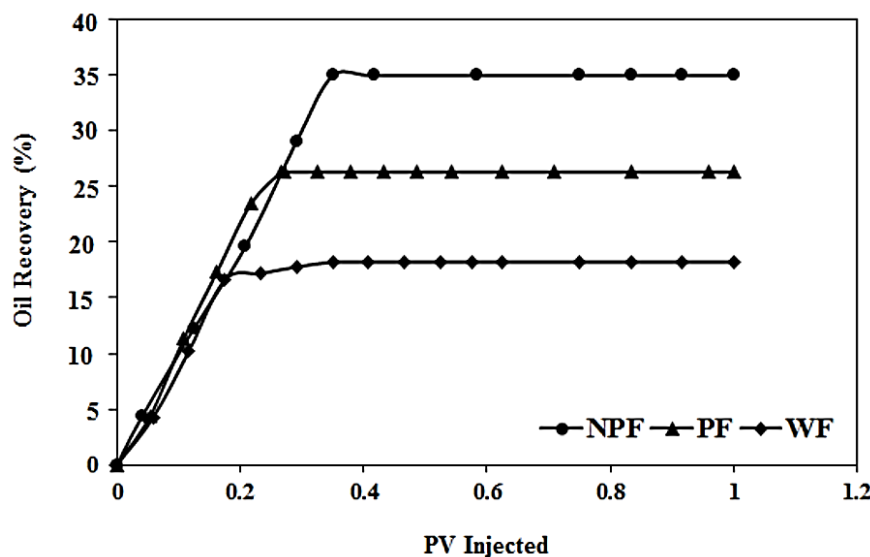


Figure 4.11 Recovery comparison between Nanoparticle-Polymer-Flood (NPF), Polymer Flood (PF) and Water Flood (WF) [217]

Nanoclay was also investigated for its viscosity and sweep efficiency improvement potential [218]. Nanoclay was proven to significantly increase the viscosity of the nanoclay-polymer solution and improve the stability of the mixture at high temperature and salinity. Cheraghian et al. [219], reported 5-6% higher recovery rate by adding nanoclay in the polymer solution. Moreover, several metal oxides such as TiO_2 [170] and FeO [220] have also been shown to improve sweep efficiency during EOR.

4.4 The Effect of Nanoparticle Parameters

4.4.1 Nanoparticle size

The size of NPs and its associated charge density have a significant effect the disjoining pressure strength. McElfresh et al. [207] concluded that smaller particles would result in higher charge density and the stronger electrostatic repulsion, assuming the particle is in stable condition. According to Hendraningrat et al. [221], smaller particles are proven to increase the recovery considerably as can be seen in Figure 4.12. The result shows that not only oil recovery but also displacement efficiency is increasing due to the smaller size of NPs. Similarly, several other experiments concluded that smaller particles would lead to the higher ultimate oil recovery [188, 222]. Another study proved that by decreased NPs' diameter from 30 nm to 18.5 nm, the structural disjoining pressure would increase for about 4.3 times [205].

Experimental Studies of Nano-EOR

For a similar mass, smaller NPs will give higher particle density and lower contact angle between fluid and rock surface. Higher particle density improves the structural disjoining pressure significantly [205]. For less hydrophilic surface, smaller NPs will spread more readily than a bigger particle. The size of the particle should be small enough not to be mechanically trapped, but big enough to avoid extra log-jamming [223]. Therefore, smaller particles are favorable for the higher oil recovery [31].

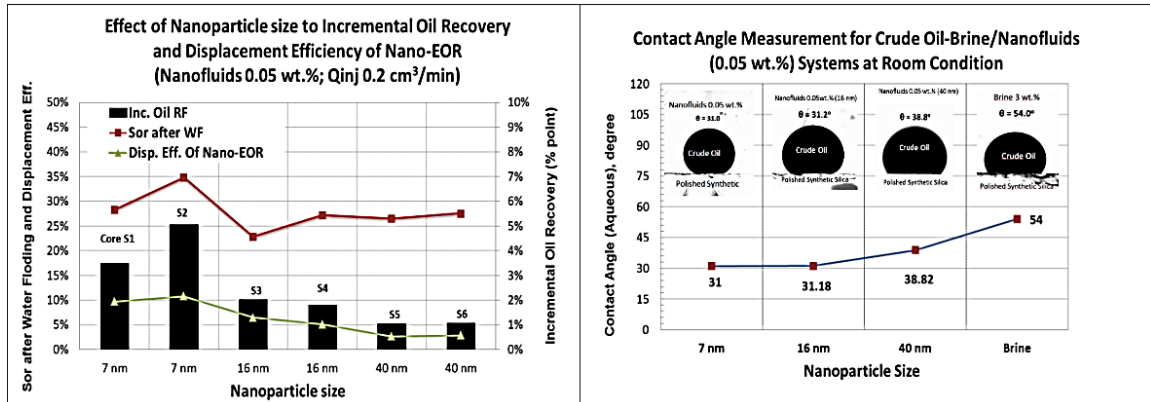


Figure 4.12 The effect of nanoparticle size [221]

4.4.2 Nanoparticle concentration

The concentration of injected NPs is one of the key parameters that determine EOR process. According to Chengara [204], disjoining pressure and Brownian motion will increase with increasing concentration which also increases the repulsion forces. Increasing concentration will also improve the displacement efficiency due to the viscosity enhancement of the nanofluid and the spreading of NPs on the grain surface [223]. The effect of concentration on the displacement efficiency and IFT can be seen in Figure 4.13. The interfacial tension between reservoir fluids was reported to significantly decrease by increasing concentration of injected NPs [28]. High concentration also leads to the higher wettability alteration effect. Based on the facts above, a higher concentration is favorable for higher oil recovery.

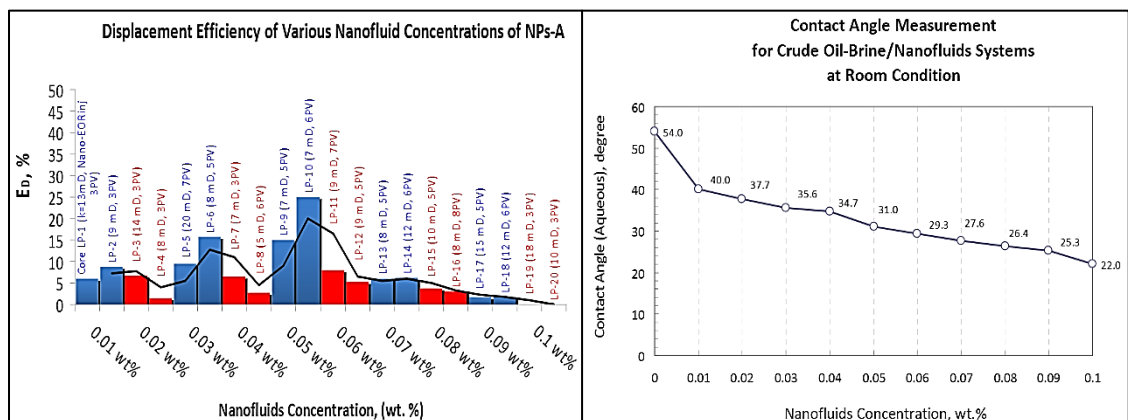


Figure 4.13 Concentration Effect on nano-EOR [216]

However, there is a certain limit on the concentration of injected NPs, since above that limit NPs will tend to block the pore throat and reduce the ultimate oil recovery. Hendraningrat et al. [28] reported the permeability and porosity impairment of Berea core for about 2% after injecting 0.5 wt.% of silica NPs. A higher concentration will improve the displacement efficiency, the wettability alteration and the IFT reduction. However, when the concentration is too high, the aggregated NPs were found to accumulate around the inlet and reduce the displacement efficiency [31].

Therefore, an optimum injected concentration is necessary to get maximum oil recovery. It is varied based on the type of nanoparticle, porous medium and the environmental condition.

4.4.3 Salinity

The salinity of the reservoir fluid and the nanofluids have a significant effect on the stability of the dispersion. Increasing salinity is proven to reduce the zeta potential of each particle which leads to easy agglomeration [207]. High ionic strength in the fluid due to the presence of salt will lead to the lower electrical repulsion between particles and allows the vdW attraction forces to dominate. As most of the rock surface are charged, it is expected that the attraction and collision will happen for particle-particle but not particle-surface [224]. Thus, in high salinity environment modification on nanoparticle is necessary to maintain the stability which can be achieved by surface modification, ionic control via surfactant, or the combination of both [223].

However, the result of a laboratory study had shown that the oil recovery increases at high salinity environment. By using high stability silica NPs, Hendraningrat et al. [31] proved that high salinity nanofluid injection could improve the wettability alteration to be more water-wet. At high salinity, the adsorption of NPs is improved due to the increasing physicochemical interaction [225]. Similarly, Kanj et al. [226] concluded from their research that increasing salinity on the dispersion did not hinder the NPs transport, but increased the adsorption on the grain surface. Increasing salinity seems to increase the adsorption of NPs and improve the recovery of the oil. However, at the same time, the stability of NPs will reduce in the high salinity environment. Therefore, the correct salinity level and surface coating are important aspects to be considered to prevent agglomeration of NPs.

4.4.4 Temperature

Since the temperature of the reservoir is always higher than the temperature at the surface, nanofluid should be able to operate at relatively high temperature for effective nano-EOR application [223]. According to Caldelas [227], the temperature has an insignificant effect on the nanoparticle retention due to the weak temperature dependence for adsorption and desorption of nanoparticle. Differently, a set of experiments by Hendraningrat et al. [221] showed that temperature significantly influences the oil recovery as can be seen in Figure 4.13. The higher temperature is favored for higher oil recovery than lower temperature. The higher temperature condition could possibly alter the reservoir fluids at the molecular level, which reduces the contact angle between the fluids.

However, the mechanism of the temperature effect is complex and difficult to explain since it involves several variables. One of the reasons is increasing the temperature tends to decrease the zeta potential of the particles. This means decreasing the stability of the nanofluid and will likely reduce the oil recovery [207]. The increment on recovery could probably be ascribed to decreasing IFT at high temperature since it weakens molecular interaction or to the increasing Brownian motion and a reduction in viscosity [221]. Since changing temperature will affect both nanofluids and the reservoir system, the effect of temperature on the recovery cannot be generalized. Therefore, further study on the temperature effect should be done to get a better understanding of the nano-EOR mechanism.

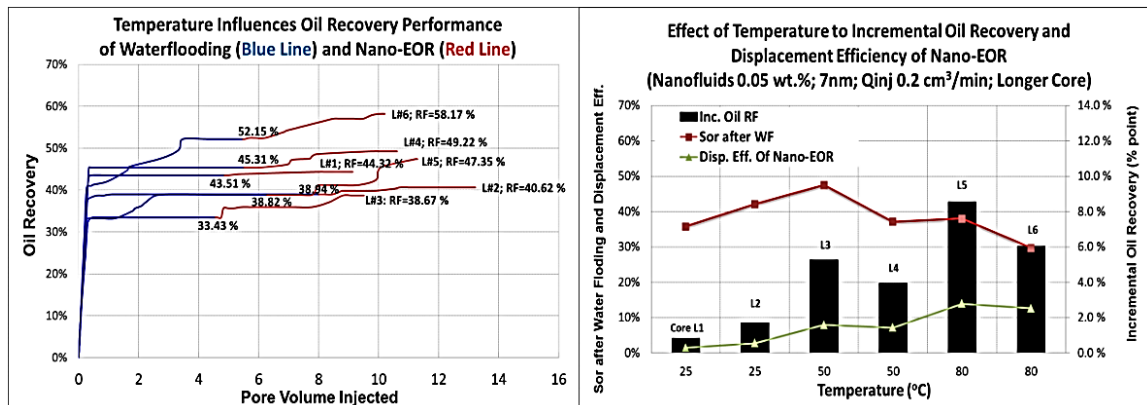


Figure 4.14 Temperature effect [221]

4.4.5 Wettability

It has been reported that increasing water wetness of the rock will increase oil recovery [228] and vice versa [189]. According to Morrow [189], strong water wetness and associated high capillary imbibition are favorable for more efficient oil displacement. However, at special cases, it had been reported that oil-wet reservoir [229] and neutral wettability [230] were proven to give higher oil recovery. Thus, wettability is playing an important role in the hydrocarbon mobility. It affects distribution and displacement process of hydrocarbon and other reservoir fluids within the matrix [22].

During nano-EOR, initial wettability will determine the magnitude of the wettability alteration. An experimental study using silica NPs showed that the highest incremental oil recovery was yielded from intermediate-wet core [221]. In intermediate-wet, oil and brine are in the equal state which reduce the possibility of the disconnected and trapped oil phase in the matrix [221]. Li [38] added that wettability affects the adsorption quantity of NPs. Water-wet and neutral-wet have higher adsorption than oil-wet media. In an oil-wet medium, the adsorption area is very close to the desorption area, which means that desorption will likely to happen.

Chapter 5 Simulation of Nanoparticle Transport

5.1 Introduction

In chapter 4, experimental studies related to the NPs for EOR have been reviewed. Extensive experimental studies have been done in the past few years to reveal the potential of NPs for EOR in the petroleum industry. In this chapter, numerical studies related to nanoparticle flow in porous media are reviewed, with considerations on particle deposition or the reaction term. Afterward, we used the most plausible model to simulate the particle transport to obtain a clear understanding of the process. We first presented the results of the visualization model, and then the transport process without and with reaction terms. Several models that have been developed for nanoparticle transport were studied. Based on that, we proposed a modified linear model. At the end of this chapter, sensitivity study on parameters affecting nanoparticle transport is presented. Experimental data from literature was used to validate the model.

5.2 Nanoparticle Flow in Porous Media

In the nano-EOR process, deeper understanding on the transport behavior of nanofluid is necessary since it is critical for the improvement of hydrocarbon recovery. As discussed in the previous chapters, nanoparticle can alter the wettability of the rock by forming attachment layers on the solid surface [29, 193]. Thus, deposition of NPs in porous media during the transport is an important mechanism for predicting the formation of nanoparticle layers. Deposition of nanoparticle is affected by several parameters such as particle velocity [225, 231], particle size [232], grain size [233], pH [234], ionic strength [235] and temperature [236].

Particle flow behavior in porous media had been widely studied both theoretically and experimentally [237, 238]. According to McDowell-Boyer [239], there are three filtration mechanism for colloidal particles flowing through porous media, i.e., filtration cake, straining and physical-chemical mechanisms, as displayed in Figure 5.1. Particles larger than the grain size will not able to pass and will form a filtration cake layer at the inlet, while particles small enough to penetrate but comparable to pore throat size will likely to stuck in the smaller throat. Differently, micro to nano size particles will be able to penetrate the media while having dominant physical-chemical interaction with grain surface [4, 239]

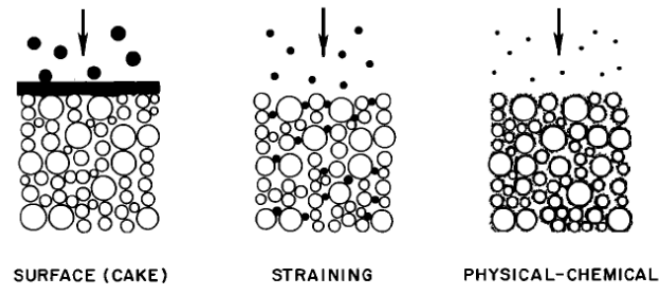


Figure 5.1 Filtration mechanism of colloidal particle transport in porous media [239]

Since NP has a size between colloidal particle (10^{-6} m) and molecules (10^{-10} m), it exhibits both colloidal and molecules characteristics [240]. Due to its small size, nanoparticle flow mechanism inside the porous media is quite complex and hard to explain. Number of forces are involved in the transport. Unlike colloidal particle in which sedimentation and interception are the dominant mechanisms [241], Brownian motion and ionic interaction are the dominant parameters on NPs flow [73, 242].

During the flow, several mechanisms are involved between particle, fluid and grain such as particle-grain collision, particle-surface static interaction, thermodynamic and hydrodynamic forces [225]. According to Derjaguin-Landau-Verwey-Overbeek (DLVO) theory [70, 243], the surface interaction consists of van der Waals (vdW) attraction and double-layer repulsion [225]. The interaction between the particle and the collector occurs due to diffusion, interception, and deposition [244] (see Figure 5.2). The transport mechanism for stable nanofluids is dominated by Brownian diffusion. While NP that transported close to the collector is adsorbed on the collector surface by interception due to the velocity difference. For NPs that have strong vdW attractions or a higher density due to agglomeration, deposition or sedimentation will occur.

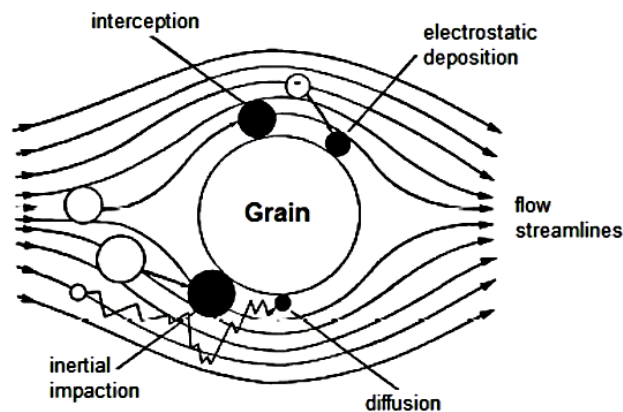


Figure 5.2 Particle-collector interaction mechanism [245]

5.3 Numerical Study Overview

Advection-dispersion equation (ADE) is extensively used for describing the particle flow in porous media. Several attempts on NP transport models based on ADE equation have been performed with some modifications and additional assumptions. One dimensional ADE equation can be expressed as Eq. 5.1 [246]:

$$\frac{\partial c}{\partial t} = D \frac{\partial^2 c}{\partial x^2} - v \frac{\partial c}{\partial x} \quad (5.1)$$

with $D \frac{\partial^2 c}{\partial x^2}$ as the dispersion term and $v \frac{\partial c}{\partial x}$ as the advection term, c is the concentration of the particle, and D is the dispersion coefficient.

The advection term describes the particle transport due to the bulk motion of the fluid as a function of velocity and concentration. For NPs flow, advection is the primary process that dominates the movement. The second process that needs to be considered is dispersion. Dispersion indicates the tendency of the particles to spread and mix due to molecular diffusion and the velocity gradient. It consists of mechanical dispersion and diffusion. In some cases, the reaction between the particles and the medium surface will occur and need to be considered in the equation.

As the reaction between NPs and solid pore surfaces is always present, the expression above (Eq. 5.1) is only valid for describing passive tracer and failed for modeling nanoparticles flow since deposition will occur [237]. Thus, the reaction term is added to accommodate the attachment of particles on the grain surface. Deposition (reaction) of particles is described as $\frac{\rho_b \partial s}{\phi \partial t}$, where ρ_b is the bulk density of the medium, ϕ is the porosity and s is the attachment concentration on solid surface. The reaction term assumes:

- a. Homogeneous porous medium;
- b. Incompressible fluid and medium
- c. Constant rate at isothermal state
- d. Dispersion occurs in a parallel direction
- e. Aggregation between NPs and chemical reaction with solid surface will not occur
- f. Dispersion coefficient of NP is similar as the tracer

The one-dimensional ADE equation with consideration of particle deposition therefore becomes Eq. 5.2.

$$\frac{\partial c}{\partial t} + \frac{\rho_b \partial s}{\phi \partial t} = D \frac{\partial^2 c}{\partial x^2} - v \frac{\partial c}{\partial x} \quad (5.2)$$

The reaction term $\frac{\rho_b \partial s}{\phi \partial t}$ can be solved by using several approaches of adsorption isotherm expressions. [247]

$$\frac{\rho_b \partial s}{\phi \partial t} = kc \quad (\text{Linear})$$

$$\frac{\rho_b \partial s}{\phi \partial t} = \frac{k_1 c_m}{1 + k_2 c_m} \quad (\text{Langmuir})$$

$$\frac{\rho_b \partial s}{\phi \partial t} = k c^n, \quad n > 1 \quad (\text{Freundlich})$$

$$\frac{\rho_b \partial s}{\phi \partial t} = k_1 c - k_2 c^2 \quad (\text{Quadratic})$$

$$\frac{\rho_b \partial s}{\phi \partial t} = k_1 e^{-\frac{k_2}{c}} \quad (\text{Exponential})$$

According to adsorption expressions above, some modification and assumption are added in deposition term to compensate NPs flow. Numerous models have been developed based on different theories such as colloidal filtration, colloidal filtration with site blocking, colloidal filtration with detachment, kinetic Langmuir model, and dual-site model (Table 5.1). These models will be discussed briefly in the next subsection.

Table 5.1 Transport flow model (modified from [237])

| Model | References | Deposition Term | |
|---------------------------------|---|--|-------|
| Colloid Filtration Theory | Yao et al. (1971) [244] | $\frac{\rho_b}{\emptyset} \frac{\partial s}{\partial t} = k_{dep} c$, $k_{dep} = \frac{3(1-\emptyset)}{2} \frac{u\alpha\eta_0}{dc}$ | (5.3) |
| Filtration Model + Maximum Site | Li et al. (2008) [231], Liu et al. (2009) [248], Cullen et al. (2010) [249] | $\frac{\rho_b}{\emptyset} \frac{\partial s}{\partial t} = k_{dep} \left(1 - \frac{s}{s_{max}}\right) c$ | (5.4) |
| Filtration Model + Detachment | Bradford et al. (2002) [250] | $\frac{\rho_b}{\emptyset} \frac{\partial s}{\partial t} = k_{dep} c - \frac{\rho b}{\emptyset} k_{det} s$ | (5.5) |
| Kinetic Langmuir Model | Wang et al. (2008) [251] | $\frac{\rho_b}{\emptyset} \frac{\partial s}{\partial t} = k_a \left(1 - \frac{s}{s_{max}}\right) c - \frac{\rho b}{\emptyset} k_d s$ | (5.6) |
| Two Site Model | Zhang et al. (2016) [237] | $\frac{\rho_b}{\emptyset} \frac{\partial s}{\partial t} = k_{irr} \left(1 - \frac{s1}{s1_{max}}\right) c + k_{ra} \left(1 - \frac{s2}{s2_{max}}\right) c - \frac{\rho b}{\emptyset} k_{rd} s2$ | (5.7) |

5.3.1 Filtration Model

Colloid filtration theory (CFT) is one of the widely used techniques for predicting particle deposition phenomenon in porous media [252]. Initially, the concept was developed by Yao et al. [244] in 1971 for simulating water and waste-water filtration phenomenon. Later on, several theoretical studies based on CFT were conducted for predicting transport behavior of pollutants [244], microbial particles [253], and nanoparticle [237, 251])

Colloid filtration theory simulates colloidal particle flow through saturated homogeneous porous media by considering hydrodynamic dispersion, particle advection and retention on solid surface [254]. It uses the first order linear reaction term with deposition constant (k_{dep}) as functions of porosity (\emptyset), sand grain diameter (dc), attachment efficiency (α), collector efficiency (η_0), and particle velocity (v). Therefore, deposition term of CFT can be expressed as Eq. 5.8 and 5.9 [244]:

$$\frac{\rho_b}{\phi} \frac{\partial s}{\partial t} = k_{dep} c \quad (5.8)$$

$$k_{dep} = \frac{3(1 - \phi)}{2d_c} v \alpha \eta_o \quad (5.9)$$

According to the Eq. 5.8 and 5.9, the depositional rate constant has a linear relation with particle velocity, attachment efficiency and collector efficiency. By assuming particle velocity similar to fluid velocity, deposition of NPs will not occur at zero velocity (no flow). However, the relation of velocity and deposition is not truly a linear relation. Benamar et al. [255] found that recovery of NP will increase with increasing flow rate, with coarsest particle dominant in effluent at a high rate. They concluded that deposition rate would increase up to a critical point then decrease with increasing rate.

Single Collector Efficiency

According to Prieve and Ruckenstein [256], particle deposition rates are the result of each transport mechanism which happened to the particles during the flow. Based on that, Tufenkji et al. [254] defined single-collector efficiency (η_o) as the sum of transport efficiency by diffusion (η_D), interception (η_I), and gravity (η_G), which can be expressed as Eq. 5.10.

$$\eta_o = \eta_D + \eta_I + \eta_G \quad (5.10)$$

Overall single-collector efficiency (η_o) can be estimated using empirical correlations that has been developed and tested by some researchers. Collector efficiency can be expressed as equations in the Table 5.2 below.

Table 5.2 Single Collector Efficiency

| References | Collector Efficiency Equation |
|----------------------|---|
| Yao-Habibian [244] | $\eta_o = 4A_s^{\frac{1}{3}} N_{PE}^{\frac{2}{3}} + \frac{3}{2} N_R^2 + N_G \quad (5.11)$ |
| Logan et al. [257] | $\eta_o = 4A_s^{\frac{1}{3}} N_{PE}^{\frac{2}{3}} + A_s N_R^{\frac{15}{8}} N_{vdW}^{\frac{1}{8}} + 0.00338 A_s N_G^{1.2} N_R^{-0.4} \quad (5.12)$ |
| Tufenkji et al [254] | $\eta_o = 2.4 A_s^{\frac{1}{3}} N_R^{-0.081} N_{PE}^{-0.715} N_{vdW}^{0.052} + 0.55 A_s N_R^{1.675} N_A^{0.125} + 0.22 N_R^{-0.24} N_G^{1.11} N_{vdW}^{0.053} \quad (5.13)$ |
| Messina et al. [258] | $\eta_o = \gamma^2 [1.5062 A_s N_R^{1.9834} + N_G (1 + 6.0187 N_R^2) + N_{PE}^{-1} (7.5609 + 4.9534 N_R^1) / (2 - 2\gamma) + A_s^{0.1259} N_G^{0.8741} (0.0442 + 0.1220 N_R^{0.4210}) + A_s^{0.3662} N_{PE}^{-0.6338} (2.9352 + 2.7480 N_R^{0.3737}) + N_G^{0.6550} N_{PE}^{-0.3450} (0.9461 + 1.1626 N_R^{0.6012}) + A_s^{0.1562} N_G^{0.5873} N_{PE}^{-0.2565} (-0.6740 - 0.7119 N_R^{0.5438})] \quad (5.14)$ |

Where A_s is the Happel correction factor, N_R is aspect ratio, N_{PE} is Peclet number, N_{vdW} is van der Waals number, N_A is attraction number and N_G is gravity number. The equations for those dimensionless parameters can be found in Eqs. 5.15-5.20 below.

$$A_s = \frac{2(1 - \gamma^5)}{2 - 3\gamma + 3\gamma^5 - 2\gamma^6}, \gamma = (1 - \phi)^{\frac{1}{3}} \quad (5.15)$$

$$N_R = d_p/d_c \quad (5.16)$$

$$N_{PE} = \frac{ud_c}{\phi D_n} \quad (5.17)$$

$$N_{vDW} = \frac{A_h}{k_B T} \quad (5.18)$$

$$N_A = \frac{A_h \phi}{12\pi\mu a_p^2 u} \quad (5.19)$$

$$N_G = \frac{2a_p^2(\rho_p - \rho_f)g\phi}{9\mu u} \quad (5.20)$$

Different with collector efficiency (η_o), attachment efficiency (α) is quite difficult to estimate since there are no theoretical and empirical approaches for estimating this parameter [237]. Attachment efficiency represents a ratio of experimental-single-collector removal efficiency (η) and calculated-single collector contact efficiency (η_o), so $\alpha = \eta/\eta_o$ [252]. The value of α is often estimated from experimental breakthrough curve [252, 259] or from matching with other parameters such as depositional constant k_{dep} and collector efficiency η_o [260]. Types of nanoparticles, surface coating and rock type are believed to affect attachment efficiency [4]. To simplify the model, attachment efficiency is assumed to be constant for similar experimental conditions.

Maximum Site

Classic colloid filtration theory does not consider the maximum capacity of sites. It means that the adsorption of particles onto the solid surface will continuously occur as long as the particles source does not stop. Taking this into consideration, Cullen et al. added maximum site (s_{max}) parameter to accommodate site blocking [249].

$$\frac{\rho_b}{\phi} \frac{\partial s}{\partial t} = k_{dep} \left(1 - \frac{s}{s_{max}}\right) c \quad (5.21)$$

Maximum site (s_{max}) can be estimated using empirical correlation [231] as a function of particle velocity and particle diameter, as in Eq. 5.22,

$$s_{max} = 19.6 \left(\left(\frac{v d_p}{D} \right)^{\frac{1}{3}} \frac{d_c}{d_M} \right)^{-1.2} \quad (5.22)$$

Where d_c is the average diameter of collector and d_M is the average diameter of the medium sand. From the equation above, velocity has direct effect on the maximum site capacity, which means at high velocity maximum adsorption capacity is smaller. Therefore, smaller particle is favorable to achieve maximum adsorption.

Detachment

Classic colloid filtration theory assumes the adsorption of NPs is irreversible and does not consider the detachment phenomena. CFT is not able to simulate a gradual increase of NP injection concentration.

Considering the detachment of NPs that are already attached to the surface, the deposition term can be modified into Eq. 5.23:

$$\frac{\rho_b}{\phi} \frac{\partial s}{\partial t} = k_{dep} c - \frac{\rho_b}{\phi} k_{det} s \quad (5.23)$$

With a new parameter k_{det} as detachment rate coefficient of NPs from solid surface. Detachment coefficient could be affected by hydrodynamic forces and surface properties, however, k_{det} can only be estimated using fitting since no theoretical and empirical approaches are available. This modified model assumes the detachment and attachment rate coefficients are constant in every position, and all of adsorption processes that occurs are reversible [261].

5.3.2 Kinetic Langmuir Model

Kinetic Langmuir model is deducted from classical colloid filtration theory that assumes the adsorption is driven by chemical potential and follows Langmuir isotherm rule as Eq. 5.24 below,

$$\frac{c}{s} = \frac{1}{s_{max} K_L} + \frac{c}{s_{max}} \quad (5.24)$$

where c is equilibrium dispersion concentration and s is equilibrium adsorption concentration, while the term K_L refer to Langmuir or equilibrium constant and s_{max} as maximum adsorption. The basic difference between this model and CFT is that the adsorption on this model is reversible with a maximum capacity of adsorption. Therefore, the deposition term can be expressed as Eq. 5.25 [251],

$$\frac{\rho_b}{\phi} \frac{\partial s}{\partial t} = k_a \left(1 - \frac{s}{s_{max}}\right) c - \frac{\rho_b}{\phi} k_d s \quad (5.25)$$

with k_a as attachment rate coefficient and k_d as detachment rate coefficient. Maximum attachment concentration can be estimated using Eq. 5.26 below assuming monolayer adsorption,

$$s_{max} = \frac{\pi}{3\sqrt{3}} d_p \rho_p \rho_s \quad (5.26)$$

Additional assumptions also need to be applied such as adsorption capacity is independent on flow condition, both attachment and detachment rate coefficients are uniform, and all adsorbed particles can be desorbed[4]. At adsorption and desorption equilibrium, the attachment concentration can be derived from Eq. 5.27.

$$s = \frac{s_m}{1 + \frac{\rho_b k_d s_{max}}{\phi k_a c}} \quad (5.27)$$

Considering all equations above, in this model all attached particles on the porous media can be removed by having enough post flush (zero particle concentration), which

is not really correct since several experiment results showed immobilized particle concentration [227, 240]. Therefore, several attempts on developing a model for describing immobilized particle had been proposed [237, 241].

5.3.3 Dual Sites Model

Dual sites model accommodates both reversible and irreversible adsorption and is considered the presence of immobilized particles. Zhang et al. [237] proposed the independent two-site model that includes both reversible and irreversible attachment each with maximum site capacity. The model assumes nanoparticle attachment to be more solute-like than colloid-like with both attachment and detachment rate coefficients independent of flow rate and the sites for attachment limited by surface area [237]. Thus, the deposition term for the dual site model can be expressed as in Eq. 5.28 and 5.29,

$$\left(\frac{\rho_b}{\phi} \frac{\partial s}{\partial t}\right)_t = \left(\frac{\rho_b}{\phi} \frac{\partial s}{\partial t}\right)_{irr} + \left(\frac{\rho_b}{\phi} \frac{\partial s}{\partial t}\right)_{rev} \quad (5.28)$$

$$\left(\frac{\rho_b}{\phi} \frac{\partial s}{\partial t}\right)_t = \left[k_{irr} \left(1 - \frac{s_1}{s_{1max}}\right) c \right] + \left[k_{ra} \left(1 - \frac{s_2}{s_{2max}}\right) c - \frac{\rho_b}{\phi} k_{rd} s_2 \right] \quad (5.29)$$

where k_{irr} is the irreversible attachment rate coefficient, k_{ra} and k_{rd} are the reversible attachment and detachment rate coefficient respectively. The term s_1 and s_2 are the reversible and irreversible attachment concentration, and s_{1max} and s_{2max} are the reversible and irreversible maximum attachment concentration respectively. However, by adding more terms, solving the equation is getting more problematic since it has six unknown parameters (D , k_{irr} , k_{ra} , k_{rd} , s_{1max} and s_{2max}) that increase the complexity and reduce the effectivity of the equation. Dispersion coefficient could be estimated by fitting with tracer dispersion curve. The parameters k_{irr} , k_{ra} , k_{rd} , s_{1max} and s_{2max} are estimated by history matching with the core flood experimental data.

5.3.4 Modified Linear Adsorption Model

Based on all the models above, we proposed simple modified linear adsorption model in this study to get a basic overview on the adsorption of NP on the solid surface. The model assumes that the concentration of the particle on the solid surface (s) is linear to the concentration of particle inside the fluid (c) and their relation can be described as Eqs. 5.30-5.31 below,

$$s = k_c c \eta_o \quad (5.30)$$

$$\frac{\rho_b}{\phi} \frac{\partial s}{\partial t} = \frac{\rho_b}{\phi} \frac{\partial (k_c c \eta_o)}{\partial t} \quad (5.31)$$

where k_c is the concentration distribution coefficient of NP between solid and fluid phases while η_o is the collector efficiency. Distribution coefficient can be obtained from history matching with experimental data and is assumed to be constant for similar NPs, porous medium and experimental condition. By combining Eq. 5.30 and 5.31 with Eq. 5.2, the final equation can be expressed as Eq. 5.32.

$$\left(1 + \frac{\rho_b}{\phi} k_c \eta_o\right) \frac{\partial c}{\partial t} = D \frac{\partial^2 c}{\partial x^2} - v \frac{\partial c}{\partial x} \quad (5.32)$$

The linear expression proposes that the equilibrium between adsorbed concentration on the solid surface and dispersed concentration in the fluid is instantly obtained. It means that changing the injected concentration will directly affect the adsorbed concentration proportionally. Thus, the adsorption is assumed to be reversible and by having enough post flush ($c = 0$), the entire adsorbed particle can be removed ($s = 0$).

Moreover, since the adsorbed concentration has a linear relation with dispersed concentration, maximum retention capacity is determined by the initial concentration and the concentration distribution coefficient, instead of a function of the surface area of the pore. Therefore, for high injected concentration (c) with high distribution coefficient ($k_c \sim 1$), the maximum retention capacity should be considered further since it may exceed the real capacity of the surface area of the porous medium.

5.4 Model Development and Parameter Study

5.4.1 Visualization Model

In order to obtain a deep understanding on how particle moves due to the 2D advection and dispersion in porous media, the visualization model was developed based on Taylor dispersion with parabolic velocity distribution, as a result of both cross-channel diffusion and longitudinal advection. The method was chosen because of the simplicity and reliability on describing particle movement. Brownian movement applied on nanoparticle flow in porous media was also considered. The random walk of the particle was generated based on random number function in MATLAB. However, the adsorption of nanoparticle on the solid surface was assumed not to occur during the transport process to simplify the model and the flow is assumed to be laminar.

Input data such as particle velocity (v) = 0.004 m/s and dispersion coefficient (D) = 5×10^{-6} m²/s were used for the visualization model. The model described nanoparticle injection behavior in 1 m porous medium with constant injection rate. The result can be found in Figure 5.3.

As illustrated in Figure 5.3, NPs are initially concentrated at the inlet of the core. Some of the particles are already slightly moved from the initial position. Gradually, with increasing time nanoparticle move and disperse toward to outlet. The random function contributes to the random movement of NPs in each time-step and position. Random walk of the particles describes the Brownian motion that dominates NPs flow in the porous media. The effect of the particle dispersion can initially be observed at T2 by the change in concentration distribution. Furthermore, at T3 and T4 the dispersion effect is more obvious to spot.

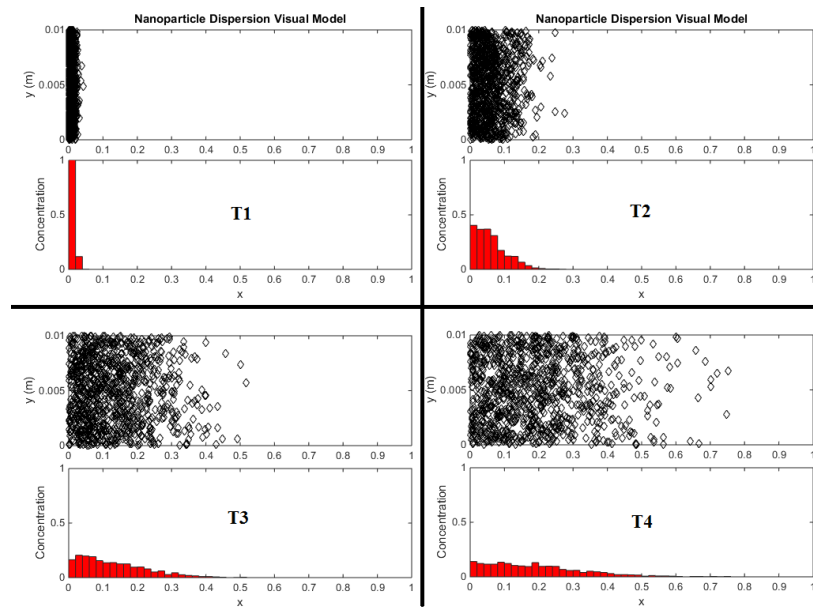


Figure 5.3 Visualization result of nanoparticle flow model

Another parameter such as velocity of the particle also plays an important role in the nanoparticles transport (see Figure 5.4). Increasing velocity will lead to the faster breakthrough at the outlet and it also significantly affects the concentration distribution of nanoparticles at each position. However, this model is only able to provide direct visualization on how dispersion will occur during particle flow. It is not able to give a precise description of the contribution of each advection and dispersion during the flow.

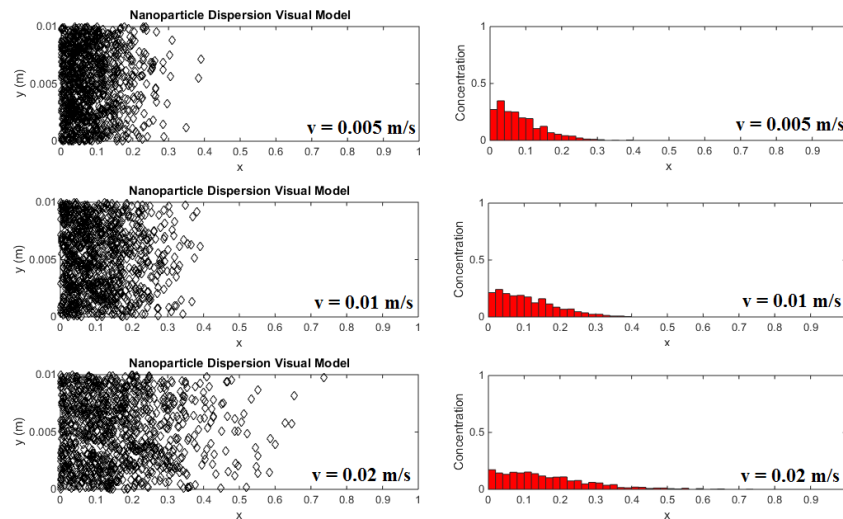


Figure 5.4 Velocity effect on particle flow behavior

5.4.2 Transport Model

To get a more accurate model for predicting NP deposition, the transport model based on ADE was suggested. Finite-difference techniques were used in this model development to solve ADE. Finite-difference approaches the solution numerically by using discretization of space and time derivatives with small time-step and spacing, so that the error could be minimized [262]. The solution of typical advection-dispersion can be seen in Figure 5.5. The concentration will move forward due to the advection,

while the dispersion is responsible for the reduced maximum concentration and alter the shape in each position.

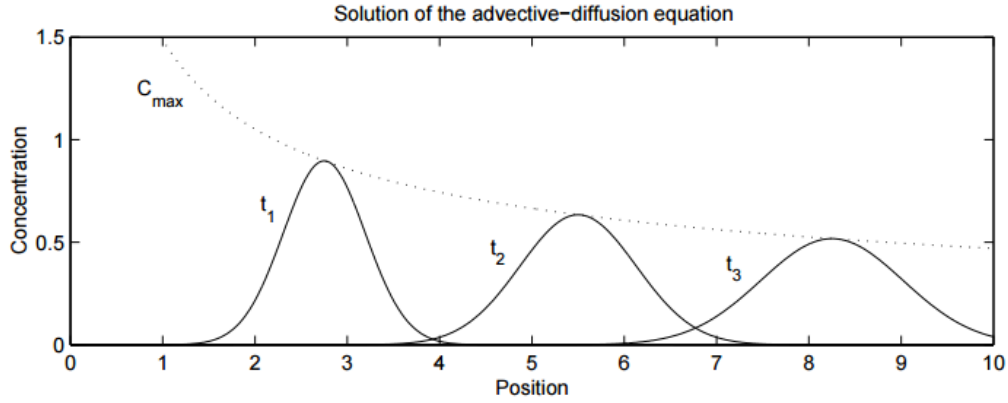


Figure 5.5 One dimension ADE solution [263]

By applying spatial and temporal discretization on advection-dispersion equation, Eq. 5.1 can be written as,

$$\frac{c_{i,j}^{n+1} - c_{i,j}^n}{\Delta t} = \frac{D}{(\Delta x)^2} (c_{i+1,j}^n - 2c_{i,j}^n + c_{i-1,j}^n) - \frac{v}{\Delta x} (c_{i+1,j}^n - c_{i,j}^n) \quad (5.33)$$

then, Eq. 5.33 can be rearranged to be Eq. 5.34.

$$c_{i,j}^{n+1} = c_{i,j}^n + \frac{D * \Delta t}{(\Delta x)^2} (c_{i+1,j}^n - 2c_{i,j}^n + c_{i-1,j}^n) - \frac{v * \Delta t}{\Delta x} (c_{i+1,j}^n - c_{i,j}^n) \quad (5.34)$$

Eq. 5.34 is the final equation and can be easily modified for the other models which are going to be investigated. Neumann stability analysis is implemented to determine the temporal discretization to get stable result. The time step based on Neumann stability can be expressed as,

$$\Delta t = \frac{\Delta x^2}{v\Delta x + 2D} \quad (5.35)$$

Input parameters such as dispersion coefficient (D) = 5×10^{-6} m²/s, particle velocity (v) = 0.004 m/s, core length 1 m, initial concentration 1 wt.% with 30s nanofluid slug injection were used. Reaction term was set to zero for this model.

The result in Figure 5.6 shows a similar trend with the proposed solution from the reference (Figure 5.5). The figure describes the concentration movement from the injection position towards the outlet of the core at each time step. Initially, nanofluid slugs were injected for about 30 seconds into the saturated porous media. The concentration of the NP in the fluid then gradually moves toward the outlet and breakthrough occurs at around $t=234$ seconds. The concentration peak point is gradually decreasing in every time step and position due to the dispersion term. The dispersion behavior of the flow is mostly affected by the magnitude of its dispersion constant.

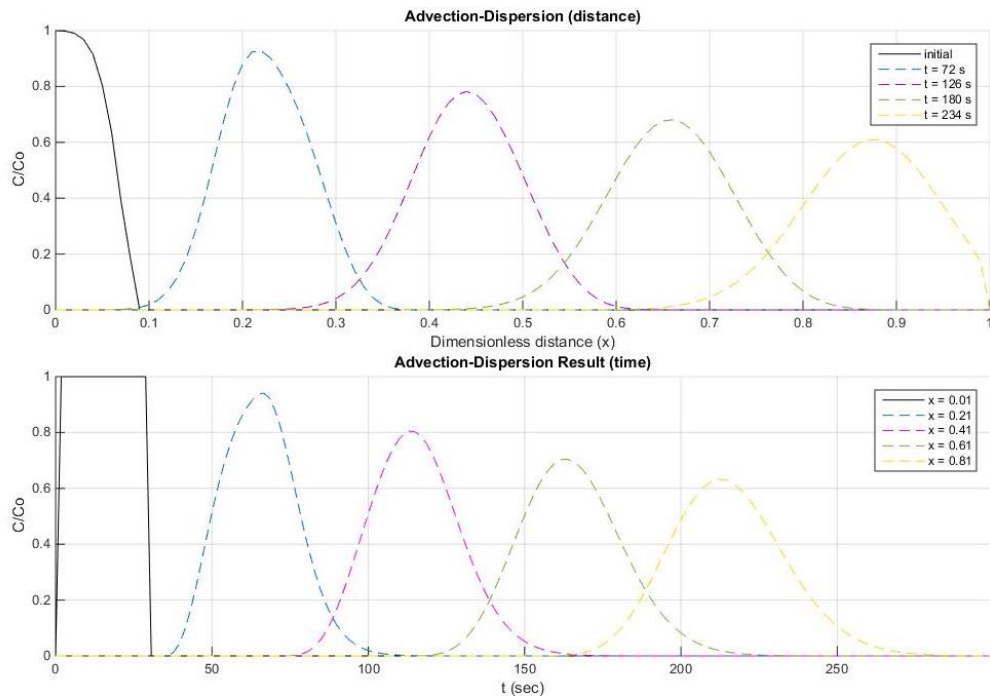


Figure 5.6 Advection-Dispersion Result

The three-dimensional plot in Figure 5.7 describes the effect of dispersion constant on the concentration distribution. It shows that at higher dispersion coefficients, the concentration is more linearly distributed which lead to lower peak concentration at every position and time-step. It simply means that higher dispersion constant will strongly distribute the concentration towards the core. While lower dispersion constant will keep the slug injection concentrated at some position. Concentration behavior at effluent ($x=L$) will also be affected due to dispersion coefficient. By using this basic advection-dispersion model, sets of numerical studies were done by adding various reaction term to accommodate NP deposition.

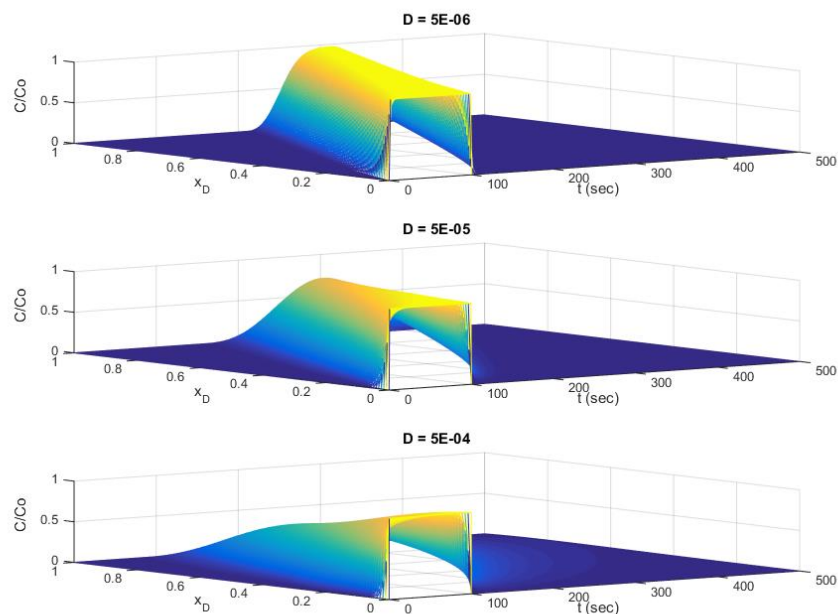


Figure 5.7 3-D plot of the effect of dispersion coefficient (D) on concentration distribution

Single Collector Efficiency Sensitivity

Several models of single-collector efficiency had been proposed for colloidal particle (see Table 5.2), however none of them was experimentally proved for NPs. Yao et al. [244] and Logan et al. [257] verified their models using experimental data with particle diameters of 0.1-7.6 μm at a velocity of $1.3 \times 10^{-3} \text{ m/s}$ [244, 257][244, 257]. Differently, Tufenkji and Elimelech [254] investigated their equation for particle diameter of 0.01-10 μm and velocity of 7×10^{-5} - $2 \times 10^{-3} \text{ m/s}$, but validated with experimental data with particle diameter of 0.1-4 μm . Thus, for compatibility check, all models were analyzed at different range of velocity and particle diameters with similar input data such as collector diameter (d_c) = 150 μm , porosity (ϕ) = 30%, Hamaker constant (A_h) = $40 \times 10^{-21} \text{ J}$, temperature (T) = 298 K, particle density (ρ_p) = 1.67 g/cm^3 and fluid density (ρ_f) = 1.0 g/cm^3 .

Sensitivity analysis was performed at velocity between $5 \times 10^{-6} \text{ m/s}$ to $5 \times 10^{-1} \text{ m/s}$ and for particle with diameter in the range of 10^{-5} m to 10^{-9} m , the results are shown in Figure 5.8. In general, the result indicates a similar trend of increasing collector efficiency by reducing the particle velocity. It confirms that at the lower velocity the tendency of the particles to deposit is increasing due to the lower hydrodynamic forces. Moreover, all the models show slightly different behavior with different particle diameter. When the velocity is 0.5 m/s, Yao-Habibian model gives the lowest efficiency for a particle with a diameter of $5 \times 10^{-7} \text{ m}$, while the other models give the lowest efficiency at diameter of $1 \times 10^{-7} \text{ m}$. However, since the size of NPs is between 10^{-9} and 10^{-8} , further investigations are focused in that particle size range.

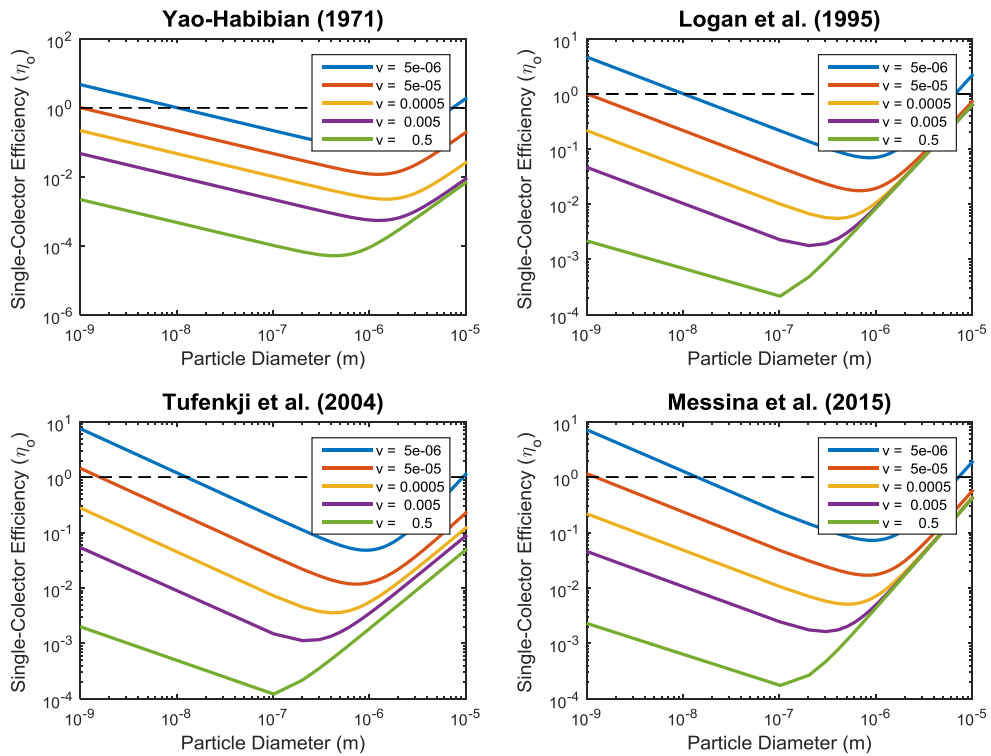


Figure 5.8 Comparison of the single-collector efficiency models at different particle diameters (10^{-5} - 10^{-9} m) and velocities (5×10^{-6} - $5 \times 10^{-1} \text{ m/s}$).

The other important observation is that the collector efficiency will increase beyond one ($\eta_o > 1$) at nano-scale diameter at very low velocity. Therefore, the result from all models seem incorrect and not representative since the value of efficiency should not be above one [4]. Due to the inability to describe the collector efficiency of nano-scale particles at really low velocity, Messina et al. [258] proposed normalized model which always has a value below one and could potentially be used for NPs model at low velocity (see Figure 5.9). However, further study with experimental validation is required for more reliable single collector model.

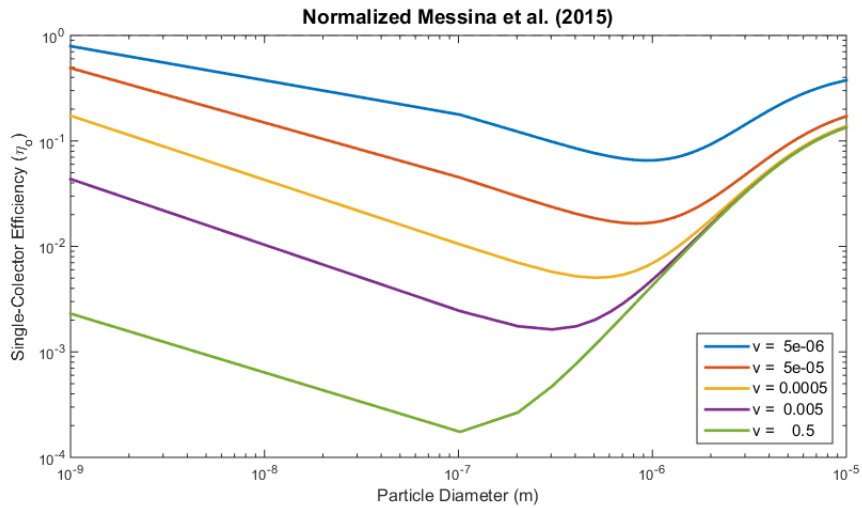


Figure 5.9 Normalized model at different particle diameters (10^{-5} - 10^{-9} m) and velocities (5×10^{-6} - 5×10^{-1} m/s)

The investigations for low particle velocity and low porosity were done for all model including the normalization model, as can be seen in Figure 5.10. At low velocity (5×10^{-6} m/s), [258] normalized-model proposed by Messina et al. is the only model with reasonable result while other models give overly high values. Differently, for low porosity case (10%) all the models have similar value at nano-scale particle diameter. Therefore, it can be seen that a lower porosity will give a lower efficiency for the nano-scale particle diameter and higher efficiency for larger particle diameter. Based on this sensitivity study, Messina’s model is used for the colloidal filtration model.

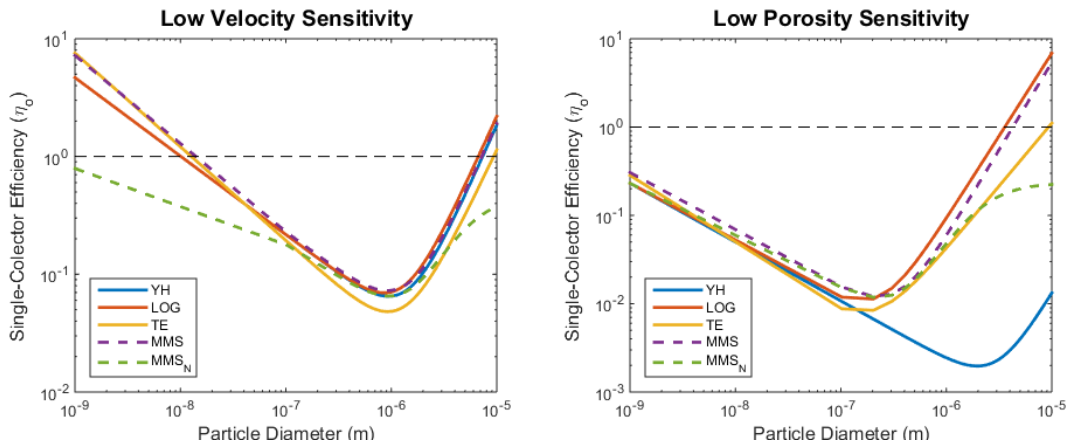


Figure 5.10 Comparison of Yao-Habibian (YH), Logan et al. (LOG), Tufenkji-Elimelech (TE), Messina et al. (MMS) single-collector efficiency model at low velocity, 5×10^{-6} m/s (left) and low permeability, 10% (right)

Colloidal Filtration Model

Unlike passive tracers, a deposition will occur due to the physiochemical attraction between the particle and solid surface during nanoparticle flow. Therefore, reaction term needs to be added to the basic advection-dispersion equation. By combining Eq. 5.2 and Eq. 5.8, colloidal filtration general equation can be expressed as Eq. 5.36.

$$\frac{\partial c}{\partial t} = D \frac{\partial^2 c}{\partial x^2} - v \frac{\partial c}{\partial x} - k_{dep} c, \quad k_{dep} = \frac{3(1-\phi)}{2dc} v \alpha \eta_o \quad (5.36)$$

The general colloidal filtration equation is solved with the following boundary and initial conditions.

$$\text{I.C. } c(x, 0) = 0, \quad s(x, 0) = 0 \quad \text{for } 0 \leq x \leq L \quad (5.37)$$

$$c(0, t) = c_o \quad \text{for } 0 \leq t \leq t_i$$

$$\text{B.C. } c(0, t) = 0 \quad \text{for } t > t_i \quad (5.38)$$

$$c_x(L, t) = 0 \quad \text{for } t > 0$$

Deposition term in colloidal filtration model is mostly influenced by deposition rate constant and the dispersed concentration of nanoparticle in the fluid. From Eq. 5.36, depositional rate constant is the function of porosity (ϕ), sand grain diameter (dc), attachment efficiency (α), collector efficiency (η_o), and particle velocity (v). All the parameters are known from experimental data, except the attachment and the single-collector efficiency. Single-collector efficiency can be estimated using several empirical equations while the attachment efficiency value should be fitted with available experimental data.

Parameter study was done on colloidal filtration model with default input as in Table 5.3. With these input data, a sensitivity study was done by varying other parameters such as collector diameter, nanoparticle diameter, dispersion coefficient, particle velocity and attachment efficiency.

Table 5.3 Data input for sensitivity study

| D | $q \left(\frac{cc}{min} \right)$ | α | $v \left(\frac{m}{s} \right)$ | L (m) | d_p (nm) | d_c (μm) | ϕ | V_{pore} (cc) | PVI |
|---------|-----------------------------------|----------|--------------------------------|------------|---------------|----------------------|--------|--------------------|-----|
| 5.0E-06 | 10 | 1.0E-04 | 0.004 | 1 | 100 | 150 | 0.45 | 15 | 3 |

The result of collector and particle diameter sensitivity study can be found in Figure 5.11. It can be seen that a smaller collector diameter is preferable for better adsorption. One of the most possible reason is that smaller collector will have strong vdW attraction forces but small repulsion forces. It also has larger surface area compared to the bigger collector. According to Eq. 5.9, the depositional rate constant is inversely proportional to the collector size. The smaller collector size will give the higher depositional rate and vice versa.

Similarly, the smaller nanoparticle size will lead to more deposition. Smaller nanoparticle size will give higher collector efficiency (at NP magnitude) which leads to lower nanoparticle recovery and higher deposition. The other important observation is a significant concentration drop in the particle diameter range from 50 nm to 10 nm, which means smaller particles will increase the NPs deposition exponentially.

Simulation of Nanoparticle Transport

Moreover, in Table 5.4, the effect of different particle and collector diameter on single-collector efficiency and depositional constant can be observed.

Table 5.4 Collector and particle diameter sensitivity study result

| Collector Diameter Sensitivity | | | Particle Diameter Sensitivity | | |
|--------------------------------|----------|-----------|-------------------------------|----------|-----------|
| d_c (nm) | η_o | k_{dep} | d_p (nm) | η_o | k_{dep} |
| 100 | 3.00E-03 | 1.40E-03 | 10 | 9.60E-02 | 3.00E-03 |
| 150 | 2.30E-03 | 6.96E-04 | 50 | 3.50E-03 | 1.10E-03 |
| 200 | 1.90E-03 | 4.31E-04 | 100 | 2.30E-03 | 6.98E-04 |
| 250 | 1.60E-03 | 2.97E-04 | 150 | 1.80E-03 | 5.43E-04 |

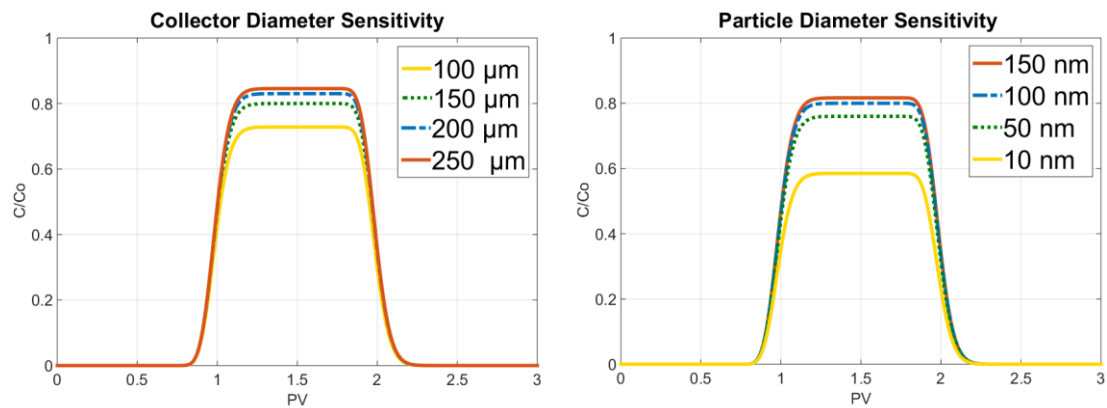


Figure 5.11 Sensitivity of collector diameter and particle diameter

Other parameters such as dispersion constant, particle velocity and attachment efficiency also have a significant contribution to the nanoparticles deposition. Figure 5.12 shows that increasing the dispersion coefficient will lead to the reduction in effluent concentration since it increases the particle distribution in the porous media. Similarly, higher attachment efficiency is favorable for higher deposition as it is directly proportional to the depositional constant, which depends on the NPs type, size and surface coating. On the other hand, higher particle velocity will reduce the deposition due to the increased hydrodynamic energy that will reduce the attachment efficiency. Therefore, lower velocity is favorable for higher nanoparticle deposition that will lead to higher oil recovery rate.

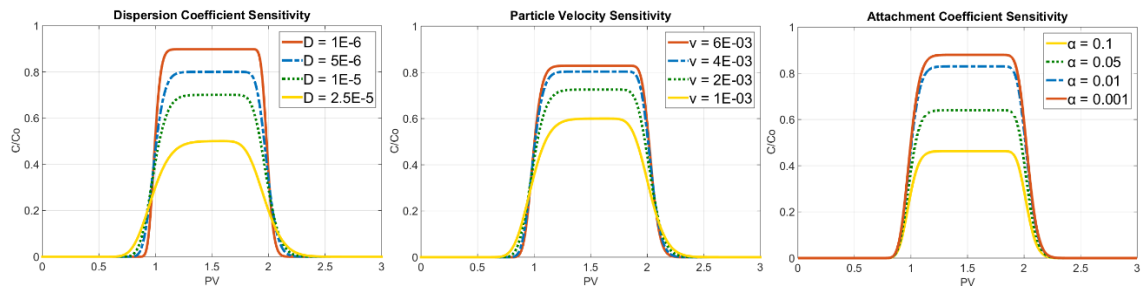


Figure 5.12 Dispersion coefficient, particle velocity and attachment efficiency sensitivity

Modified Linear Model

We further proposed a model using a linear relation between adsorbed concentration on solid and dispersed concentration in the liquid, as expressed in Eq. 5.30. Concentration distribution coefficient was introduced and the relation between adsorbed and dispersed concentration is shown in Figure 5.13. By adding the linear relation and collector efficiency to the main ADE equation, the final expression for modified linear model can be expressed as Eq. 5.39.

$$\left(1 + \frac{\rho_b}{\phi} k_c \eta_o\right) \frac{\partial c}{\partial t} = D \frac{\partial^2 c}{\partial x^2} - v \frac{\partial c}{\partial x} \tag{5.39}$$

The model was solved using the finite-difference method with similar boundary and initial conditions as for Eq. 5.37 and 5.38. Then, by using the same input data as the previous model (Table 5.3), sensitivity studies were done with various distribution coefficients.

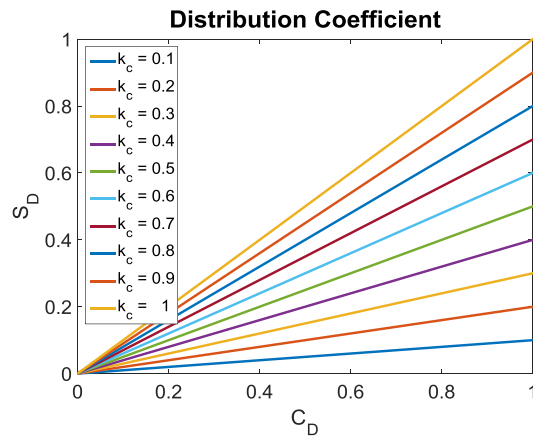


Figure 5.13 Linear relation on distribution coefficient

Two types of sensitivity studies were done using modified linear model to investigate the effect of the distribution coefficient on the deposition of NPs in the porous media. The results are presented in Figure 5.14. The first sensitivity study was conducted by varying the distribution coefficient ($k_c=0.1-0.4$) to understand its effect on the effluent concentration profile. From Figure 5.14, increasing the distribution coefficient will delay the breakthrough and increase the deposition at the same time. According to the effluent data, the NPs have late breakthrough compared to the tracers. This phenomenon indicates that adsorptions occur during the NPs flow.

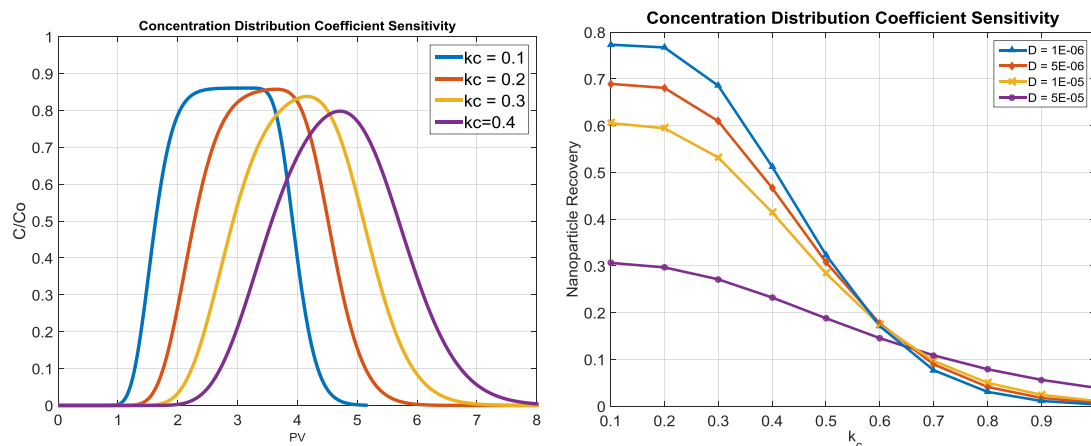


Figure 5.14 Sensitivity study result of: A. the concentration profile at effluent (left) and B. nanoparticle recovery (right)

The second study was done to understand the effect of various dispersion coefficient (D) at different distribution coefficient (k_c) on the nanoparticle recovery at the effluent. The results are presented in Figure 5.14 B and Table 5.5. In correlation with the previous sensitivity study (Figure 5.11), reducing distribution coefficient will increase nanoparticle recovery. It means less NPs are deposited. Moreover, at higher dispersion coefficient (D), increasing the distribution coefficient (k_c) will not significantly affect the nanoparticle recovery as at lower dispersion coefficient (D). However, at some critical point of k_c , changing the dispersion coefficient will not affect the recovery. Our hypothesis is that advection will dominate the flow at this point, while dispersion will not significantly affect the flow.

Table 5.5 Sensitivity study result on the different dispersion coefficient and distribution coefficient

| D = 1E-06 | | D = 5E-06 | | D = 1E-05 | | D = 5E-05 | |
|-----------|-------|-----------|-------|-----------|-------|-----------|-------|
| k_c | R | k_c | R | k_c | R | k_c | R |
| 0.2 | 0.767 | 0.2 | 0.681 | 0.2 | 0.595 | 0.2 | 0.297 |
| 0.4 | 0.513 | 0.4 | 0.467 | 0.4 | 0.415 | 0.4 | 0.233 |
| 0.6 | 0.171 | 0.6 | 0.177 | 0.6 | 0.174 | 0.6 | 0.146 |
| 0.8 | 0.031 | 0.8 | 0.041 | 0.8 | 0.050 | 0.8 | 0.079 |
| 1 | 0.004 | 1 | 0.007 | 1 | 0.011 | 1 | 0.040 |

5.5 Experimental Data Validation

In this section, core-flooding data are used as the input for both colloidal filtration model and modified linear model. The selection of four experimental results from Murphy [240] was based on the data quality and the experimental condition which matches with our model assumption. Laboratory studies were done by injecting slugs of coated salt-tolerant silica NPs (Exp. 66-67) and iron oxides (Exp. 91-92) into saturated Boise sand pack media. Constant injection rate was set for each run and recovery of NPs at the effluent was recorded. The experiments data can be seen in Table 5.6 that includes the pore volume injection (PVI) and the effluent recovery (R_{exp}).

Table 5.6 Experimental Data [240]

| Ex | NPs type | q (cc/min) | v (m/s) | Ci (wt.%) | PVI | Φ (%) | d _c (μm) | d _p (nm) | R _{exp} |
|----|-------------|------------|----------|-----------|-----|------------|---------------------|---------------------|------------------|
| 66 | Silica | 10 | 3.70E-03 | 5 | 3 | 47.6 | 177-210 | 15 | 0.84 |
| 67 | Silica | 1 | 3.70E-04 | 5 | 3 | 47.9 | 177-210 | 15 | 0.83 |
| 91 | Iron Oxides | 1 | 3.80E-04 | 0.1 | 2.9 | 46.4 | 150-180 | 150 | 0.47 |
| 92 | Iron Oxides | 8.4 | 3.10E-03 | 0.1 | 3.1 | 47.3 | 150-180 | 150 | 0.79 |

Plots of concentration profile (concentration vs pore volume) at effluent for each experiment were extracted from the literature. They will be used in the history matching process. Tracer concentration data was also added for each run to help the data fitting process. Using the input data in Table 5.6 and fitting with effluent concentration plot, both CFT and ML models are validated.

Colloidal Filtration Theory (CFT) Model

Transport and deposition of nanoparticle were predicted by applying Colloidal Filtration Theory model. Parameters such as dispersion coefficients (D) were matched with the tracers as assumed before that the dispersion coefficients for both were similar. Single collector efficiency (η_o) was calculated by using Messina et al. model and the attachment efficiency (α) was matched with the experimental data. Then, by using single collector and attachment efficiency, depositional rate coefficients were calculated.

The result of the simulation using CFT model can be seen in Table 5.7. The simulation result shows that CFT model gives a relatively accurate prediction for Experiments 66-67 and a poor result for Experiments 91-92. A significant error is found for the simulation of Exp. 91. The reason is that the Exp. 91 data is quite unique compared to the other experimental results, since it only recovered 47% of total injected concentration while others recovered almost the same as the injected concentration. This happened due to the finite retention capacity which is not possible to predict using CFT unless the deposition rate is small [240].

Table 5.7 Colloidal Filtration Theory Result

| Ex | D | η_o | α | k _{dep} | R _{exp} | R _{sim} | Error |
|----|----------|----------|----------|------------------|------------------|------------------|-------|
| 66 | 1.75E-05 | 9.27E-03 | 2.00E-03 | 3.65E-04 | 0.84 | 0.71 | 15.3% |
| 67 | 8.00E-06 | 9.27E-03 | 2.00E-03 | 3.65E-04 | 0.83 | 0.83 | 0.5% |
| 91 | 1.01E-06 | 7.57E-03 | 1.50E-02 | 1.51E-04 | 0.47 | 0.72 | 53.6% |
| 92 | 3.00E-06 | 1.92E-03 | 1.50E-02 | 4.70E-04 | 0.79 | 0.90 | 13.5% |

Experiments 66 and 67 were conducted by using salt tolerant silica NPs with an average diameter of 15 nm coated with specific polymer for stability enhancement. Attachment efficiency for this specific nanoparticle was calculated to be $\alpha = 2.00E-03$. Deposition rate constants were calculated for both Exp. 66 and 67, followed with concentration profile at effluent using filtration model. The effluent histories with the simulation results for both Exp. 66-67 can be seen in Figure 5.15.

The effluent history for both Exp. 66 and 67 shows delay in breakthrough compared to the tracer data and simulation result. Experiment 66 has slightly earlier breakthrough than Exp. 67 due to higher flowrate. However, both have similar trend lines. Concentration in both experiments increase gradually until a maximum point and then drop drastically at the post-flush period. Differently, the tracer and simulation result have similar breakthrough time, at which concentration increase to some point (maximum concentration of tracer) and then have a plateau period before post-flush. The only difference between tracer and the simulation result is the plateau at maximum concentration. Our simulation result always has a lower concentration than tracer data due to the deposition of the NPs.

At post-flush, the experimental data drop at an earlier stage with the gradual reduction in concentration. While, simulation and tracer data have later breakthrough with a drastic drop in concentration. The overall result shows that simulation-66 recovers only 71% of the total injected concentration, while simulation-67 recovers 83%. Compared to the experimental data, the error in simulation-66 is 15.3 % while simulation-67 is 0.5%. The discrepancy in the result is probably due to the velocity difference.

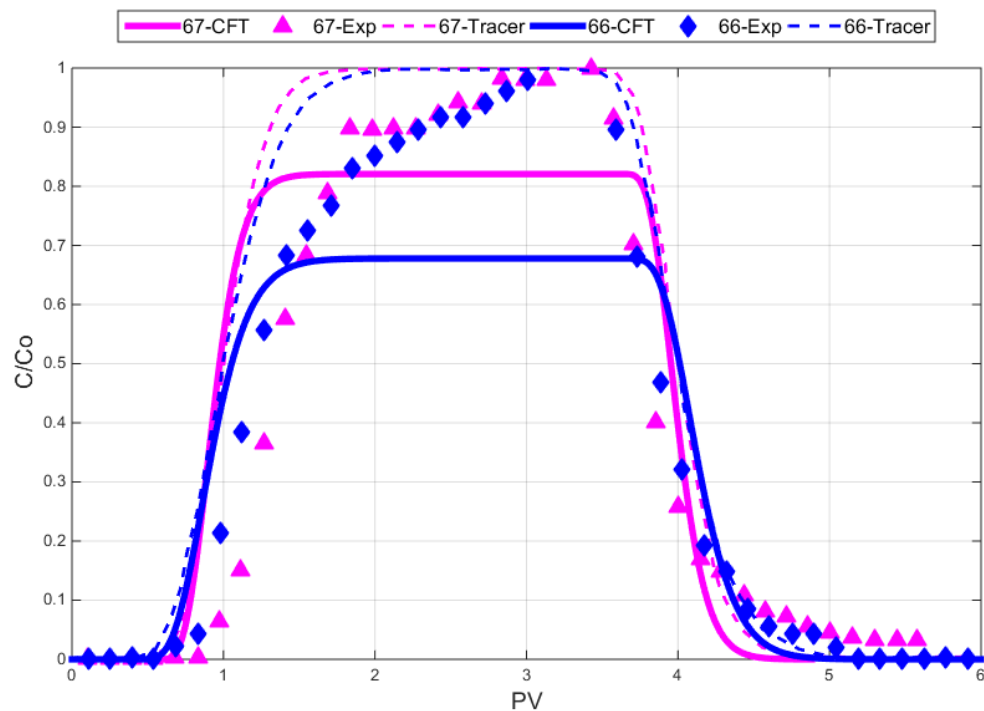


Figure 5.15 Effluent data and simulation using Colloidal Filtration Theory (CFT) result of experiments 66 and 67

For Experiment 91 and 92, coated iron oxides NP with an average diameter of 150 nm were used [240]. Attachment efficiency was matched by using both effluent history data, and was calculated to be $1.50E-02$. The value was then used for the calculation of depositional rate constant. Figure 5.16 shows the result of the simulations and effluent history data for both Exp. 91 and 92.

The experimental data shows very late breakthrough for both Exp. 91 and 92. The difference in delay between both experiments is noticeable. After breakthrough, both experiments show a different trend in concentration increment. The effluent concentration increases slowly for Exp. 91 and drastically for Exp. 92. It means that more NPs adsorption occurs in Exp. 91. This is due to the velocity difference between both experiments. High particle velocity will result in high hydrodynamic energy. It leads to the detachment of adsorbed particles. Moreover, simulations and tracer data for both experiments show similarity in breakthrough time and the concentration gradient.

The filtration model (CFT) for Exp. 91 and 92 failed to match the initial nanoparticle effluent curve. On the other hand, the post-flush curve for Exp. 92 is well matched with simulation result. The simulation-91 is quite close to the post-flush history. The error for simulation-92 is acceptable at around 13.5%. On the other hand, the error for simulation-91 is really high. We can conclude that CFT is unable to simulate NPs flow at low velocity with massive adsorption. Therefore, another model is proposed to get a better result with less error.

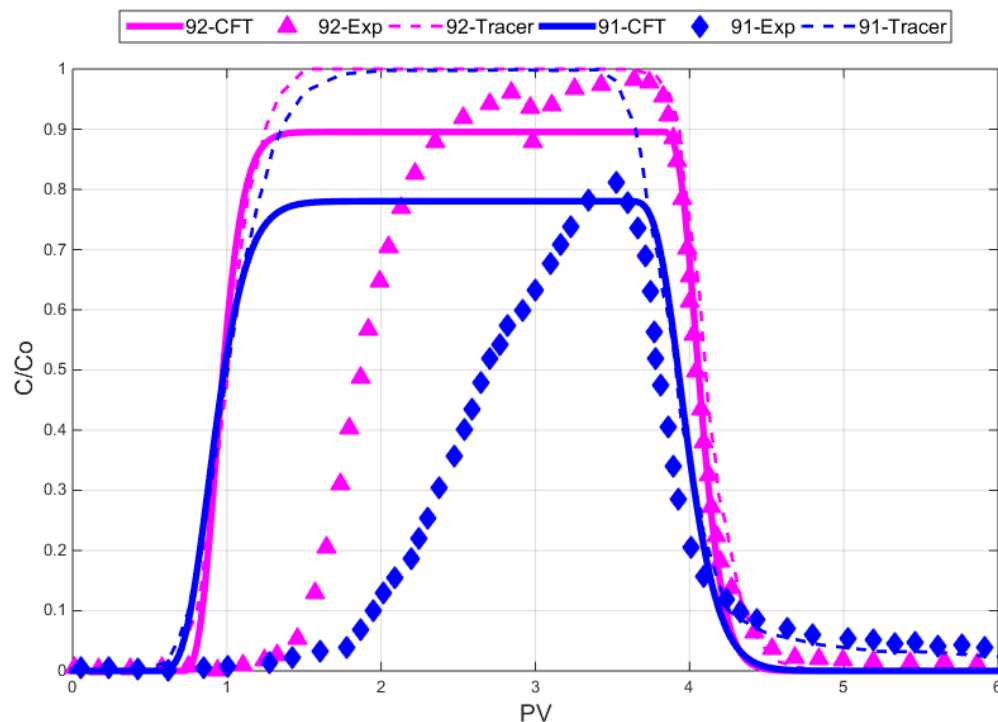


Figure 5.16 Effluent data and simulation using Colloidal Filtration Theory (CFT) result of experiments 91 and 92

Modified Linear (ML) Model

Modified Linear model was proposed to simulate the same experimental data. Unlike colloidal transport model in which the rate of adsorbed concentration is linear to the dispersed concentration, in modified linear model direct relation between adsorbed and dispersed concentration is assumed. The collector efficiency is added to the equation for accommodating the effect of diffusion, interception and gravity on the model. The collector efficiency is calculated using Messina et al. [258] model. Therefore, a new constant (k_c), concentration distribution coefficient, is introduced. The value of k_c is obtained from the fitting with effluent history data point.

The result of the simulation can be seen in Table 5.8. In general, by using modified linear model, the nanoparticle recovery results are improved with lower error value than the previous filtration model. For all experimental data, the errors are reduced except for Exp. 67. It increased from 0.5% to 1.4% which is however still acceptable. Differently, for Exp. 91 the error is significantly reduced from 53.6 % to 7.8%.

Table 5.8 Modified Linear Result

| Ex | D | η | k_c | R_{exp} | R_{sim} | Error |
|----|----------|----------|----------|-----------|-----------|-------|
| 66 | 8.80E-06 | 6.57E-03 | 1.50E-02 | 0.84 | 0.81 | 3.8% |
| 67 | 4.50E-07 | 3.18E-02 | 4.00E-03 | 0.83 | 0.82 | 1.4% |
| 91 | 3.20E-07 | 9.71E-03 | 6.00E-02 | 0.47 | 0.43 | 7.8% |
| 92 | 2.10E-06 | 2.44E-03 | 1.35E-01 | 0.79 | 0.75 | 5.1% |

Effluent histories and the simulation results for Experiment 66 and 67 can be seen in Figure 5.17. The simulations are done by matching the distribution coefficient value, and the best fit values are 1.50E-02 and 4.00E-03 for Ex. 66 and 67 respectively. Collector efficiency is also calculated for each experiment.

From figure 5.13, simulations and experimental data have similar breakthrough time and are well matched to the initial concentration profile. However, at the post-flush period, the experimental data concentration drops at an early time with a gradual reduction in the end, while simulation results give slightly late, but significant, concentration drop. Both simulation results have a plateau region at the maximum concentration and are unable to be matched with the gradual rising profile from the experimental data. However, the early plateau of Exp. 67 can be matched correctly by the model. The simulated concentration recoveries are relatively good with errors at approximately 3.8% and 1.4% for Ex. 66-67 respectively.

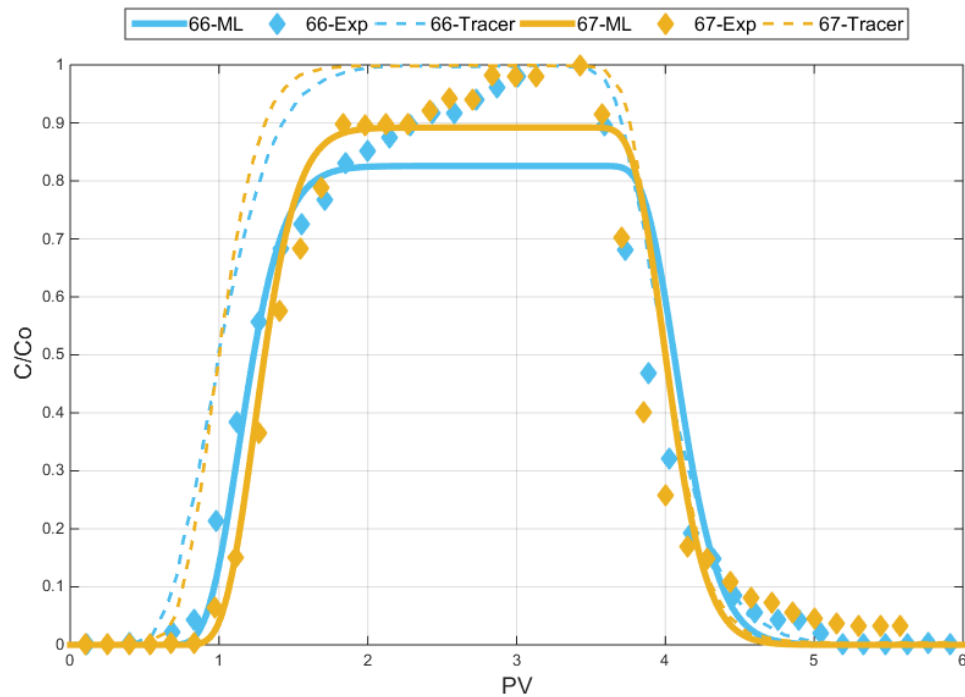


Figure 5.17 Effluent data and simulation using Modified Linear (ML) result of experiments 66 and 67

For the Experiments 91 and 92, the results of the simulation and the effluent history are presented in Figure 5.18. The breakthrough time of Exp. 92 and the simulation are perfectly matched. Differently, the breakthrough time for the simulation-91 is quite late compared to the effluent history. The initial concentration profile of simulation-92 is fitted properly to the effluent history but failed to match the post flush concentration drop profile. On the contrary, for the Exp. 91, the simulation cannot perfectly follow the rising profile of experiment data and failed to correctly match the post-flush period. The simulated Exp. 91 has the higher concentration and lower error on the recoverable concentration (7.8%) than CFT model. Likewise, the Ex. 92 simulation result gives 5.1% error on predicting recoverable nanoparticle concentration.

A simple approach using the linear relation between adsorbed and dispersed NPs concentration is proven to be reliable enough to simulate the deposition and the flow of NPs in porous media. Therefore, at the next section, the modified linear model and filtration model are compared to the more complex model using dual sites which are reversible and irreversible.

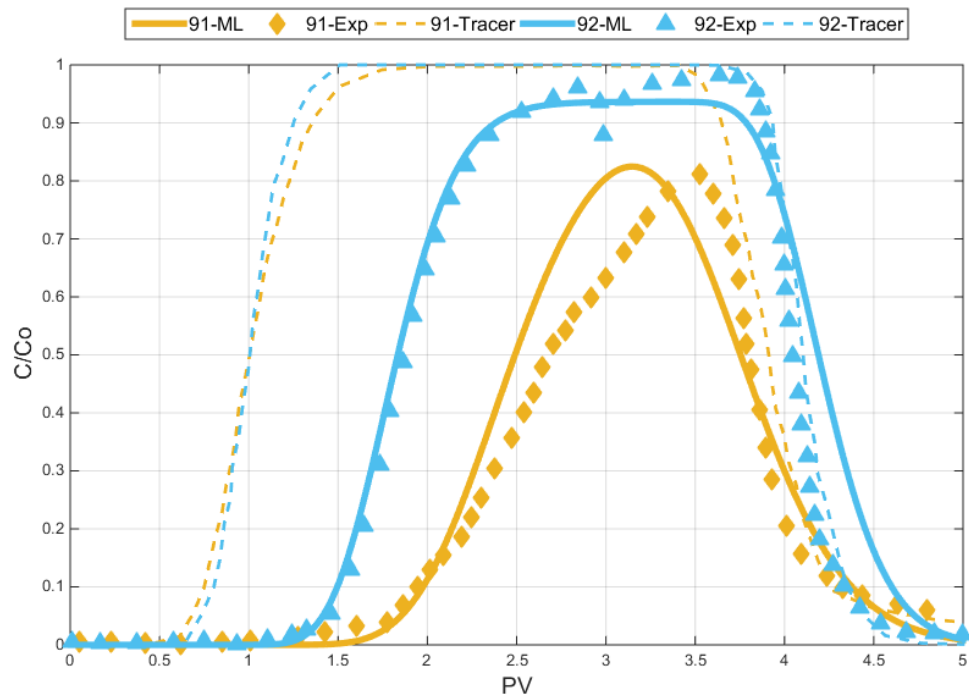


Figure 5.18 Effluent data and simulation using Modified Linear (ML) result of experiments 91 and 92

Comparison with Two-site Model

Independent two-site model (ISTM) were suggested by Zhang [4] to accommodate both reversible and irreversible adsorption during nanoparticle transport. The fact that NPs interactions with each other and the collector (sand grain) are similar at the static condition, leads to a conclusion that heterogeneity of the collector surface is the main cause of the different type of adsorption (reversible and irreversible). By assuming there are immobilized adsorbed particles, continuous post-flush injection is not able to recover the particles from the porous media. The immobilized adsorption concentration depends on the collector surface and the capacity of each site.

By introducing dual types of adsorption, the equation in the model becomes more complicated with six unknown parameters (D , k_{irr} , k_{ra} , k_{rd} , $s_{1\ max}$ and $s_{2\ max}$). Those parameters are varied based on NPs and porous media type, at selected experimental conditions. By using ISTM, Zhang [4] predicted all the parameters in Table 5.9. Because there is no empirical equation for most of the parameters, the only way to obtain those values is by history matching. Even though the simulation can be matched with the historical data, matching process of six unknown parameters can be problematic and reduce the flexibility of the model. Therefore, a comparative study is done to get an idea on how simple models, which are easier to solve and have higher flexibility, are compared to the more complex ones.

Simulation of Nanoparticle Transport

Table 5.9 Independent Two-site Model (Zhang)

| Ex | $s_{1\ max}$ | $s_{2\ max}$ | k_{irr} | k_{ra} | k_{rd} | R_{exp} | R_{sim} |
|----|--------------|--------------|-----------|----------|----------|-----------|-----------|
| 91 | 5.75E-04 | 2.87E-01 | 7.00E-03 | 1.20E-04 | 5.00E-04 | 0.47 | 0.41 |
| 92 | 5.75E-04 | 2.87E-01 | 7.00E-03 | 1.20E-04 | 5.00E-04 | 0.79 | 0.67 |

In this section only Experiment 91 and 92 were considered for the study. The result of the comparative study between the three models can be found in Table 5.10. In general, colloidal filtration model has the biggest error compared to the others. Filtration model tends to overestimate the recovery value for about 53.6% (Exp. 91) higher than the experimental data. On the other hand, both modified linear and two-site model have lower result than the effluent history. The reason for overestimated result by CFT is because this model has a similar breakthrough as tracers, which is too early for the real nanoparticle breakthrough. Differently, ML and ISTM models have more accurate breakthrough time due to the matched parameters.

Table 5.10 Model Comparison Result with the Dual Site Model [4]

| Ex | R_{exp} | R_{CFT} | R_{ML} | R_{ISTM} | ϵ_{CFT} | ϵ_{ML} | ϵ_{ISTM} |
|----|-----------|-----------|----------|------------|------------------|-----------------|-------------------|
| 91 | 0.47 | 0.72 | 0.43 | 0.41 | 53.6% | 7.8% | 12.8% |
| 92 | 0.79 | 0.90 | 0.75 | 0.67 | 13.5% | 5.1% | 15.2% |

Overall, modified linear has more accurate result compared to the other models. The error for both Exp. 91 and 92 are below 10%, while the two-site model has error larger than 10%. However, the smaller error does not mean that the model is more valid and reliable since the effluent profile matching data should be considered as well. The result of the fitting history data can be seen in Figure 5.19 for both experiments.

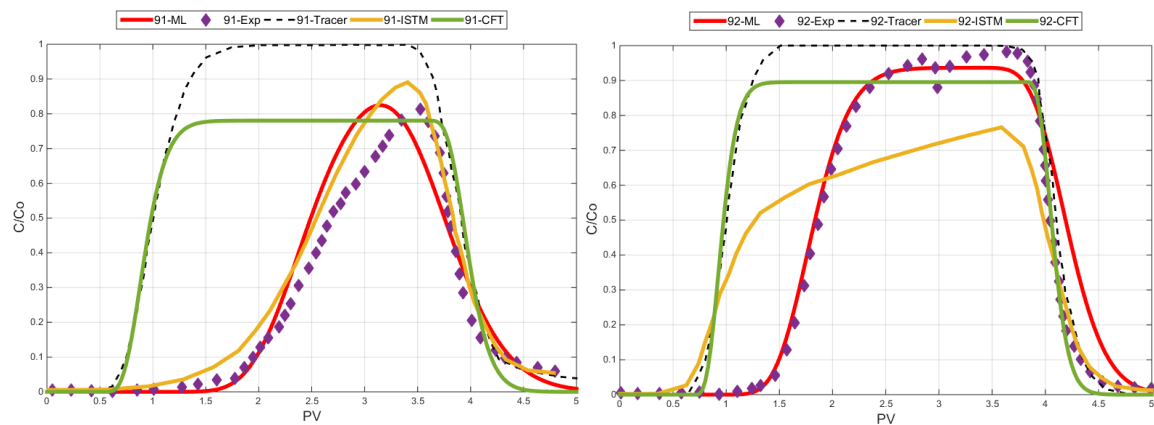


Figure 5.19 Model comparison for experiment 91 and experiment 92

The result of Exp. 91 shows that both ML and ISTM result are quite close to the effluent data while CFT is matched with tracer instead of the effluent. The breakthrough time of ISTM is more accurate than ML. Even though the ISTM model does not perfectly fit with the initial concentration profile, it has a similar gradient with the historical data and at the post-flush period, the simulation is fairly fitted. Conversely, ML is unable to match the concentration gradient at both initial and after the post-flush period.

On the other hand, for Ex. 92, the ML result is perfectly matched to the initial profile and poorly matched at the post-flush. It shows that the breakthrough for ISTM is too early. In this case, ISTM is unable to match effluent history data at both initial and post-flush period. Thus, from similar experimental condition using iron oxides NPs at a different velocity and pore volume injection, it can be concluded that linear model is quite reliable on predicting nanoparticle deposition. However, different setup, experimental condition, and NPs type can lead to the different result and need to be investigated further.

Chapter 6 Conclusion and Future Research

6.1 Conclusion Remarks

Massive studies on the application of nanotechnology in petroleum industry especially for EOR have been done and shown promising results. Nano-EOR is proposed to substitute the existing chemical EOR for improving the oil recovery efficiency with several advantages: (1) NPs can improve the fluid performance by only using small amount of materials, (2) improvement in heat and mass transfer lead to the possible application in high-temperature condition, (3) high flexibility for combining with other materials such as surfactant and polymer. Various types of NPs (organic and inorganic) are confirmed to be able to increase the oil recovery up to 20% additional in oil recovery. They can improve the oil recovery through several mechanisms such as IFT reduction, wettability alteration, disjoining pressure, and viscosity control. Some parameters, like NPs' concentration, size, temperature, wettability, and salinity, are proven to affect the performance of nano-EOR.

In this thesis, the retention mechanism of NPs in the porous media are studied theoretically. Brownian motion and interception can bring the NPs close enough to the collector surface. Then, the interaction of NPs according to DLVO theory will take place with the domination of van der Waals attraction. Thus, those particles have a close affinity to the collector surface and are adsorbed easily.

Four different single-collector efficiency models based on empirical equation are investigated. The sensitivity study of single-collector efficiency models reveals that smaller particles are favored for better adsorption. The contact efficiency increases as particle velocity decreases since it is proportional to the hydrodynamic force which is the main force of desorption. The Brownian motion is the dominant force for NPs adsorption on the solid surface, compared to gravity and interception. However, small particles with low velocity lead to the overestimation efficiency above 100% which is not possible in real life. This is because the models are built for the colloidal particle with micron size magnitude. Therefore, the normalized model is used to predict the single-collector efficiency for the nanoparticles.

From the experimental data, it can be concluded that the effluent history of NPs shows, (a) delay in NPs breakthrough compared to tracer data, (b) gradually increasing concentration after breakthrough, (c) drop concentration during the post-flush period, (d) retained NPs inside porous media after post-flush.

To simulate the behavior of NPs in the porous media, two transport models are developed based on advection-dispersion equation (ADE). Since ADE is in the partial differential form, finite difference method is used to solve. Neumann stability analysis is also applied to obtain a stable result from the simulation. The result from ADE is then confirmed with the reference, and it shows the similar trend.

The classical colloidal filtration theory (CFT) is used to predict colloidal particle transport in the porous medium. In this research, CFT is developed for predicting NPs

transport behavior. The result shows that CFT is failed to predict the effluent history data. This model cannot match the concentration profile of NPs but success to fit with tracer data.

Modified linear (ML) model is proposed by the author to simplify the transport model of nanoparticle. This model assumes the adsorption of NPs is linearly proportional to the injected NPs concentration. Adsorption in this model is reversible and can be detached with enough post-flush. This model shows that it can predict the effluent history quite good. However, the post-flush period is difficult to match by using this model.

Independent dual site model (ISTM) is obtained from the literature and then compared with the ML and CFT. The model assumes there are two kinds of adsorption that occur during the NPs transport, which are irreversible and reversible. The comparison shows that both ISTM and ML can simulate the behavior of NPs. ML has slightly better result than ISTM model. Therefore, by using simple linear adsorption model, the transport of NPs can be predicted.

6.2 Challenges and Future Research

The future development of nano-EOR has many challenges. The main challenges in the petroleum industry, especially in nano-EOR are the technology limitation, economical aspect of the project, environmental and health issues. Even though considerable studies proved that NPs could increase the oil recovery, most of them are limited to small laboratory scale and not yet applicable for real field implementation. There are several limitations that hinder the application of NPs in field scale.

1. Preparation of stable nanofluids for larger scale application is not yet possible. As NPs tend to agglomerate under reservoir condition (high temperature, pressure, and salinity), the preparation of homogenous NPs suspension still become a challenge.
2. Several mechanisms on improving the recovery in nano-EOR have been proposed. However, the mechanisms and its affecting parameters are not clearly understood. The interactions between NPs and rock properties need to be studied further.
3. The development of fundamental understanding on nano-EOR is limited. The lack of theoretical and numerical investigation on nano-EOR seems to be one of the reasons. Most of numerical studies refer to the colloidal particle model which is not perfectly described NPs behavior. The models are also limited on the physical interactions of NPs and have not yet considered the chemical interactions.
4. Due to the fast research and development of nanotechnology, the health and safety studies are left behind and need to catch up. One of the important challenges for NPs development is its effect on human body. Due to nano-scale size, NPs can be easily inhaled by human and potentially deposited inside the lung.

According to several challenges presented above, some future researches on nano-EOR are suggested as follows.

1. Advance researches on the preparation of stable nanofluids need to be done with economic aspect consideration.
2. Several NPs are proved to exhibit different characteristic and mechanism for EOR. However, there has not yet research proposed on the mixture nanofluids application. New application and better performance can be revealed by enabling two or more nanofluids functioning together.
3. Pilot projects of nano-EOR for practical uses need to be done intensively. The project will improve the understanding of the nano-EOR mechanisms in the real condition. Optimization studies on a nano-EOR parameter are also recommended to improve the recovery and cost efficiency.
4. The experiments need to be done to confirm the adsorption and desorption behavior during the NPs flow. Reversible and irreversible adsorption need be studied further, experimentally and theoretically. As it brings significant effect to the deliverability of NPs to the target zone.
5. Integrated research on the health and safety of NPs must be done extensively to prevent the risk afflicting human and the environment.

Bibliography

1. Das, S.K., et al., *Nanofluids: science and technology*. 2007: John Wiley & Sons.
2. Taniguchi, N. *On the basic concept of nanotechnology*. in *Proc. Intl. Conf. Prod. Eng. Tokyo, Part II, Japan Society of Precision Engineering*. 1974.
3. Weiss, P.S., *A Conversation with Dr. Heinrich Rohrer: STM Co-inventor and One of the Founding Fathers of Nanoscience*. acsnano, 2007.
4. Zhang, T., *Modeling of Nanoparticle Transport in Porous Media*. PhD, 2012.
5. Roco, M.C., *National Nanotechnology Initiative -Past, Present, Future*. PREPRINT Handbook on Nanoscience, Engineering and Technology, 2007. **2**: p. 1-326.
6. Bawarski, W.E., et al., *Emerging nanopharmaceuticals*. *Nanomedicine: Nanotechnology, Biology and Medicine*, 2008. **4**(4): p. 273-282.
7. Marcato, P.D. and N. Durán, *New aspects of nanopharmaceutical delivery systems*. *Journal of nanoscience and nanotechnology*, 2008. **8**(5): p. 2216-2229.
8. Lu, W., et al., *Gold nano-popcorn-based targeted diagnosis, nanotherapy treatment, and in situ monitoring of photothermal therapy response of prostate cancer cells using surface-enhanced Raman spectroscopy*. *Journal of the American Chemical Society*, 2010. **132**(51): p. 18103-18114.
9. Müller, S., *Magnetic fluid hyperthermia therapy for malignant brain tumors—an ethical discussion*. *Nanomedicine: Nanotechnology, Biology and Medicine*, 2009. **5**(4): p. 387-393.
10. Webster, T.J., et al., *Nano-biotechnology: carbon nanofibres as improved neural and orthopaedic implants*. *Nanotechnology*, 2003. **15**(1): p. 48.
11. Ghormade, V., M.V. Deshpande, and K.M. Paknikar, *Perspectives for nano-biotechnology enabled protection and nutrition of plants*. *Biotechnology advances*, 2011. **29**(6): p. 792-803.
12. Poizot, P., et al., *Nano-sized transition-metal oxides as negative-electrode materials for lithium-ion batteries*. *Nature*, 2000. **407**(6803): p. 496-499.
13. Rao, C.e.N.e.R., et al., *Graphene: the new two - dimensional nanomaterial*. *Angewandte Chemie International Edition*, 2009. **48**(42): p. 7752-7777.
14. Song, Y. and C. Marcus, *Hyperpolarized Silicon Nanoparticles: Reinventing Oil Exploration*. International Presentation, 2007.
15. Sharma, M.M., *A New Family of Nanoparticle Based Drilling Fluids*. 2012: p. 8-10.
16. Ju, B. and T. Fan, *Enhanced Oil Recovery By Flooding With Hydrophilic Nanoparticles*. *China Particuology*, 2006. **4**: p. 41-46.
17. Kong, X., *Applications of Micro and Nano Technologies in the Oil and Gas Industry- An Overview of the Recent Progress*. Society of Petroleum Engineering, 2010.
18. Mohajeri, A., et al., *Hydrodesulphurization Nanocatalyst, Its Use and a Process for Its Production*. 2009, Google Patents.
19. Gavrielatos, E., R. Mohan, and O. Shoham, *EFFECT OF INTERMEDIATE WETTABILITY NANOPARTICLES ON OIL-WATER EMULSION STABILITY*. *Journal of Petroleum Science and Engineering*, 2017.
20. Hendraningrat, L. and O. Torsæter, *Metal oxide-based nanoparticles: revealing their potential to enhance oil recovery in different wettability systems*. *Applied Nanoscience*, 2015. **5**(2): p. 181-199.
21. Li, S., *An experimental investigation of Enhanced Oil Recovery Mechanisms in Nanofluid Injection Process*, in *NTNU*. 2016. p. 430-442.
22. Fletcher, A. and J. Davis. *How EOR can be transformed by nanotechnology*. in *SPE Improved Oil Recovery Symposium*. 2010. Society of Petroleum Engineers.
23. Zhang, T., et al. *Foams and emulsions stabilized with nanoparticles for potential conformance control applications*. in *SPE International Symposium on Oilfield Chemistry*. 2009. Society of Petroleum Engineers.
24. Espinoza, D.A., et al. *Nanoparticle-stabilized supercritical CO2 foams for potential mobility control applications*. in *SPE Improved Oil Recovery Symposium*. 2010. Society of Petroleum Engineers.
25. Ju, B., et al. *A study of wettability and permeability change caused by adsorption of nanometer structured polysilicon on the surface of porous media*. in *SPE Asia Pacific Oil and Gas Conference and Exhibition*. 2002. Society of Petroleum Engineers.
26. Onyekonwu, M.O., Naomi, *Investigating the Use of Nanoparticles in Enhancing Oil Recovery*. *SPE Journal*, 2010.
27. Hendraningrat, L., et al., *Improved oil recovery by nanofluids flooding: an experimental study*. *SPE Kuwait International Petroleum Conference and Exhibition*, 2012: p. SPE 163335.

28. Hendraningrat, L., S. Li, and O. Torsæter, *A coreflood investigation of nanofluid enhanced oil recovery*. Journal of Petroleum Science and Engineering, 2013. **111**: p. 128-138.
29. Hendraningrat, L., O. Torsæter, and others, *Understanding Fluid-Fluid and Fluid-Rock Interactions in the Presence of Hydrophilic Nanoparticles at Various Conditions*. SPE Asia Pacific Oil & Gas Conference and Exhibition, 2014.
30. Hendraningrat, L. and O. Torsæter. *Unlocking the potential of metal oxides nanoparticles to enhance the oil recovery*. in *Offshore Technology Conference-Asia*. 2014. Offshore Technology Conference.
31. Hendraningrat, L., *Unlocking the Potential of Hydrophilic Nanoparticles as Novel Enhanced Oil Recovery Method : An Experimental Investigation*. 2015.
32. McNaught, A.D. and A.D. McNaught, *Compendium of chemical terminology*. Vol. 1669. 1997: Blackwell Science Oxford.
33. Christian, P., et al., *Nanoparticles: structure, properties, preparation and behaviour in environmental media*. Ecotoxicology, 2008. **17**(5): p. 326-343.
34. Bhushan, B., *Springer handbook of nanotechnology*. 2010: Springer Science & Business Media.
35. Meehan, D.N., *The Impact of Nanotechnology on Oil and Gas Economics*. The Way Ahead, 2011. **7**(03): p. 18-19.
36. Horikoshi, S. and N. Serpone, *Introduction to nanoparticles*. Microwaves in Nanoparticle Synthesis: Fundamentals and Applications, 2013: p. 1-24.
37. Wijesena, R. [cited 2017 13 June]; Available from: <https://niniti.com/nanoscale-why-size-matter/>.
38. Li, S., *An Experimental Investigation of Enhanced Oil Recovery Mechanisms in Nanofluid Injection Process*. 2016.
39. McBain, S.C., H.H. Yiu, and J. Dobson, *Magnetic nanoparticles for gene and drug delivery*. International journal of nanomedicine, 2008. **3**(2): p. 169.
40. Hannink, R.H. and A.J. Hill, *Nanostructure control of materials*. 2006: Woodhead Publishing.
41. Benjamin, J.S., *Dispersion strengthened superalloys by mechanical alloying*. Metallurgical transactions, 1970. **1**(10): p. 2943-2951.
42. Verkoeijen, D., et al., *Determining granule strength as a function of moisture content*. Powder technology, 2002. **124**(3): p. 195-200.
43. Yadav, T.P., R.M. Yadav, and D.P. Singh, *Mechanical milling: a top down approach for the synthesis of nanomaterials and nanocomposites*. Nanoscience and Nanotechnology, 2012. **2**(3): p. 22-48.
44. Koch, C.C. and J. Whittenberger, *Mechanical milling/alloying of intermetallics*. Intermetallics, 1996. **4**(5): p. 339-355.
45. Yang, H. and P. McCormick, *Mechanically activated reduction of nickel oxide with graphite*. Metallurgical and Materials Transactions B, 1998. **29**(2): p. 449-455.
46. Lü, L., M. Lai, and W. Liang, *Magnesium nanocomposite via mechanochemical milling*. Composites science and technology, 2004. **64**(13): p. 2009-2014.
47. Ding, J., et al., *Ultrafine Co and Ni particles prepared by mechanochemical processing*. Journal of Physics D: Applied Physics, 1996. **29**(9): p. 2365.
48. Sheibani, S., et al., *Structural evolution in nano-crystalline Cu synthesized by high energy ball milling*. Materials Letters, 2007. **61**(14): p. 3204-3207.
49. Wang, G., et al., *Layer - By - Layer Dendritic Growth of Hyperbranched Thin Films for Surface Sol-Gel Syntheses of Conformal, Functional, Nanocrystalline Oxide Coatings on Complex 3D (Bio) silica Templates*. Advanced Functional Materials, 2009. **19**(17): p. 2768-2776.
50. Yu, W. and H. Xie, *A review on nanofluids: preparation, stability mechanisms, and applications*. Journal of Nanomaterials, 2012. **2012**: p. 1.
51. Davidson, A., C. Huh, and S.L. Bryant. *Focused magnetic heating utilizing Superparamagnetic nanoparticles for improved oil production applications*. in *SPE International Oilfield Nanotechnology Conference and Exhibition*. 2012. Society of Petroleum Engineers.
52. Ghadimi, A., R. Saidur, and H. Metselaar, *A review of nanofluid stability properties and characterization in stationary conditions*. International Journal of Heat and Mass Transfer, 2011. **54**(17): p. 4051-4068.
53. Amanullah, M. and A. Al-Tahini, *Nano-Technology- Its Significance in Smart Fluid Development for Oil and Gas Field Application*. SPE Saudi Arabia Section Technical Symposium and Exhibition, 2009: p. 1-12.
54. Hoelscher, K.P., et al. *Application of nanotechnology in drilling fluids*. in *SPE international oilfield nanotechnology conference and exhibition*. 2012. Society of Petroleum Engineers.
55. Rahmani, A.R., et al., *Crosswell magnetic sensing of superparamagnetic nanoparticles for subsurface applications*. SPE Journal, 2014.
56. Apaleke, A.S., A.A. Al-Majed, and M.E. Hossain, *Drilling Fluid: State of The Art and Future Trend*. North Africa Technical Conference and Exhibition, 2012: p. 20-22.
57. Amanullah, M., M.K. AlArfaj, and Z.A. Al-abdullatif. *Preliminary test results of nano-based drilling fluids for oil and gas field application*. in *SPE/IADC Drilling Conference and Exhibition*. 2011. Society of Petroleum Engineers.

58. Cheraghian, G., et al. *Application of TiO₂ and fumed silica nanoparticles and improve the performance of drilling fluids*. in *AIP Conference Proceedings*. 2014. AIP.
59. Dimens, N. and S. Issue, *The great potential of nanomaterials in drilling and drilling fluid application*. 2014. **5**: p. 463-471.
60. Al-Shehri, A.A., et al. *Illuminating the reservoir: Magnetic nanomappers*. in *SPE Middle East Oil and Gas Show and Conference*. 2013. Society of Petroleum Engineers.
61. Li, J. and M. Meyyappan, *Real time oil reservoir evaluation using nanotechnology*. 2011, Google Patents.
62. AfzaliTabar, M., et al., *Preference of multi-walled carbon nanotube (MWCNT) to single-walled carbon nanotube (SWCNT) and activated carbon for preparing silica nanohybrid pickering emulsion for chemical enhanced oil recovery (C-EOR)*. *Journal of Solid State Chemistry*, 2017. **245**: p. 164-173.
63. Cheraghian, G., *Effects of nanoparticles on wettability: A review on applications of nanotechnology in the enhanced Oil recovery*. *International Journal of Nano Dimension*, 2015. **6**(5): p. 443.
64. Ehtesabi, H., M.M. Ahadian, and V. Taghikhani, *Enhanced heavy oil recovery using TiO₂ nanoparticles: investigation of deposition during transport in core plug*. *Energy & Fuels*, 2014. **29**(1): p. 1-8.
65. Guo, F. and S. Aryana, *An experimental investigation of nanoparticle-stabilized CO₂ foam used in enhanced oil recovery*. *Fuel*, 2016. **186**: p. 430-442.
66. Ogolo, N., O. Olafuyi, and M. Onyekonwu. *Enhanced oil recovery using nanoparticles*. in *SPE Saudi Arabia section technical symposium and exhibition*. 2012. Society of Petroleum Engineers.
67. Trefalt, G. and M. Borkovec, *Overview of DLVO Theory*. 2014.
68. Derjaguin, B., *A theory of interaction of particles in presence of electric double layers and the stability of lyophobic colloids and disperse systems*. *Progress in Surface Science*, 1993. **43**(1-4): p. 1-14.
69. Derjaguin, B. and L. Landau, *Theory of the stability of strongly charged lyophobic sols and of the adhesion of strongly charged particles in solutions of electrolytes*. *Progress in Surface Science*, 1993. **43**(1-4): p. 30-59.
70. Verwey, E., W, and, Overbeek. J. Th. G, 1948.
71. Fedele, L., et al., *Experimental stability analysis of different water-based nanofluids*. *Nanoscale research letters*, 2011. **6**(1): p. 300.
72. Singh, A.K. and V.S. Raykar, *Microwave synthesis of silver nanofluids with polyvinylpyrrolidone (PVP) and their transport properties*. *Colloid and Polymer Science*, 2008. **286**(14-15): p. 1667-1673.
73. Bera, A. and H. Belhaj, *Application of nanotechnology by means of nanoparticles and nanodispersions in oil recovery - A comprehensive review*. *Journal of Natural Gas Science and Engineering*, 2016. **34**: p. 1284-1309.
74. Kapusta, S.D., L. Balzano, and P. te Riele, *Nanotechnology Applications in Oil and Gas Exploration and Production*. *International Petroleum Technology Conference*, 2012: p. 5.
75. Bennetzen, M.V. and K. Mogensen, *Novel Applications of Nanoparticles for Future Enhanced Oil Recovery*. *International Petroleum Technology Conference*, 2014: p. 10-12.
76. Schröder, L., et al., *Molecular imaging using a targeted magnetic resonance hyperpolarized biosensor*. *Science*, 2006. **314**(5798): p. 446-449.
77. Cassidy, M., et al., *In vivo magnetic resonance imaging of hyperpolarized silicon particles*. *Nature nanotechnology*, 2013. **8**(5): p. 363-368.
78. Ravindra Jahagirdar, S., *Oil-Microbe Detection Tool Using Nano Optical Fibers*. *SPE Western Regional and Pacific Section AAPG Joint Meeting*, 2008. **31**.
79. Berlin, J.M., et al., *Engineered Nanoparticles for Hydrocarbon Detection in Oil-Field Rocks*. 2011: p. 11-13.
80. LIU, H., X. JIN, and B. DING, *Application of nanotechnology in petroleum exploration and development*. *Petroleum Exploration and Development*, 2016. **43**: p. 1107-1115.
81. Pratyush, S. and B. Sumit, *Nano-robots system and methods for well logging and borehole measurements*. 2008, Google Patents.
82. Cai, J., et al., *Decreasing water invasion into Atoka shale using nonmodified silica nanoparticles*. *SPE Drilling & Completion*, 2012. **27**(01): p. 103-112.
83. Xu, Z.-c. *Application of Nanotechnology on Borehole Wall Stability in Gas-Liquid Medium Transition During Gas Drilling*. in *SPE Annual Technical Conference and Exhibition*. 2012. Society of Petroleum Engineers.
84. McDonald, M.J. *A novel potassium silicate for use in drilling fluids targeting unconventional hydrocarbons*. in *SPE Canadian Unconventional Resources Conference*. 2012. Society of Petroleum Engineers.
85. Srivatsa, J.T. and M.B. Ziaja. *An experimental investigation on use of nanoparticles as fluid loss additives in a surfactant-polymer based drilling fluids*. in *International Petroleum Technology Conference*. 2011. International Petroleum Technology Conference.

86. Aderibigbe, A.A., et al., *Detection of Propping Agents in Fractures using Magnetic Susceptibility Measurements Enhanced by Magnetic Nanoparticles*. SPE Annual Technical Conference and Exhibition, 2014: p. 27-29.
87. Contreras, O., et al. *Application of in-house prepared nanoparticles as filtration control additive to reduce formation damage*. in *SPE International Symposium and Exhibition on Formation Damage Control*. 2014. Society of Petroleum Engineers.
88. Gurluk, M.R., et al. *The Effect of Different Brine Solutions on the Viscosity of VES Micelles*. in *SPE European Formation Damage Conference & Exhibition*. 2013. Society of Petroleum Engineers.
89. Ho, C.Y., et al., *Rheological Behaviour of Graphene Nano-sheets in Hydrogenated Oil-based Drilling Fluid*. *Procedia Engineering*, 2016. **148**: p. 49-56.
90. Murtaza, M., M. Rahman, and A. Al-Majed. *Mechanical and Microstructural Studies of Nanoclay Based Oil Well Cement Mix under High Pressure and Temperature Application*. in *International Petroleum Technology Conference*. 2016. International Petroleum Technology Conference.
91. Santra, A.K., P. Boul, and X. Pang. *Influence of nanomaterials in oilwell cement hydration and mechanical properties*. in *SPE International Oilfield Nanotechnology Conference and Exhibition*. 2012. Society of Petroleum Engineers.
92. Quercia, G., et al., *Influence of olivine nano-silica on hydration and performance of oil-well cement slurries*. *Materials & Design*, 2016. **96**: p. 162-170.
93. Jafariesfad, N., et al. *Nano-Sized MgO with Engineered Expansive Property for Oil Well Cement Systems*. in *SPE Bergen One Day Seminar*. 2016. Society of Petroleum Engineers.
94. De la Roi, R., C. Egyed, and J.-P. Lips. *Nano-engineered oil well cement improves flexibility and increases compressive strength: A laboratory study*. in *SPE International Oilfield Nanotechnology Conference and Exhibition*. 2012. Society of Petroleum Engineers.
95. Khan, W., et al. *MWCNT for Enhancing Mechanical Properties of Oil Well Cement for HPHT Applications*. in *SPE/IADC Middle East Drilling Technology Conference and Exhibition*. 2016. Society of Petroleum Engineers.
96. Sun, X., et al., *Rheology, curing temperature and mechanical performance of oil well cement: Combined effect of cellulose nanofibers and graphene nano-platelets*. *Materials & Design*, 2017. **114**: p. 92-101.
97. Sengupta, S. and A. Kumar. *Nano-Ceramic Coatings-A Means of Enhancing Bit Life and Reducing Drill String Trips*. in *IPTC 2013: International Petroleum Technology Conference*. 2013.
98. Chakraborty, S., et al. *The Trick Is The Surface-Functionalized Nanodiamond PDC Technology*. in *SPE International Oilfield Nanotechnology Conference and Exhibition*. 2012. Society of Petroleum Engineers.
99. Mueller, H., et al., *Lubricants for drilling fluids*. 2004, Google Patents.
100. Moh'd Husein, M. and G. Hareland, *Drilling fluids with nano and granular particles and their use for wellbore strengthening*. 2013, Google Patents.
101. Roddy, C.W., et al., *Cement compositions and methods utilizing nano-clay*. 2013, Google Patents.
102. Roddy, C.W., *Cement compositions and methods utilizing nano-hydraulic cement*. 2016, Google Patents.
103. Kühn, K.-D., *Bone cement mixture and x-ray contrast medium as well as method for their preparation*. 2006, Google Patents.
104. Junwen, W., et al., *A nano-particle foam unloading agent applied in unloading liquid of deep gas well*. *EXPLOR. DEVELOP*, 2016. **43**: p. 695-700.
105. Sun, Z., G. Jing, and Z. Tu, *Effect of Modified nano-silica/EVA on Flow Behavior and Wax Crystallization of Model Oils with Different Wax Content*. *Journal of Dispersion Science and Technology*, 2017(just-accepted).
106. Bhatia, K.H. and L.P. Chacko. *Ni-Fe nanoparticle: An innovative approach for recovery of hydrates*. in *Brasil Offshore*. 2011. Society of Petroleum Engineers.
107. !!! INVALID CITATION !!!
108. Huang, T. and J.B. Crews, *Nanotechnology applications in viscoelastic surfactant stimulation fluids*. *SPE Production & Operations*, 2008. **23**(04): p. 512-517.
109. Crews, J.B., T. Huang, and W.R. Wood. *The future of fracturing-fluid technology and rates of hydrocarbon recovery*. in *SPE Annual Technical Conference and Exhibition*. 2008. Society of Petroleum Engineers.
110. Crews, J.B. and A.M. Goma. *Nanoparticle associated surfactant micellar fluids: an alternative to crosslinked polymer systems*. in *SPE International Oilfield Nanotechnology Conference and Exhibition*. 2012. Society of Petroleum Engineers.
111. Li, L., G.A. Al-Muntasheri, and F. Liang. *Nanomaterials-Enhanced High-Temperature Fracturing Fluids Prepared with Untreated Seawater*. in *SPE Annual Technical Conference and Exhibition*. 2016. Society of Petroleum Engineers.
112. Ghahfarokhi, R.B., *Nano-proppants for fracture conductivity*. 2016, Google Patents.

113. Al-Muntasheri, G., et al., *High temperature fracturing fluids with nano-crosslinkers*. 2015, Google Patents.
114. Wasan, D.T. and A.D. Nikolov, *Spreading of nanofluids on solids*. *Nature*, 2003. **423**(6936): p. 156.
115. Onyekonwu, M.O. and N.A. Ogolo. *Investigating the use of nanoparticles in enhancing oil recovery*. in *Nigeria Annual international conference and exhibition*. 2010. Society of Petroleum Engineers.
116. Ogolo, N., O. Olafuyi, and M. Onyekonwu, *Enhanced Oil Recovery Using Nanoparticles*. Saudi Arabia Section Technical Symposium and Exhibition, 2012: p. 9.
117. Ju, B. and T. Fan, *Experimental study and mathematical model of nanoparticle transport in porous media*. *Powder Technology*, 2009. **192**: p. 195-202.
118. Ahmadi, M.-A., et al., *Experimental investigation the effect of nanoparticles on micellization behavior of a surfactant: application to EOR*. *Petroleum Science and Technology*, 2016. **34**(11-12): p. 1055-1061.
119. Ahmadi, M.A. and J. Sheng, *Performance improvement of ionic surfactant flooding in carbonate rock samples by use of nanoparticles*. *Petroleum Science*, 2016. **13**(4): p. 725-736.
120. Ahmadi, M.-A., et al., *Evaluation of the ability of the hydrophobic nanoparticles of SiO₂ in the EOR process through carbonate rock samples*. *Petroleum Science and Technology*, 2016. **34**(11-12): p. 1048-1054.
121. Suleimanov, B., F. Ismailov, and E. Veliyev, *Nanofluid for enhanced oil recovery*. *Journal of Petroleum Science and Engineering*, 2011. **78**(2): p. 431-437.
122. Saien, J., F. Moghaddamnia, and H. Bamdadi, *Interfacial Tension of Methylbenzene–Water in the Presence of Hydrophilic and Hydrophobic Alumina Nanoparticles at Different Temperatures*. *Journal of Chemical & Engineering Data*, 2013. **58**(2): p. 436-440.
123. Esmaeilzadeh, P., et al., *Effect of ZrO₂ nanoparticles on the interfacial behavior of surfactant solutions at air–water and n-heptane–water interfaces*. *Fluid Phase Equilibria*, 2014. **361**: p. 289-295.
124. Esmaeilzadeh, P., A. Bahramian, and Z. Fakhroueian, *Adsorption of anionic, cationic and nonionic surfactants on carbonate rock in presence of ZrO₂ nanoparticles*. *Physics Procedia*, 2011. **22**: p. 63-67.
125. Moghadam, T.F. and S. Azizian, *Effect of ZnO nanoparticles on the interfacial behavior of anionic surfactant at liquid/liquid interfaces*. *Colloids and Surfaces A: Physicochemical and Engineering Aspects*, 2014. **457**: p. 333-339.
126. Mensah, A., A. Opeyemi, and M. Shaibu. *Effect of nano-particles (Al, Al₂O₃, Cu, CuO) in emulsion treatment and separation*. in *Paper SPE-16750 8eMS, Pre-sented at the Nigeria Annual International Conference and Exhibition, Lagos, Nigeria, 30th July e 1st August*. 2013.
127. Ying, J.Y. and T. Sun, *Research needs assessment on nanostructured catalysts*. *Journal of Electroceramics*, 1997. **1**(3): p. 219-238.
128. Scott, S.L., C.M. Crudden, and C.W. Jones, *Nanostructured catalysts*. 2008: Springer Science & Business Media.
129. Hamed Shokrlu, Y. and T. Babadagli. *Effects of nano-sized metals on viscosity reduction of heavy oil/bitumen during thermal applications*. in *Canadian Unconventional Resources and International Petroleum Conference*. 2010. Society of Petroleum Engineers.
130. Shokrlu, Y.H. and T. Babadagli. *Transportation and interaction of nano and micro size metal particles injected to improve thermal recovery of heavy-oil*. in *SPE Annual Technical Conference and Exhibition*. 2011. Society of Petroleum Engineers.
131. Hamed Shokrlu, Y. and T. Babadagli, *In-situ upgrading of heavy oil/bitumen during steam injection by use of metal nanoparticles: A study on in-situ catalysis and catalyst transportation*. *SPE Reservoir Evaluation & Engineering*, 2013. **16**(03): p. 333-344.
132. Shokrlu, Y.H. and T. Babadagli, *Viscosity reduction of heavy oil/bitumen using micro-and nano-metal particles during aqueous and non-aqueous thermal applications*. *Journal of Petroleum Science and Engineering*, 2014. **119**: p. 210-220.
133. Alomair, O.A., K.M. Matar, and Y.H. Alsaeed, *Experimental study of enhanced-heavy-oil recovery in Berea sandstone cores by use of nanofluids applications*. *SPE Reservoir Evaluation & Engineering*, 2015. **18**(03): p. 387-399.
134. Kisielowski, C., et al., *Imaging MoS₂ Nanocatalysts with Single - Atom Sensitivity*. *Angewandte Chemie International Edition*, 2010. **49**(15): p. 2708-2710.
135. Hansen, L.P., et al., *Atomic - Scale Edge Structures on Industrial - Style MoS₂ Nanocatalysts*. *Angewandte Chemie International Edition*, 2011. **50**(43): p. 10153-10156.
136. Patiño, J.E. and F.B. Cortés, *Nanocatalysts for hydrocracking and methods of their use*. 2016, Google Patents.
137. Sotto, A., et al., *Doping of polyethersulfone nanofiltration membranes: antifouling effect observed at ultralow concentrations of TiO₂ nanoparticles*. *Journal of Materials Chemistry*, 2011. **21**(28): p. 10311-10320.
138. Mohammadi, M., et al., *Inhibition of asphaltene precipitation by TiO₂, SiO₂, and ZrO₂ nanofluids*. *Energy & Fuels*, 2011. **25**(7): p. 3150-3156.

139. Ko, S., et al. *Accelerated Oil Droplet Separation from Produced Water Using Magnetic Nanoparticles*. in *SPE Annual Technical Conference and Exhibition*. 2014. Society of Petroleum Engineers.
140. Kapusta, S., L. Balzano, and P.M. Te Riele. *Nanotechnology applications in oil and gas exploration and production*. in *International Petroleum Technology Conference*. 2011. International Petroleum Technology Conference.
141. Negin, C., S. Ali, and Q. Xie, *Application of nanotechnology for enhancing oil recovery – A review*. Petroleum, 2016.
142. Miranda, C.R., L.S.d. Lara, and B.C. Tonetto. *Stability and mobility of functionalized silica nanoparticles for enhanced oil recovery applications*. in *SPE International Oilfield Nanotechnology Conference and Exhibition*. 2012. Society of Petroleum Engineers.
143. Metin, C.O., J.R. Baran, and Q.P. Nguyen, *Adsorption of surface functionalized silica nanoparticles onto mineral surfaces and decane/water interface*. Journal of Nanoparticle Research, 2012. **14**(11): p. 1246.
144. Wang, L., et al., *The study of thermal stability of the SiO₂ powders with high specific surface area*. Materials chemistry and physics, 1999. **57**(3): p. 260-263.
145. Shahrabadi, A., et al. *Experimental investigation of HLP nanofluid potential to enhance oil recovery: A mechanistic approach*. in *SPE International Oilfield Nanotechnology Conference and Exhibition*. 2012. Society of Petroleum Engineers.
146. Hendraningrat, L., S. Li, and O. Torsaeter. *Enhancing oil recovery of low-permeability berea sandstone through optimised nanofluids concentration*. in *SPE Enhanced Oil Recovery Conference*. 2013. Society of Petroleum Engineers.
147. Maghzi, A., et al., *Pore-scale monitoring of wettability alteration by silica nanoparticles during polymer flooding to heavy oil in a five-spot glass micromodel*. Transport in porous media, 2011. **87**(3): p. 653-664.
148. Sharma, T., G.S. Kumar, and J.S. Sangwai, *Comparative effectiveness of production performance of Pickering emulsion stabilized by nanoparticle–surfactant–polymer over surfactant–polymer (SP) flooding for enhanced oil recovery for Brownfield reservoir*. Journal of Petroleum Science and Engineering, 2015. **129**: p. 221-232.
149. Sharma, T. and J.S. Sangwai, *Silica nanofluids in polyacrylamide with and without surfactant: Viscosity, surface tension, and interfacial tension with liquid paraffin*. Journal of Petroleum Science and Engineering, 2017.
150. Sharma, T., S. Iglauer, and J.S. Sangwai, *Silica Nanofluids in an Oilfield Polymer Polyacrylamide: Interfacial Properties, Wettability Alteration, and Applications for Chemical Enhanced Oil Recovery*. Industrial & Engineering Chemistry Research, 2016. **55**(48): p. 12387-12397.
151. Johnston, K.P. and S.R. da Rocha, *Colloids in supercritical fluids over the last 20 years and future directions*. The Journal of Supercritical Fluids, 2009. **47**(3): p. 523-530.
152. Enick, R.M., et al. *Mobility and Conformance Control for CO₂ EOR via Thickeners, Foams, and Gels--A Literature Review of 40 Years of Research and Pilot Tests*. in *SPE improved oil recovery symposium*. 2012. Society of Petroleum Engineers.
153. AttarHamed, F., M. Zoveidavianpoor, and M. Jalilavi, *The incorporation of silica nanoparticle and alpha olefin sulphonate in aqueous CO₂ foam: Investigation of foaming behavior and synergistic effect*. Petroleum Science and Technology, 2014. **32**(21): p. 2549-2558.
154. !!! INVALID CITATION !!! [155].
155. Kim, I., et al., *Size-dependent properties of silica nanoparticles for Pickering stabilization of emulsions and foams*. Journal of Nanoparticle Research, 2016. **18**(4): p. 1-12.
156. Jafarnezhad, M., M.S. Giri, and M. Alizadeh, *Impact of SnO₂ nanoparticles on enhanced oil recovery from carbonate media*. Energy Sources, Part A: Recovery, Utilization, and Environmental Effects, 2017. **39**(1): p. 121-128.
157. Youssif, M.I., et al., *Silica nanofluid flooding for enhanced oil recovery in sandstone rocks*. Egyptian Journal of Petroleum, 2017.
158. Hafshejani, L.D., et al., *Synthesis and characterization of Al₂O₃ nanoparticles by flame spray pyrolysis (FSP)—Role of Fe ions in the precursor*. Powder Technology, 2016. **298**: p. 42-49.
159. Chang, H. and Y.-C. Chang, *Fabrication of Al₂O₃ nanofluid by a plasma arc nanoparticles synthesis system*. Journal of Materials Processing Technology, 2008. **207**(1): p. 193-199.
160. Tsuzuki, T. and P.G. McCormick, *Mechanochemical synthesis of nanoparticles*. Journal of materials science, 2004. **39**(16): p. 5143-5146.
161. Giraldo, J., et al., *Wettability alteration of sandstone cores by alumina-based nanofluids*. Energy & Fuels, 2013. **27**(7): p. 3659-3665.
162. Zaid, H.M., N. Yahya, and N.R.A. Latiff. *The effect of nanoparticles crystallite size on the recovery efficiency in dielectric nanofluid flooding*. in *Journal of Nano Research*. 2013. Trans Tech Publ.
163. Joonaki, E. and S. Ghanaatian, *The application of nanofluids for enhanced oil recovery: effects on interfacial tension and coreflooding process*. Petroleum Science and Technology, 2014. **32**(21): p. 2599-2607.

164. Nazari Moghaddam, R., et al., *Comparative study of using nanoparticles for enhanced oil recovery: wettability alteration of carbonate rocks*. Energy & Fuels, 2015. **29**(4): p. 2111-2119.
165. Haroun, M.R., et al. *Smart nano-EOR process for Abu Dhabi carbonate reservoirs*. in *Abu Dhabi International Petroleum Conference and Exhibition*. 2012. Society of Petroleum Engineers.
166. Shekhawat, D.S., et al. *Magnetic Recovery-Injecting Newly Designed Magnetic Fracturing Fluid with Applied Magnetic Field for EOR*. in *SPE Asia Pacific Hydraulic Fracturing Conference*. 2016. Society of Petroleum Engineers.
167. Nassar, N.N., M.E. Al-Jabari, and M.M. Husein. *Removal of asphaltenes from heavy oil by nickel nano and micro particle adsorbents*. in *Proceedings of the IASTED International Conference*. 2008.
168. Nwideo, L., et al. *Nanofluids for Enhanced Oil Recovery Processes: Wettability Alteration Using Zirconium Oxide*. in *Offshore Technology Conference Asia*. 2016. Offshore Technology Conference.
169. Ehtesabi, H., et al., *Enhanced heavy oil recovery in sandstone cores using tio2 nanofluids*. Energy & Fuels, 2013. **28**(1): p. 423-430.
170. Cheraghian, G., *Effects of titanium dioxide nanoparticles on the efficiency of surfactant flooding of heavy oil in a glass micromodel*. Petroleum Science and Technology, 2016. **34**(3): p. 260-267.
171. Cheraghian, G., *Effect of nano titanium dioxide on heavy oil recovery during polymer flooding*. Petroleum Science and Technology, 2016. **34**(7): p. 633-641.
172. Tajmiri, M., et al., *Wettability Alteration of Sandstone and Carbonate Rocks by Using ZnO Nanoparticles in Heavy Oil Reservoirs*. Iranian Journal of Oil & Gas Science and Technology, 2016. **4**(4): p. 50-66.
173. Latiff, N.R.A., et al. *Novel enhanced oil recovery method using dielectric zinc oxide nanoparticles activated by electromagnetic waves*. in *National Postgraduate Conference (NPC), 2011*. 2011. IEEE.
174. Adil, M., et al., *Effect of Dispersion Stability on Electrorheology of Water-Based ZnO Nanofluids*. Energy & Fuels, 2016. **30**(7): p. 6169-6177.
175. Karimi, A., et al., *Wettability alteration in carbonates using zirconium oxide nanofluids: EOR implications*. Energy & Fuels, 2012. **26**(2): p. 1028-1036.
176. Moslan, M.S., et al. *Wettability Alteration of Dolomite Rock Using Nanofluids for Enhanced Oil Recovery*. in *Materials Science Forum*. 2016. Trans Tech Publ.
177. Fakirov, S., D. Bhattacharyya, and S.M. Panamoottil, *Converting of bulk polymers into nanosized materials with controlled nanomorphology*. International Journal of Polymeric Materials and Polymeric Biomaterials, 2014. **63**(15): p. 777-793.
178. Rao, J.P. and K.E. Geckeler, *Polymer nanoparticles: preparation techniques and size-control parameters*. Progress in Polymer Science, 2011. **36**(7): p. 887-913.
179. ShamsiJazeyi, H., et al., *Polymer - coated nanoparticles for enhanced oil recovery*. Journal of Applied Polymer Science, 2014. **131**(15).
180. Wang, L., et al. *Preparation of microgel nanospheres and their application in EOR*. in *International Oil and Gas Conference and Exhibition in China*. 2010. Society of Petroleum Engineers.
181. Shen, M. and D.E. Resasco, *Emulsions stabilized by carbon nanotube– silica nanohybrids*. Langmuir, 2009. **25**(18): p. 10843-10851.
182. Li, X.-M., D. Reinhoudt, and M. Crego-Calama, *What do we need for a superhydrophobic surface? A review on the recent progress in the preparation of superhydrophobic surfaces*. Chemical Society Reviews, 2007. **36**(8): p. 1350-1368.
183. Yan, Y., et al., *Carbon nanotube catalysts: recent advances in synthesis, characterization and applications*. Chemical Society Reviews, 2015. **44**(10): p. 3295-3346.
184. Villamizar, L.C., et al. *Interfacially active SWNT/silica nanohybrid used in enhanced oil recovery*. in *SPE Improved Oil Recovery Symposium*. 2010. Society of Petroleum Engineers.
185. Kadhum, M.J., et al. *Propagation of carbon nanotube hybrids through porous media for advancing oilfield technology*. in *SPE International Symposium on Oilfield Chemistry*. 2015. Society of Petroleum Engineers.
186. Alnarabiji, M.S., et al., *The Influence of Hydrophobic Multiwall Carbon Nanotubes Concentration on Enhanced Oil Recovery*. Procedia Engineering, 2016. **148**: p. 1137-1140.
187. Khilar, K.C. and H.S. Fogler, *Migrations of fines in porous media*. Vol. 12. 1998: Springer Science & Business Media.
188. Sun, X., et al., *Application of Nanoparticles in Enhanced Oil Recovery: A Critical Review of Recent Progress*. Energies, 2017. **10**(3): p. 345.
189. Morrow, N.R., *Wettability and its effect on oil recovery*. Journal of Petroleum Technology, 1990. **42**(12): p. 1,476-1,484.
190. Wang, Y., et al., *Surfactant induced reservoir wettability alteration: Recent theoretical and experimental advances in enhanced oil recovery*. Petroleum Science, 2011. **8**(4): p. 463-476.
191. Maerker, J. and W. Gale, *Surfactant flood process design for Loudon*. SPE reservoir engineering, 1992. **7**(01): p. 36-44.

192. Hammond, P.S. and E. Unsal, *Spontaneous Imbibition of Surfactant Solution into an Oil-Wet Capillary: Wettability Restoration by Surfactant– Contaminant Complexation*. Langmuir, 2011. **27**(8): p. 4412-4429.
193. Al-Anssari, S., et al., *Wettability alteration of oil-wet carbonate by silica nanofluid*. Journal of colloid and interface science, 2016. **461**: p. 435-442.
194. Torsater, O., S. Li, and L. Hendraningrat. *A coreflood investigation of nanofluid enhanced oil recovery in low-medium permeability Berea sandstone*. in *SPE International Symposium on Oilfield Chemistry*. 2013. Society of Petroleum Engineers.
195. Roustaei, A. and H. Bagherzadeh, *Experimental investigation of SiO₂ nanoparticles on enhanced oil recovery of carbonate reservoirs*. Journal of Petroleum Exploration and Production Technology, 2015. **5**(1): p. 27-33.
196. Towler, B.F., et al., *Spontaneous Imbibition Experiments of Enhanced Oil Recovery with Surfactants and Complex Nano-Fluids*. Journal of Surfactants and Detergents, 2017. **20**(2): p. 367-377.
197. Chatzis, I. and N.R. Morrow, *Correlation of capillary number relationships for sandstone*. Society of Petroleum Engineers Journal, 1984. **24**(05): p. 555-562.
198. Melrose, J., *Role of capillary forces in detennining microscopic displacement efficiency for oil recovery by waterflooding*. Journal of Canadian Petroleum Technology, 1974. **13**(04).
199. Munshi, A., et al., *Effect of nanoparticle size on sessile droplet contact angle*. Journal of Applied Physics, 2008. **103**(8): p. 084315.
200. Roustaei, A., et al. *An experimental investigation of polysilicon nanoparticles' recovery efficiencis through changes in interfacial tension and wettability alteration*. in *SPE International Oilfield Nanotechnology Conference and Exhibition*. 2012. Society of Petroleum Engineers.
201. Derjaguin, B. and N. Churaev, *Structural component of disjoining pressure*. Journal of Colloid and Interface Science, 1974. **49**(2): p. 249-255.
202. Basu, S. and M.M. Sharma, *Measurement of critical disjoining pressure for dewetting of solid surfaces*. Journal of Colloid and Interface Science, 1996. **181**(2): p. 443-455.
203. Bergeron, V., *Forces and structure in thin liquid soap films*. Journal of Physics: Condensed Matter, 1999. **11**(19): p. R215.
204. Chengara, A., et al., *Spreading of nanofluids driven by the structural disjoining pressure gradient*. Journal of Colloid and Interface Science, 2004. **280**: p. 192-201.
205. Kondiparty, K., et al., *Wetting and spreading of nanofluids on solid surfaces driven by the structural disjoining pressure: statics analysis and experiments*. Langmuir, 2011. **27**(7): p. 3324-3335.
206. Wasan, D., A. Nikolov, and K. Kondiparty, *The wetting and spreading of nanofluids on solids: Role of the structural disjoining pressure*. Current Opinion in Colloid & Interface Science, 2011. **16**: p. 344-349.
207. Mcelfresh, P., D. Holcomb, and D. Ector, *Application of Nanofluid Technology to Improve Recovery in Oil and Gas*. SPE International Oilfield Nanotechnology Conference, 2012: p. 1-6.
208. Piech, M. and J.Y. Walz, *Direct measurement of depletion and structural forces in polydisperse, charged systems*. Journal of colloid and interface science, 2002. **253**(1): p. 117-129.
209. Green, D.W. and G.P. Willhite, *Enhanced oil recovery*. Vol. 6. 1998: Henry L. Doherty Memorial Fund of AIME, Society of Petroleum Engineers Richardson, TX.
210. Wang, J. and M. Dong, *Optimum effective viscosity of polymer solution for improving heavy oil recovery*. Journal of Petroleum Science and Engineering, 2009. **67**(3): p. 155-158.
211. Sheng, J., *Modern chemical enhanced oil recovery: theory and practice*. 2010: Gulf Professional Publishing.
212. Ramsden, D. and K. McKay, *Degradation of polyacrylamide in aqueous solution induced by chemically generated hydroxyl radicals: Part I—Fenton's reagent*. Polymer degradation and stability, 1986. **14**(3): p. 217-229.
213. Ramsden, D. and K. McKay, *The degradation of polyacrylamide in aqueous solution induced by chemically generated hydroxyl radicals: Part II—Autoxidation of Fe²⁺*. Polymer degradation and stability, 1986. **15**(1): p. 15-31.
214. Maghzi, A., et al., *An experimental investigation of silica nanoparticles effect on the rheological behavior of polyacrylamide solution to enhance heavy oil recovery*. Petroleum Science and Technology, 2013. **31**(5): p. 500-508.
215. Zeyghami, M., R. Kharrat, and M. Ghazanfari, *Investigation of the applicability of nano silica particles as a thickening additive for polymer solutions applied in EOR processes*. Energy Sources, Part A: Recovery, Utilization, and Environmental Effects, 2014. **36**(12): p. 1315-1324.
216. Cheraghian, G. and L. Hendraningrat, *A review on applications of nanotechnology in the enhanced oil recovery part B: effects of nanoparticles on flooding*. International Nano Letters, 2015. **6**: p. 1-10.
217. Yousefvand, H. and A. Jafari, *Enhanced oil recovery using polymer/nanosilica*. Procedia Materials Science, 2015. **11**: p. 565-570.
218. Cheraghian, G. and S. Khalilinezhad, *Effect of nanoclay on heavy oil recovery during polymer flooding*. Petroleum Science and Technology, 2015. **33**(9): p. 999-1007.

219. Cheraghian, G., *Thermal resistance and application of nanoclay on polymer flooding in heavy oil recovery*. Petroleum Science and Technology, 2015. **33**(17-18): p. 1580-1586.
220. Tarek, M. and A.H. El-Banbi. *Comprehensive Investigation of Effects of Nano-Fluid Mixtures to Enhance Oil Recovery*. in *SPE North Africa Technical Conference and Exhibition*. 2015. Society of Petroleum Engineers.
221. Hendraningrat, L., S. Li, and O. Torsæter, *Effect of Some Parameters Influencing Enhanced Oil Recovery Process using Silica Nanoparticles : An Experimental Investigation*. Society of Petroleum Engineers, 2013: p. 1-10.
222. El-Diasty, A.I., *The Potential of Nanoparticles to Improve Oil Recovery in Bahariya Formation, Egypt: An Experimental Study*. SPE Asia Pacific Enhanced Oil Recovery Conference, 2015.
223. El-diasty, A.I., et al., *Understanding the Mechanism of Nanoparticles Applications in Enhanced Applications of Nanoparticles in EOR*. Paper SPE 175806 - North Africa Technical Conference (Cairo / Egipto), 2015. **000**: p. 1-19.
224. Somasundaran, P. and G. Agar, *The zero point of charge of calcite*. Journal of Colloid and Interface Science, 1967. **24**(4): p. 433-440.
225. Zhang, T., et al., *Investigation of nanoparticle adsorption during transport in porous media*. SPE Journal, 2014.
226. Kanj, M.Y., J.J. Funk, and Z. Al-Yousif. *Nanofluid coreflood experiments in the ARAB-D*. in *SPE Saudi Arabia Section Technical Symposium*. 2009. Society of Petroleum Engineers.
227. Caldelas, F.M., et al. *Factors governing distance of nanoparticle propagation in porous media*. in *SPE Production and Operations Symposium*. 2011. Society of Petroleum Engineers.
228. Owens, W. and D. Archer, *The effect of rock wettability on oil-water relative permeability relationships*. Journal of Petroleum Technology, 1971. **23**(07): p. 873-878.
229. Cooke, C., R. Williams, and P. Kolodzie, *Use of Centrifugal Measurements of Wettability to Predict Oil Recovery*. 1974, US Department of the Interior, Report of Investigations.
230. Morrow, N.R., *A review of the effects of initial saturation, pore structure and wettability on oil recovery by waterflooding*. 1987.
231. Li, Y., et al., *Investigation of the transport and deposition of fullerene (C60) nanoparticles in quartz sands under varying flow conditions*. Environmental science & technology, 2008. **42**(19): p. 7174-7180.
232. Sasidharan, S., et al., *Coupled effects of hydrodynamic and solution chemistry on long-term nanoparticle transport and deposition in saturated porous media*. Colloids and Surfaces A: Physicochemical and Engineering Aspects, 2014. **457**: p. 169-179.
233. Shen, C., et al., *Effects of solution chemistry on straining of colloids in porous media under unfavorable conditions*. Water resources research, 2008. **44**(5).
234. Sadeghi, G., et al., *Systematic study of effects of pH and ionic strength on attachment of phage PRD1*. Ground Water, 2011. **49**(1): p. 12-19.
235. Tufenkji, N. and M. Elimelech, *Breakdown of colloid filtration theory: Role of the secondary energy minimum and surface charge heterogeneities*. Langmuir, 2005. **21**(3): p. 841-852.
236. Syngouna, V.I. and C.V. Chrysikopoulos, *Interaction between viruses and clays in static and dynamic batch systems*. Environmental science & technology, 2010. **44**(12): p. 4539-4544.
237. Zhang, T., et al., *Mechanistic Model for Nanoparticle Retention in Porous Media*. Transport in Porous Media, 2016: p. 1-20.
238. El-amin, M.F., A. Salama, and S. Sun, *Modeling and Simulation of Nanoparticle Transport in a Two-Phase Flow in Porous Media*. SPE International Oilfield Nanotechnology Conference and Exhibition, 2012: p. 12-14.
239. McDowell - Boyer, L.M., J.R. Hunt, and N. Sitar, *Particle transport through porous media*. Water Resources Research, 1986. **22**(13): p. 1901-1921.
240. Murphy, M.J., *Experimental analysis of electrostatic and hydrodynamic forces affecting nanoparticle retention in porous media*. 2012.
241. Seetha, N., et al., *Upscaling of nanoparticle transport in porous media under unfavorable conditions: Pore scale to Darcy scale*. Journal of Contaminant Hydrology, 2017.
242. Elimelech, M. and C.R. O'Melia, *Kinetics of deposition of colloidal particles in porous media*. Environmental science & technology, 1990. **24**(10): p. 1528-1536.
243. Derjaguin, B. and L. Landau, *The theory of stability of highly charged lyophobic sols and coalescence of highly charged particles in electrolyte solutions*. Acta Physicochim. URSS, 1941. **14**(633-52): p. 58.
244. Yao, K.-M., M.T. Habibiyan, and C.R. O'Melia, *Water and waste water filtration. Concepts and applications*. Environmental science & technology, 1971. **5**(11): p. 1105-1112.
245. Rajagopalan, R. and C. Tien, *Single collector analysis of collection mechanisms in water filtration*. The Canadian Journal of Chemical Engineering, 1977. **55**(3): p. 246-255.
246. Freyberg, D.L., *A natural gradient experiment on solute transport in a sand aquifer: 2. Spatial moments and the advection and dispersion of nonreactive tracers*. Water Resources Research, 1986. **22**(13): p. 2031-2046.
247. Logan, A.J., et al., *Transport and fate of Cryptosporidium parvum oocysts in intermittent sand filters*. Water Research, 2001. **35**(18): p. 4359-4369.

248. Liu, X., et al., *Mobility of multiwalled carbon nanotubes in porous media*. Environmental science & technology, 2009. **43**(21): p. 8153-8158.
249. Cullen, E., et al., *Simulation of the subsurface mobility of carbon nanoparticles at the field scale*. Advances in water resources, 2010. **33**(4): p. 361-371.
250. Bradford, S.A., et al., *Physical factors affecting the transport and fate of colloids in saturated porous media*. Water Resources Research, 2002. **38**(12).
251. Wang, Y., et al., *Transport and retention of nanoscale C60 aggregates in water-saturated porous media*. Environmental science & technology, 2008. **42**(10): p. 3588-3594.
252. Tufenkji, N. and M. Elimelech, *Deviation from the classical colloid filtration theory in the presence of repulsive DLVO interactions*. Langmuir, 2004. **20**(25): p. 10818-10828.
253. Harvey, R.W. and S.P. Garabedian, *Use of colloid filtration theory in modeling movement of bacteria through a contaminated sandy aquifer*. Environmental science & technology, 1991. **25**(1): p. 178-185.
254. Tufenkji, N. and M. Elimelech, *Correlation equation for predicting single-collector efficiency in physicochemical filtration in saturated porous media*. Environmental science & technology, 2004. **38**(2): p. 529-536.
255. Benamar, A., et al., *Particle transport in a saturated porous medium: Pore structure effects*. Comptes Rendus Geoscience, 2007. **339**(10): p. 674-681.
256. Prieve, D.C. and E. Ruckenstein, *Effect of London forces upon the rate of deposition of Brownian particles*. AIChE Journal, 1974. **20**(6): p. 1178-1187.
257. Logan, B., et al., *Clarification of clean-bed filtration models*. Journal of Environmental Engineering, 1995. **121**(12): p. 869-873.
258. Messina, F., D.L. Marchisio, and R. Sethi, *An extended and total flux normalized correlation equation for predicting single-collector efficiency*. Journal of colloid and interface science, 2015. **446**: p. 185-193.
259. Ryan, J.N., et al., *Bacteriophage PRD1 and silica colloid transport and recovery in an iron oxide-coated sand aquifer*. Environmental science & technology, 1999. **33**(1): p. 63-73.
260. Redman, J., et al., *Filtration of recombinant Norwalk virus particles and bacteriophage MS2 in quartz sand: Importance of electrostatic interactions*. Environmental Science & Technology, 1997. **31**(12): p. 3378-3383.
261. Zhang, H., et al., *Enhanced Oil Recovery Driven by Nanofilm Structural Disjoining Pressure: Flooding Experiments and Microvisualization*. Energy & Fuels, 2016. **30**(4): p. 2771-2779.
262. Kajishima, T. and K. Taira, *Computational Fluid Dynamics: Incompressible Turbulent Flows*. 2016: Springer.
263. Socolofsky, S.A. and G.H. Jirka, *Special topics in mixing and transport processes in the environment*. Engineering—lectures, fifth ed., Coastal and Ocean Engineering Division, Texas A&M University, 2005.

Appendix

Visual Model of Nanoparticle Dispersion

```
clear
close all

b=0.01; %m/s
u0=0.05; %m/s
N=1000;
x=zeros(N,1);
y=b*rand(N,1);
D=10^-6; %m^2/s
dt=0.1; %s
NT=10;

xedges=[0:0.02:1]; %for histogram
t(1)=0;
sigmax2(1)=0; %variance in x direction
%Taylor dispersion
for n=1:NT,
    up=4*u0*y/b.*(1-y/b)-2*u0/3;
    x=abs(x+randn(N,1)*(2*D*dt)^0.5+up*dt);
    y=y+randn(N,1)*(2*D*dt)^0.5;
    for i=1:N,
        if y(i) < 0,
            y(i) = abs(y(i));
        elseif y(i) > b,
            y(i) = 2*b - y(i);
        end
    end
    t(n+1)=t(n)+dt;
    numx=histc(x,xedges);
    numxd=numx/500;
    sigmax2(n+1)=var(x);
    subplot(2,1,1)
    plot(x,y,'kx')
    xlabel('x')
    ylabel('y (m)')
    title('Nanoparticle Dispersion Visual Model')
    axis([0 1 0 b])
    subplot(2,1,2)
    bar(xedges,numxd,'histc')
    xlabel('x')
    ylabel('Concentration')
    axis([0 1 0 1])
    %axis([-xmax xmax -ymax ymax])
    pause(0.01)
end
```

Advection-Dispersion Code

```
clear all;

%Parameter definition
D = 5*10^-6;
v = 0.004;
L = 1;
F = 0.9;
k = 0;
ts = 400;
dx = 0.01;
dtAD=dx*dx/(v*dx+2*D);           % unsplit time step from Neumann stability
analysis
dt=F*dtAD;

%Spatial and time discretization
x= 0:dx:L;
t= 0:dt:ts;

[mx nx] = size (x);
[mt nt] = size (t);
c=zeros (nx,nt); %initial c
pv= zeros (1,nt);

%initial condition
for i=2:nt-1
    if (t(i)>=0 && t(i)<=30)
        c(1,i) = 1;
    end
end
c1=max(max(c));

%Main finite difference
for n=2:nt
    for i=2:nx-1
        c(i,n) = c(i,n-1)+((D*dt)/dx^2)*(c(i+1,n-1)-2*c(i,n-1)+c(i-1,n-1))-
(v*dt/(dx))*(c(i,n-1)-c(i-1,n-1))-k*c(i,n-1);
    end
end
c=c/c1

for n=2:nt
%    if pv(n-1) >= 2.7
        dpv=v/L*dt;
%    else
%        dpv=v1/L*dt;
%    end
    pv(n)=pv(n-1)+dpv;
end

%plot
hold on;
figure (1)
```

```

for x=1:20:nx-1
    plot(t,c(x,:), 'color',[rand rand rand]);
end
grid on;
axis tight;
xlabel ('t (sec)');
ylabel ('C/co');
Lx=dx*(1:20:nx-1);
Lx= num2str (Lx');
Legend (Lx);

for t=10:30:nt
    plot(x,c(:,t), 'color',[rand rand rand]);
end
grid on;
axis tight;
xlabel ('x');
ylabel ('C/co');
Lt=dt*(10:30:nt);
Lt= num2str(Lt');
Legend (Lt);
%
```

Single-Collector Efficiency Code

```

clear all; clc; clf

%Input definition (in SI Unit)
por= 0.3;%porosity
dc= 150*10^-6; %collector diameter (m)
Ah = 40*10^-21 ; %Hammaker (J)
kb = 1.38064852*(10^-23); %boltzman constant
T = 298; % Temperature (K)
myu = 1.2 *10^-3; %kg m-1 s-1
rhop = 1.67*10^3; %particle density
rhof = 999; %fluid density
g = 9.81 ; %gravity

%Parameter Definition
dp= linspace (10^-9,10^-5, 100);
v = [0.000005,0.00005,0.0005,0.005,0.5];
N= length(dp);
M= length(v);
%matrix defininition
Nr=zeros (M,N); Na=zeros (M,N); Ng=zeros (M,N); effD=zeros (M,N); effI=zeros
(M,N); effG=zeros (M,N);
TE=zeros (M,N);
MMS=zeros (M,N);
MMSn=zeros (M,N);
LOG=zeros (M,N);
YH=zeros (M,N);

for n=1:M
    for i=1:N
        %sub parameter calculation
        Dn= kb*T/(3*pi*myu*dp(i)); %Diffussion Coeff (m2/s)
        gam=(1-por)^(1/3);
        As=2*(1-gam^5 )/((2-3*gam+3*(gam^5)-2*(gam^6)));
        Nr(n,i)=dp(i)/dc;
        Npe=(v(n)*dc)/(Dn*por);
        Nvdw=Ah/(kb*T);
        Na(n,i)=(Ah*por)/(12*pi*myu*(dp(i)/2)^2*v(n));
        Ng(n,i)=(2*((dp(i)/2)^2)*(rhop-rhof)*g*por)/(9*myu*v(n));

        %main calculation
        effD(n,i)=(2.4*As^(1/3)*Nr(n,i)^(-0.081)*Npe^(-0.715)*Nvdw^0.052);
        effI(n,i)=(0.55*As*Nr(n,i)^1.675*Na(n,i)^0.125);
        effG(n,i)=(0.22*Nr(n,i)^(-0.24)*Ng(n,i)^1.11*Nvdw^0.053);
        TE(n,i)= effD(n,i)+effI(n,i)+effG(n,i);
        MMS(n,i)= gam^2*(1.5062*As*Nr(n,i)^1.9834+7.5609*Npe^-1/(2-
2*gam)+Ng(n,i)+As^0.3662*Npe^-
0.6338*(2.9352+2.7480*Nr(n,i)^0.3737)+0.9461*Ng(n,i)^0.6550*Npe^-0.3450);
        MMSn(n,i)= MMS(n,i)/((1+6.0098*As*Nr(n,i)^1.9834)+gam^2*7.5609*Npe^-
1/(2-2*gam)+Ng(n,i)+As^0.3662*Npe^-
0.6338*(2.9352+2.7480*Nr(n,i)^0.3737)+2.7972*Ng(n,i)^0.6550*Npe^-0.3450);
        LOG(n,i)= 4*As^(1/3)*Npe^(-
2/3)+(As*Nr(n,i)^(15/8)*Nvdw^(1/8))+0.00338*As*Ng(n,i)^1.2*Nr(n,i)^-0.4);
        YH(n,i)= 4*As^(1/3)*Npe^(-2/3)+(3/2)*Nr(n,i)^2+Ng(n,i);
    end
end

```

```

%plot
V= num2str (v');
V= strcat({'v = '},V);
Mo=char( 'YH', 'LOG', 'TE', 'MMS', 'MMS_N');
y= ones (M,N);

figure (1)
subplot(2,2,3)
    loglog(dp,TE); hold on;
    loglog(dp,y, '--k'); hold on;
    title('Tufenkji et al. (2004)')
    xlabel('Particle Diameter (m)')
    ylabel('Single-Collector Efficiency ( $\eta_o$ ) ')
    legend (V)
subplot(2,2,4)
    loglog(dp,MMS); hold on;
    loglog(dp,y, '--k'); hold on;
    title('Messina et al. (2015)')
    xlabel('Particle Diameter (m)')
    ylabel('Single-Collector Efficiency ( $\eta_o$ ) ')
    legend (V)
subplot(2,2,2)
    loglog(dp,LOG); hold on;
    loglog(dp,y, '--k'); hold on;
    title('Logan et al. (1995)')
    xlabel('Particle Diameter (m)')
    ylabel('Single-Collector Efficiency ( $\eta_o$ ) ')
    legend (V)
subplot(2,2,1)
    loglog(dp,YH); hold on;
    loglog(dp,y, '--k'); hold on;
    title('Yao-Habibian (1971)')
    xlabel('Particle Diameter (m)')
    ylabel('Single-Collector Efficiency ( $\eta_o$ ) ')
    legend (V)

figure (2)
    loglog(dp,YH(1,:)); hold on;
    loglog(dp,LOG(1,:)); hold on;
    loglog(dp,TE(1,:)); hold on;
    loglog(dp,MMS(1,:)); hold on;
    loglog(dp,MMSn(1,:)); hold on;
    loglog(dp,y, '--k'); hold on;
    xlabel('Particle Diameter (m)')
    ylabel('Single-Collector Efficiency ( $\eta_o$ ) ')
    legend (Mo)

figure (3)
    loglog(dp,MMSn); hold on;
    loglog(dp,y, '--k'); hold on;
    title('Normalized Messina et al. (2015)')
    xlabel('Particle Diameter (m)')
    ylabel('Single-Collector Efficiency ( $\eta_o$ ) ')
    legend (V)

```

Nanoparticle Transport Code

```
clear all;

%Parameter definition
D = 2.1*10^-6; % Diffusion m2/s
q1 = 8.33*0.01667*10^-6; %volumetric flow rate m3/sec
A = 4.49*10^-5; % Area m3
v1 = q1/A; % velocity m/s
vpore=14.8*10^-6; % Pore volume m3
L = 0.3; %Length m
F = 0.9; %safety factore
ts = 500; %total time step
dx = 0.01; %time step
%Depositional Coef Parameter
por = 0.473; %Porosity
dp = 100 *10^-9; %particle diameter
dc = 150 *10^-6 ;%collector diameter m
rhop = 1.52 *10^3 ; %particles density kg/m3
rhof = 1.1 *10^3 ; %fluids density kg/m3
rhob = 1.28*10^3 ; %bulk density kg/m3
eta = collector (por,dp,dc,v1,rhop,rhof); %Collector Eff
alp = 0.01; %Attachment Eff (Can be adjusted)
k1 = 3*(1-por)/(2*dc)*v1*alp*eta; %Depositional Coeff
%parameter PV related
PVIt=2.2; % PV total injected slug
PVItt=PVIt*vpore/q1; %convert in time
dtAD=dx*dx/(v1*dx+2*D); % unsplit time step from von Neumann stability
analysis
dt=F*dtAD;
ka= 0.135;
Kap = 1+((rhob/por)*ka*eta);

%Spatial and time discretization
x= 0:dx:L;
t= 0:dt:ts;
[mx nx] = size (x);
[mt nt] = size (t);
c=zeros (nx,nt); %initial c
pv=zeros (1,nt); %for PV plot

%initial condition
for i=2:nt-1
    if (t(i)>=0 && t(i)<=PVItt)
        c(1,i) = 0.1;
    end
end
c1=max(max(c));

%Main finite difference

for n=2:nt
    for i=2:nx-1
        c(i,n) = c(i,n-1)+((D*dt)/(Kap*dx^2))*(c(i+1,n-1)-2*c(i,n-1)+c(i-1,n-1))-
(v1*dt/(Kap*dx)*(c(i,n-1)-c(i-1,n-1)));
    end
end
```

```

c=c/c1;
for n=2:nt
    dpv=v1/L*dt;
    pv(n)=pv(n-1)+dpv;
end

Area= trapz (pv,c(nx-1,:));
Recovery = Area/3;
plot(pv,c(nx-1,:), 'g'); hold on;
axis ([0 5 0 1]);
title ('E92');
grid on;

xlabel ('PV');
ylabel ('C/co');

%Experimental data
Ex=xlsread('E92.xlsx')
pvexp=Ex(:,1); cexp=Ex(:,2);
plot(pvexp,cexp, 'bd');

%Tracer data
Ext=xlsread('E92-tracer.xlsx')
pvexp=Ext(:,1); cexp=Ext(:,2);
plot(pvexp,cexp, 'k--');
%
%Tracer data
Ext=xlsread('E92-ISTM.xlsx')
pvexp=Ext(:,1); cexp=Ext(:,2);
plot(pvexp,cexp, 'm');

```